UNIVERSITY of TRIPOLI
Faculty of Science
Department of Geophysics

Integration of Geophysical Study of Cenozoic Structural Evolution in The Maradah Trough and Adjacent Area, Central Sirt Basin, Libya

Submitted By
Mohammed Saied Emhemmed Al-Ezabi

Name of Supervisors
Supervisor: Bashir Mohamed Youshah
Professor
Co- Supervisor: Mohammed Abdullah Saleem
Associated Professor

Thesis was submitted in partial Fulfilment of requirements for the degree of Master in Geophysics

Date (12 / 04 / 2023)

Declaration

I Mohammed Saied Emhemmed Al-Ezabi. the undersigned hereby confirm that the work contained in this thesis / dissertation, unless otherwise referenced is the researcher's own work, and has not been previously submitted to meet requirements of an award at this University or any other higher education or research institution, I furthermore, cede copyright of this thesis in favour of University of Tripoli.

Student name: Mohammed Saied Al-Ezabi

Signature: .....

Date: 12 / 04 / 2023

University of Tripoli
Faculty of Science
Department of

Title

Integration of Geophysical Study of Cenozoic Structural Evolution in The Maradah Trough and Adjacent Area, Central Sirt Basin, Libya

Student name
Mohammed Saied Emhemmed Al-Ezabi

This dissertation has been approved by the examination committee:

Dr. Ahmed Salem Saheel (External examiner)……
(Libyan Petroleum institute - Tripoli)

Dr Muftah Ali Abuaisha (Internal examiner)……
(University of Tripoli – Tripoli

Dr. Mohammed Abdullah Saleem (Co-supervisor)……
(Libyan Petroleum institute - Tripoli)

Dr.Bashir Mohamed Youshah (Supervisor)……
(University of Tripoli - Tripoli)

Dr. Fathi Goma Al- Sghair
Head of Graduate Studies and Training Office

Prof. Ramadan E. Eljadi
Dean of the Faculty

……..…… ……..……

12 / 04 / 2023

المُلخّــص

تدمج هذه الدراسة البيانات الجاذبية والمغناطيسية والبيانات الجيولوجية في محاولة لفهم الهياكل الجيولوجية الرئيسية السطحية وتحت السطحية في مرتفع مرادا ، فالهدف من هذه الدراسة هو تحليل البيانات الجاذبية والمغناطيسية لتحديد الصفات التكتونية لمنطقة الدراسة والمنطقة المجاورة لها ، والواقعة في الجزء الأوسط من حوض سرت بليبيا. والبيانات المستخدمة في هذه الدراسة هي 8871 قيمة شادة جاذبية، تم توفيرها من معهد النفط الليبي (LPI). في حين ان البيانات المغناطيسية هي 3231 نقطة شبكية، تم الحصول عليها من مشروع توحيد اللوح الأفريقي المغناطيسي لرسم الخرائط المغناطيسية (AMMP) من قبل معهد النفط الليبي. وقد تمت إزالة الحقل المرجعي الجيومغناطيسي الارضي (IGRF) باستخدام المعادلة الدولية من البيانات الأصلية، تم هذا العمل باستخدام برنامج جيوسوفت.

بدايةً ، تضمن العمل بشكل رئيسي معالجة و تحليل البيانات الجاذبية ، و قد أظهرت العديد من الشواذ الجاذبية ، فقد اظهرت منطقة الشمال قيم عُليا بلغت(3.2-) ملي جال (بمنصة الجهمة). في حين اظهرت منطقة مُرتفع مرادا قيم دُنيا تراوحت مابين (33.5- : 33-) ملي جال.

فبعد التحليل الجاذبي قد ظهرت معظم السمات الجيولوجية التركيبية في منطقة الدراسة باتجاه الشمال الغربي - الجنوب الشرقي ، والتي تتعلقت بتاريخ الصدع الذي حدث في فترة الزمن الطباشيري، هذا الصدع قد أثر على حَوض سرت بأكمله.

تم تطبيق العديد من التقنيات على الشادة الجاذبية والشادة المغناطيسية الكلية لتحديد التراكيب تحت السطحية. منها المشتقة الأفقية الكلية لبيانات الجاذبية والبيانات المغناطيسية ، الاستمرار التصاعدي بمستويات مختلفة ، الفصل خرائط الجاذبية، وفصل خرائط المغناطسية ، اختزال خرائط مغناطيسية الى قطب، وخرائط الجاذبية الزائفة، تحليل أويلر ثلاثي الأبعاد.

تم تمييزه بوضوح من خلال تحليل خرائط المشتقة الأفقية الكلية لبيانات الجاذبية المغناطيسية تراكيباً جيولوجية مختلفة في الجزء الجنوبي من منطقة الدراسة.كانت فيها قيم التدرج العليا باتجاه عام (شمال شمال شرق- جنوب جنوب غرب) و باتجاه عام اخر شمال – جنوب. في حين تم تطبيق الاستمرار التصاعدي على الشاذة الجاذبية من أجل تحسين و اظهار التراكيب الجيولوجية العميقة باستعمال مستويات مختلفة من التردد القطعي (10كم ، 15كم ، 20كم ، 25كم ، 50 كم ، 75 كم)، قد ظهرت افضل النتائج عند مستوى تصاعدي 25كم.

وقد تميز الشذوذ الجاذبي الناتج من تحليل من خريطة الجاذبية المحلية بقيم موجبة سادت الجزء الشمالي و كانت باتجاه عام شمال غرب - وجنوب شرق ، بينما كان اتجاهها العام بالجزء الجنوبي والاوسط الشمال الغربي – الجنوب الشرقي. و في الجزء الجنوبي من منطقة الدراسة ظهر امتداداً ملحوظاً باتجاه عام شمال - جنوب هذا الميل يمثل منطقة مُرتفع مرادا.

في حين اظهر تحليل البيانات المغناطسية (TMI) شذوذاً مغناطيسيًا عاليًا بقيمة 115 نانو تيسلا، في منطقة الشمال. وفي جزء من منطقة الدراسة بمُرتفع مرادا اظهر شذوذاً مغناطيسيا منخفضاً بقيمة 50- نانو تيسلا.

وعندا التحليل المغناطسي لخرائط شذوذ الجاذبية الزائفة والقطبية المغناطيسية المختزلة للقطب قد ظهرت معظم السمات الجيولوجية التركيبية في منطقة الدراسة باتجاه عام شمال – جنوب.

وقد تميزت خرائط اختزال مغناطيسية الى قطب بوجود شواذ مختلطة مابين قيم المنخفضة و العالية. تراوحت هذه القيم مابين قرائتي (28 : 135) نانو تيسلا ، لُوحظت بوضوح في منطقة منصة زُلطن.

خرائط شذوذ الجاذبية الزائفة التي تم الحصول عليها من بيانات الكثافة المغناطيسية الكلية، وقد تم احتساب قيمة الكثافة 1 جم/سم^3 ، و قيمة التمغنُط 0.5 جاوس. يتيح لنا هذا المرشح ازالة تاثير القطب على خرائط المغناطسية ليتسنى العمل عليها و كانها خرائط جاذبية.

وقد بينت طريقة تحليل أويلر ثلاثي الأبعاد أن عمق سطح العلوي لشواذالجاذبية يتراوح بين 3400 م الى 9600 م.بينما تراوح عمق العلوي لشواذ المغناطيسي 3200 م الى 9200 م

و باستخدام طرق النمذجة لمحاكاة الطبقات السفلية و القاع، فقد ظهر النموذج عمقاً تقريبا تحت منطقة مُرتفع مرادا يُـقدر بقُرابة 1.2 كم ، بينما تراوح عمقهُ فوق المناطق العميقة 4.2 كم. في حين ان كان عمق سطح القاع 3.2 كم تحت اغلب الشواذ الاخرى.

ABSTRACT

This study integrates the gravity and magnetic data and geological data in an effort to understand the surface and subsurface major geological structures in Maradah Trough. The aim of this study is analysis of gravity and magnetic data to delineate the tectonic features of the study area and adjacent area, which located in the central part of Sirt Basin of Libya. The data that used in this study is about 8871 gravity values were made available from Libyan Petroleum Institute (LPI). The magnetic data made available from African Magnetic Mapping Project (AMMP) by Libyan Petroleum Institute, which about 3231 gridded point. The International Geomagnetic Reference Field (IGRF) was removed from the original data using Geosoft Package software. Based on analysis of the Bouguer gravity map, it showed numerous anomalies varying from high gravity anomaly expression in the north (Al Jahamah Platform) with the maximum value -3.2 mGal to low gravity expression in the Maradah Trough with minimum value -33 mGal. The most structural features in the study area are characterized by NW-SE trend directions, which related to the Late Cretaceous rift that affect the entire of the Sirt Basin.

Several techniques were applied to the Bouguer gravity and total magnetic intensity to delineate subsurface structures. Total horizontal derivative for gravity and magnetic data, upward continuation to different levels, regional gravity and residual maps were obtained, while magnetic maps were obtained Reduction to the pole and pseudo gravity maps,3D Euler Deconvolution.

gravity anomalies map generally reflects structural trend N-S direction.
Fault lineaments can be interpreted as structural trends according to the total horizontal derivative maps of gravity and magnetic data. In the southern portion of the study area, which is clearly highlighted by the total horizontal derivative, high gradient

values delineate the NNE-SSW and N-S lineaments. Upward continuation was applied to the Bouguer gravity anomaly in order to enhance the deep-seated features (regional gravity map) by using various of cutoff-wave numbers 10,15,20,25,50,75 km. Finally, it had found that the best cutoff-wave number is 25 km. The residual gravity anomaly is calculated by separated the regional anomaly from Bouguer anomaly. The residual gravity anomaly was characterized by positive anomaly in the northern part dominant NW-SE trend, and also the trends in southern and central part were orientation NW-SE trending anomalies. A strong N-S trend was in the southern part of the study area which reflects to the Hagfa Trough (Maradah Trough). The Total Magnetic Intensity (TMI) map reflects high magnetic anomaly with value of 115 nT in north.

part of study area (Al Jahamah Platform) and reflects low magnetic anomaly with value -50 nT in the Maradah Trough. Both the Reduction to magnetic Pole and Pseudo Reduction to the Pole (RTP) map was characterized by low and high frequencies anomalies. The elongated negative anomalies with values between -28 to -135 nT were observed over Zaltan Platform. These anomalies were characterized by high frequency and high amplitude. Pseudo gravity anomaly is obtained from TMI used a density contrast 1 g/cc and magnetization was 0.5 gauss such that transformation makes the TMI behaves like gravity data.

It was demonstrated by applying 3D Euler Deconvolution analysis method that the depth of the upper surface of the gravitational anomalies ranged from 3400 m to 9600 m. meanwhile, the depth of the upper surface of the magnetic anomalies ranged from 3200 m to 9200 m.

The foundation beneath the gravity Trough s is rather shallow (approximately 2.1 km), but it is quite deep (about 4.2 km) beneath the positive anomalies, where the basement

surface indicates a maximum depth of 3.2 Km, according to the gravity models that were built in this study.

Dedication

It is with great gratitude that I dedicate my dissertation work to my family and friends. A special feeling of gratitude to my loving parents, whose words of encouragement and push for tenacity ring in my ears.

I also dedicate this dissertation to my many friends who have supported me throughout the process. I will always appreciate all they have done.

Acknowledgments

first and foremost, I have to thank my research supervisors, Prof. Bashir Youshah**.**

Dr. Mohammed Saleem. Without their assistance and dedicated involvement in every step throughout the process, this thesis would have never been accomplished. I would like to thank you very much for your support and understanding over these past years.

I am also grateful to Prof. Ramadan Al-Jadi, lecturer, in the Department of Geophysics. I am extremely thankful and indebted to him for sharing expertise, and sincere and valuable guidance and encouragement extended to me.

I take this opportunity to express gratitude to all of the Department faculty members for their help and support. I also thank my parents for the unceasing encouragement, support and attention.

I would like to thank Libyan Petroleum Institute (LPI) and Al-Haroug Oil operation who provided me with the Gravity, magnetic data and logs data which I have used in my study.

Finally, I must express my very profound gratitude to my parents for providing me with unfailing support and continuous encouragement throughout my years of study and through the process of researching and writing this thesis. This accomplishment would not have been possible without them. Thank you.

I also place on record, my sense of gratitude to one and all, who directly or indirectly, have lent their hand in this venture.

Author
Mohammed.S. Al-Ezabi

Table of contents

List of Figures:

List of Tables:

XIII

Chapter 1

1.1 Introduction

Sirt basin is one of the major extension basins in the world located in the central north onshore Libya. It is bounded by the Tripolitanian, Ghadamis and Gargaf zones to the west, the Tibisti and Kufrah zones to the south, the Cyrenaica zone to the east, and the Mediterranean Sea to the north, Sirt basin consisting of several Trough s and platforms, in which there are a lot of structural and stratigraphic traps have been formed. the study area (part of Maradah Trough and adjacent area) which is part of this basin located between the geographical coordinates, longitudes 19º00`E - 20º00`E and latitudes 28º00`N - 29º00`N (Figure 1.1).

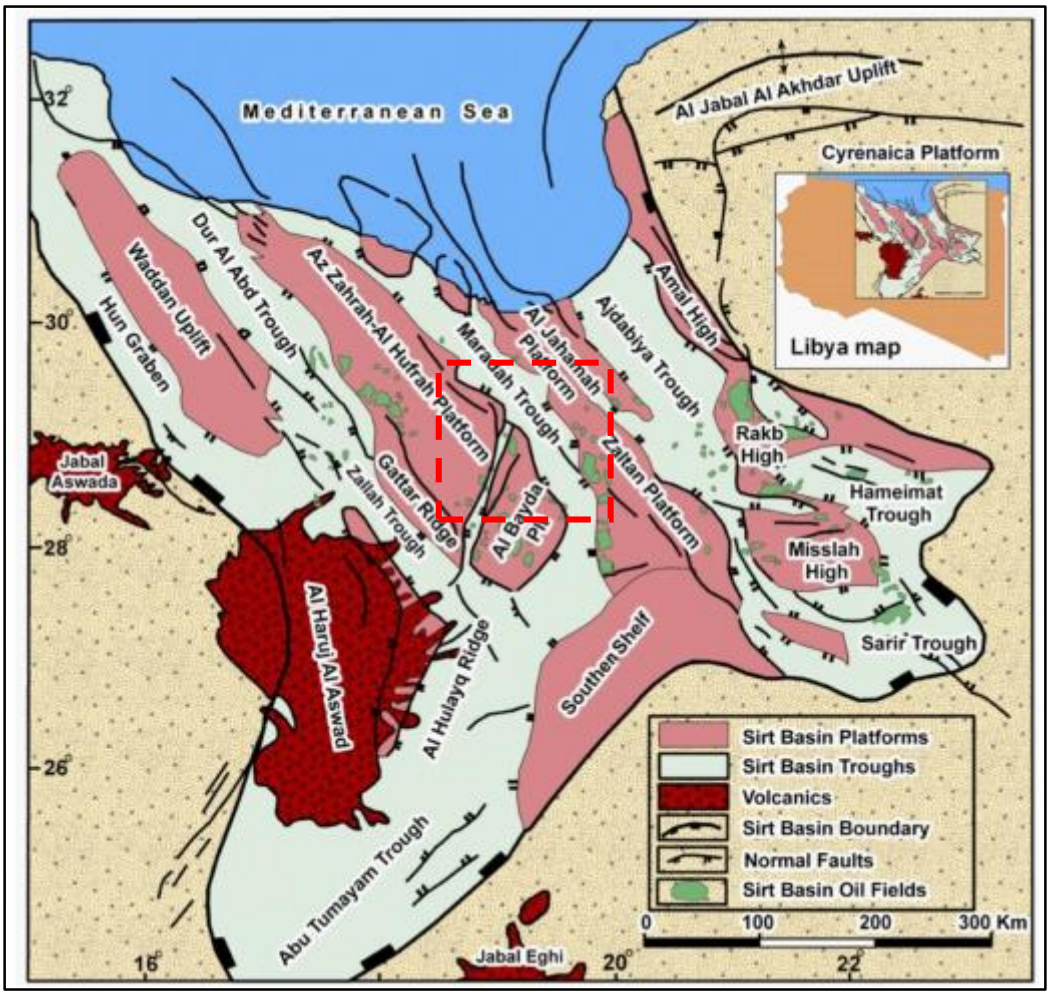

Figure 1. 1: The tectonic framwork of Sirt Basin, shows that the basin is differentiated into several positive and negative tectonic elements delimated by normal faults. (Modified after Mozoughi and Taleb, 1981; Bellini and Masa, 1980). Insert map of Sirt Basin in Libya the study area (red rectangular)

Based on the application of these methods, we can analyze the accurate data of each method using a combination of borehole data available in the area in order to obtain the most accurate results.

1.2 Aims and Objectives

The study aims to delineate and define the structural framework in the area, by which the geometry and the depth of the expected hydrocarbon traps can be located and defined. This main aim could be approached by defining the following:

1. The gravity anomalies sources.
2. The magnetic anomalies source.

Also, the research seeks to determine the major and minor structures and faults and to locate and track them in both directions laterally and deeply. It also will include a brief study on the tectonic setting of this basin.

1.3 Dataset

A variety of geophysical and geological data have been obtained and will be used in this project, represented by the four main types of data, gravity, magnetic, seismic, and borehole data which provided by several companies working in the country as described below:

- Borehole Data

  The complete sets of borehole logs (Sonic, Density, Gamma-ray, Resistivity, and Lithology) for 45oil and gas wells distributed in the area are available for the study.

- Gravity Data

There is about 8871 gravity station covered the study area (Maradah Trough s and adjacent area), the gravity data originally was collected by Libyan Petroleum Institute LPI for the Libyan Gravity Project and distributed in the area as shown in Figure1.3. The survey points are placed regularly and orthogonal to cover the area which is semi-square as shown, the smallest spacing was 500 meters and the largest spacing was approximately 1.2 km.

1.4 Software used in analysis.

Various software has been used to carry out different analyses on one or more of the datasets. The main ones are:

- OASIS MONTAJ software (version 6.4)

This software was used to process and interpret the gravity and magnetic data, the software is including a rich set of features that provide ease of use and enable the user to access the data set, process, map, and apply the interpretation filters.

- GM-SYS modelling capability

This sub-software of OASIS MONTAJ, models and displays the gravity data simultaneously, including the surface data, response curves and well information.

1.5 Thesis structure

This dissertation is divided into three main parts:

Part I: includes the general background, scope and purpose of the thesis, followed by the Data set and Software that I have used.

Part II: describes the geological and stratigraphic background of the area, reviews past work on its tectonic development through time, and also gives a brief description of the main reservoirs.

Part III: This section comprises the majority of the thesis, and does include the author's original work created during gravity and magnetic processing of the Maradah Trough and its adjacent area.

Part IIII: Part III's conclusions are discussed, and they are set in the context of the basin's evolution.

Chapter 2

Geology Background

This chapter is split into two parts. First, a brief description of the geological setting of the region will be provided. A summary of the Sirt Basin's basic stratigraphy, tectonics, and major structures was also provided in the second section.

2.1 Introduction

Libya is one of the North African countries. It shares its borders with Tunisia and Algeria on the west, Egypt on the east, Sudan on south-east Niger, and Chad on the south, while in the north is located on the Mediterranean coast. It is one of the largest oil and natural gas producing countries in Africa. Most of its production is from oil fields which are distributed in the major sedimentary basins in Libya (Figure 2.1). According to Energy Intelligence Research (Kendall, 2008), in 2003 Libya was the 11th largest exporter of petroleum in the world. Libya reached the peak of 3.3 million barrels a day in 1970 and currently produces only about 900.000 barrels of crude a day, due to the political circumstances that dominated the country last then years. According to National Oil Corporation (NOC), only around 30 percent of Libya has been explored for hydrocarbons, Libya wants to return production to previous peak levels. There are about 320 producer fields with a total reserve exceeding 50 billion barrels of oil and 40 trillion cubic feet of gas (Rusk2002).

The evolution of sedimentary basins of Libya was controlled by a tectonic movement that include: 1-A compressional early Paleozoic Pan-African event, 2-The Hercynian Orogeny, 3 - Extension related to Cretaceous, middle Tertiary and Holocene events starting with the southern Tethys and evolving into the Mediterranean.

The main producing basins of Libya are in order of importance the Sirt, Ghadamis, Murzuq, and the offshore Tripolitania basin.

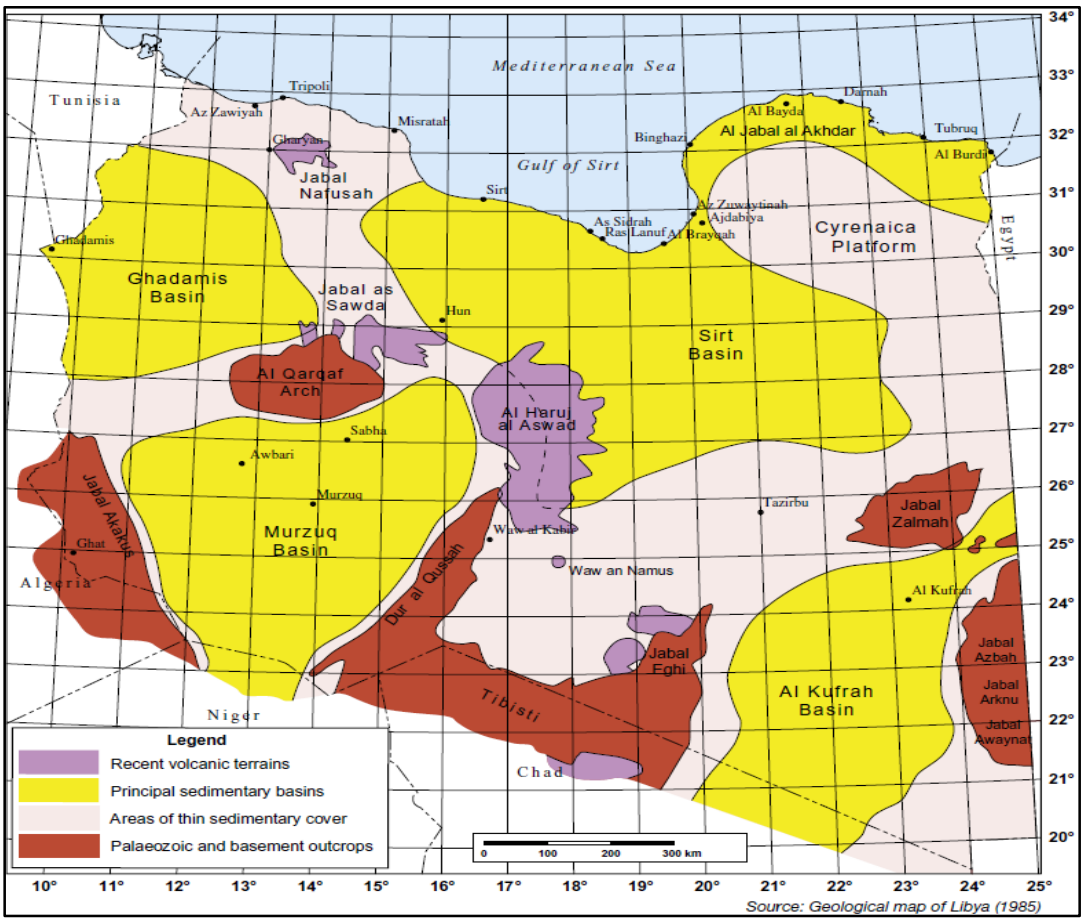

Figure 2. 1: The major Sedimentary basins (Geoligcal map of libya 1985).

Epeirogeny movements with vertical nature are limited to up-arching and faulting and included Mesozoic-Tertiary basins of Sirt and Cyrenaica (NE Libya). Tectonic movements occurring in northern Libya were responsible for the large sedimentary sequences in Libyan basins. The generation and entrapment of hydrocarbons in Libya were controlled by the tectonic history of each basin (Hassan & Kendall, 2014).

The Sirt Basin contains some sixteen giant oil fields with about 117 billion barrels of in-place proven recoverable oil. These form 89% of all the discovered Libyan petroleum reserves. This basin is considered to be the most prolific oil basin in North

Africa with an oil gravity that ranges between 44 and 32 APIs, and Sulphur content of between 0.15 and 0.66%. The Sirt Basin includes Cretaceous and Paleocene reservoir sequences and the Upper Cretaceous Sirt Shale is a major source rock for this basin (Hallett, 2002).

The Ghadamis intracratonic Basin consists of up to 6000 m of dominantly clastic Paleozoic through Mesozoic strata with an estimated 3 billion bbl of recoverable oil. The Upper Silurian Akakus Formation and the Tadrart - OuanKasa Formations are the most prolific oil-producing horizons. (Hallett, 2002; Rusk, 1999).

The Muzurq Basin is filled with Cambrian through Quaternary deposits, with a maximum total thickness of more than 3000 m in the central part of the Basin. In the area to the north, where oil reserves are some 1 billion barrels, the potential reservoirs include the Memouniat, Akakus, and Tadrart- OuanKasa sandstones. The major source of rock in this basin is the Silurian Tanezzuft Shale (Hallett, 2002; Rusk, 1999).

The Eastern Tripolitania Basin is the offshore basin, which is a highly faulted, deep Trough , that extends from the Gulf of Gabes to the northwestern margin of the Sirt Basin. The eastern sector is some 20,000 km^2in extent and is essentially unexplored, with only one dry hole (up to the year 2000); known accumulations are 100-150 km west of the area (Hallett, 2002; Rusk, 1999).

2.2 Sirt Basin Overview

The Sirt Basin is one of the youngest sedimentary basins in Libya and covers an approximate area of 600,000 km^2 (Hallett, 2002) in north-central Libya and contains a sedimentary deposit sequence reaching a thickness of approximately 7500 m.

It is located along the North African continental margin and bounded by the Gulf of Sirt along the Mediterranean coast and extends to beyond latitude 26°N south. This

basin is characterized by a series of northwest-trending platforms and Trough s, which stretch 600 km in the east-west direction from the Hun Graben in the west to the Cyrenaica Platform in the east. It is bounded to the south by the Tibisti Massif and to the west by the Al Qarqaf Uplift and the Ghadamis and Murzuq basins. The topography of the Sirt basin is variable from 150 m above sea level in the Dahra platform to 750 m below sea level in the north of the Agedabia Trough . The lowest part is situated close to the coastline near the Gulf of Sirt and coincides with the tectonic subsidence calculated by (Abadi, 2002) for the most recent phase (49 Ma - present). More than 7 km of sediment thickness was accumulated in the deepest part of the basin (Agedabia Trough) in the eastern part of the Sirt Basin, of Mesozoic and

Cenozoic age (98.9Ma-0Ma) (Elakkari, 2005; Galushkin, El Maghbi, &El Gtlawi, 2014; Hallett, 2002).

The Sirt Basin is a late Mesozoic and Tertiary continental rift, triple junction, in northern Africa that borders a relatively stable Paleozoiccraton and cratonic sag basins along its southern margins (Figure 2.2). The province extends offshore into the Mediterranean Sea, with the northern boundary drawn at the 2,000-meter (m) isobath (Hallett, 2002).

The majority content of the known hydrocar0bons reserved in the Sirt Basin was formed during the Mesozoic. The sediment configuration within the basins was controlled by basement structures which divided the entire basin into a series of Trough s and platforms (Figure 2.2).

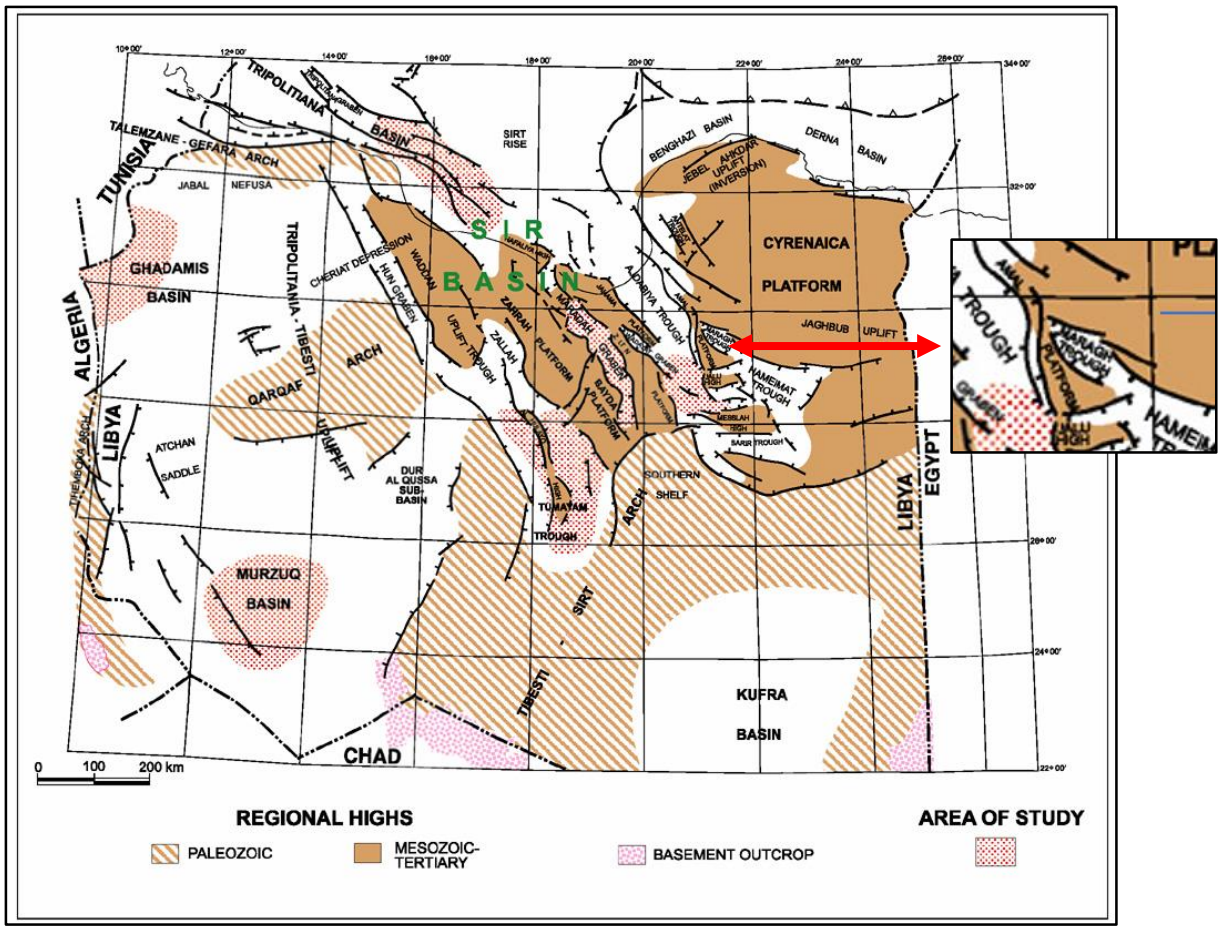

Figure 2. 2: Structural elements of the Sirt Basin, showing oil and gas fields. and Trough s and grabens, platforms (Rusk 2002)

The south and southeast boundaries of the Sirt Basin are drawn at the Precambrian-Paleozoic contact along the Nubian Uplift and its northeast-trending extension termed the Southern Shelf (Figure 2.2) also referred to as the Northeast Tibesti Arch / Alma Arch uplift by some authors (Tawadros, Rasul, &Elzaroug, 2001).

The Sirt Basin formed in a more dramatic manner. The basin underwent regional uplift, tensional and compressional faulting, and Trough subsidence, resulting in an NW trending horst and graben structural style (Figure 2.2) of considerable relief (Ahlbrandt, 2001).

The Cyrenaica Shelf (also referred to as a platform, including both basin and uplift) forms the eastern and northeastern border.

The western border, generally called the Western Shelf, is a combination of the Nubian Uplift and a northwest-trending extension called the Fezzan Uplift (Tripoli- As Sawda Arch); the latter feature intersects the Nafusa(Teleman- Gefara) Arch, an east-west-trending arch along the other west margin of the province (Ahlbrandt, 2001; Elakkari, 2005; Tawadros, 2001).

2.3 Stratigraphy of the Sirt Basin

The stratigraphical sequence of the Sirt Basin is characterized by much reduced or

completely absent Paleozoic rocks. The Cambro-Ordovician is the only Paleozoic sequence with a wide distribution in the Sirt Basin, except in some paleo-high areas where it is absent as at the western edge of the Beda and Zelten platforms. The Silurian and Devonian is present in scattered areas in the western part of the basin, whereas the Carboniferous and Permian are completely unrepresented. The pre-Cretaceous Mesozoic (Triassic and Jurassic) is characterized by a thin succession of rocks (where present) located in the northeastern part of the basin where it is associated with a very thin Lower Cretaceous sequence. The Lower Cretaceous is however thicker and more widespread in the south-eastern part of the basin (Sarir Trough). (Figure 2.3).

Many previous studies have been made of the stratigraphical succession in the Sirt

basin (Conent & Goudarzi.1967; Pomeyrol, 1968; Williams,1968; Conely,1971; Barr & Weegar, 1972; Clifford, Grund & Musrati, 1980; Hammuda, 1980; Van Houten,1980; Massa & Delort,1 1984; Gumati & Kanes, 1985; Butt, 1986 and others). The stratigraphical figure given below is modified by Rusk 2002

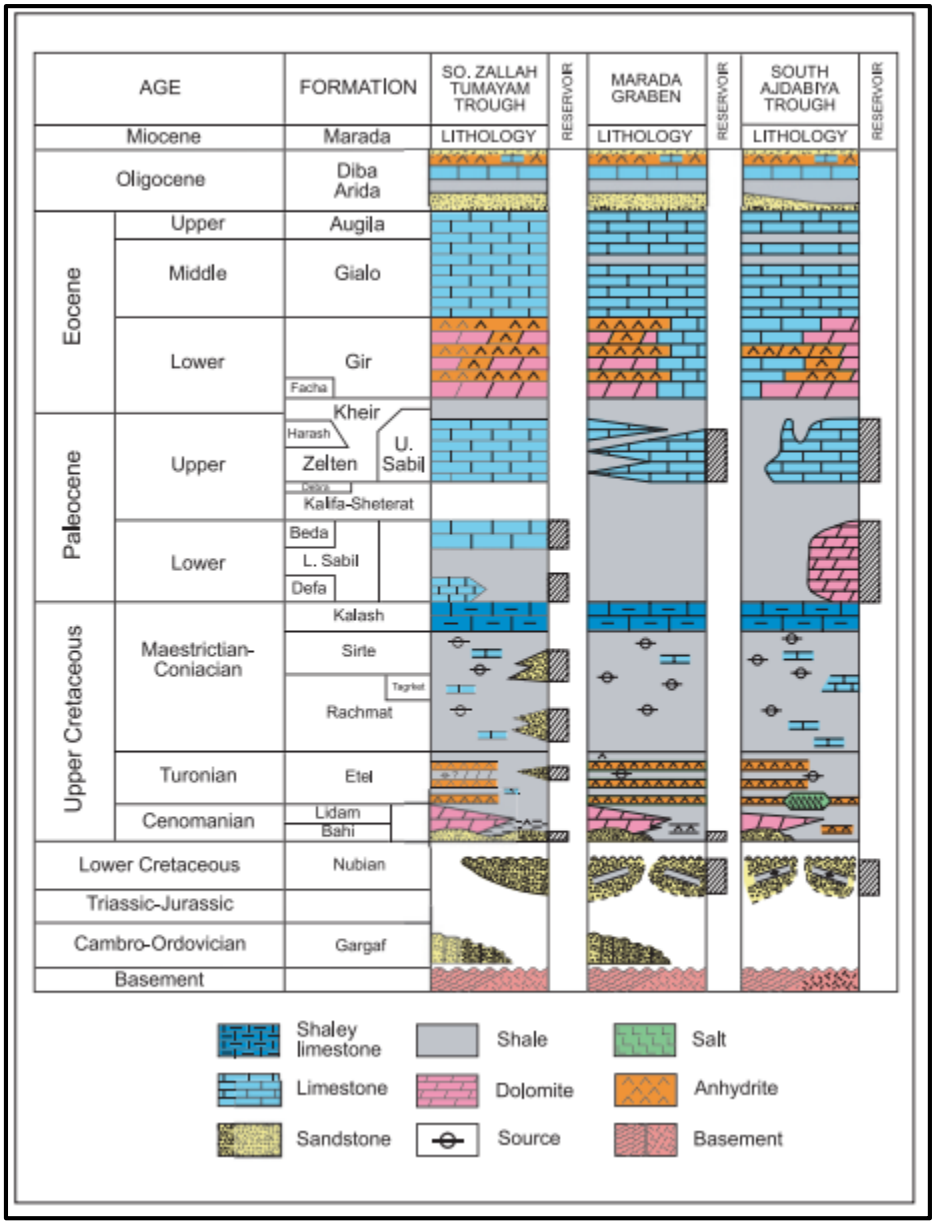

Figure 2. 3: Stratigraphic column of the Sirt Basin highlighting the lithologies of the formations, the reservoir units of the oil fields demonstrate age, formations, lithology, main reservoir-oil fields, and its tectonic events. (Rusk 2002)

Within the Sirt basin, five sedimentary sequences were dominated, which is typical of rift complex configuration. (Abadi, 2002) (Figure 2.3, 2.4 & 2.5).

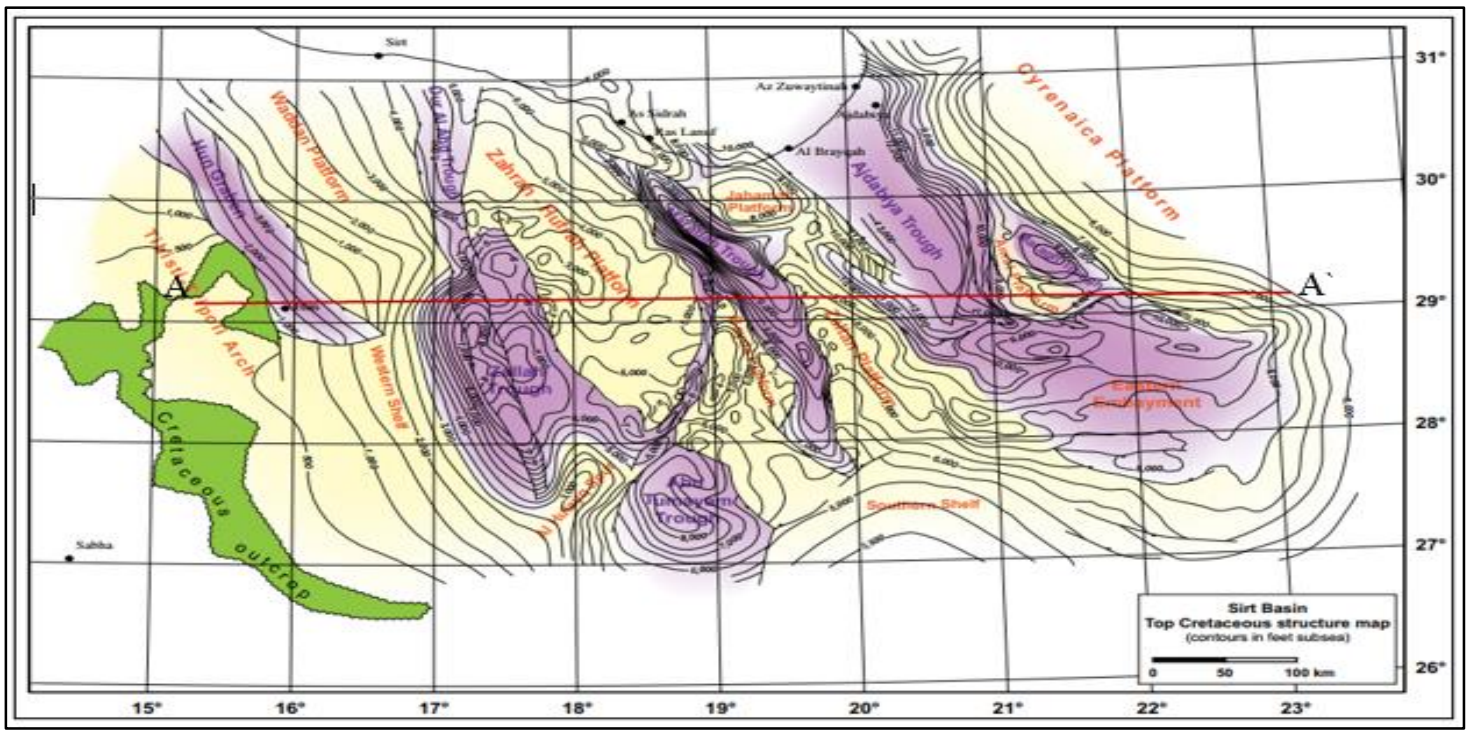

Figure 2. 4 : Regional Structure Map of Sirt Basin. Source: Nubian Consulting Ltd- Don Hallett & Clark

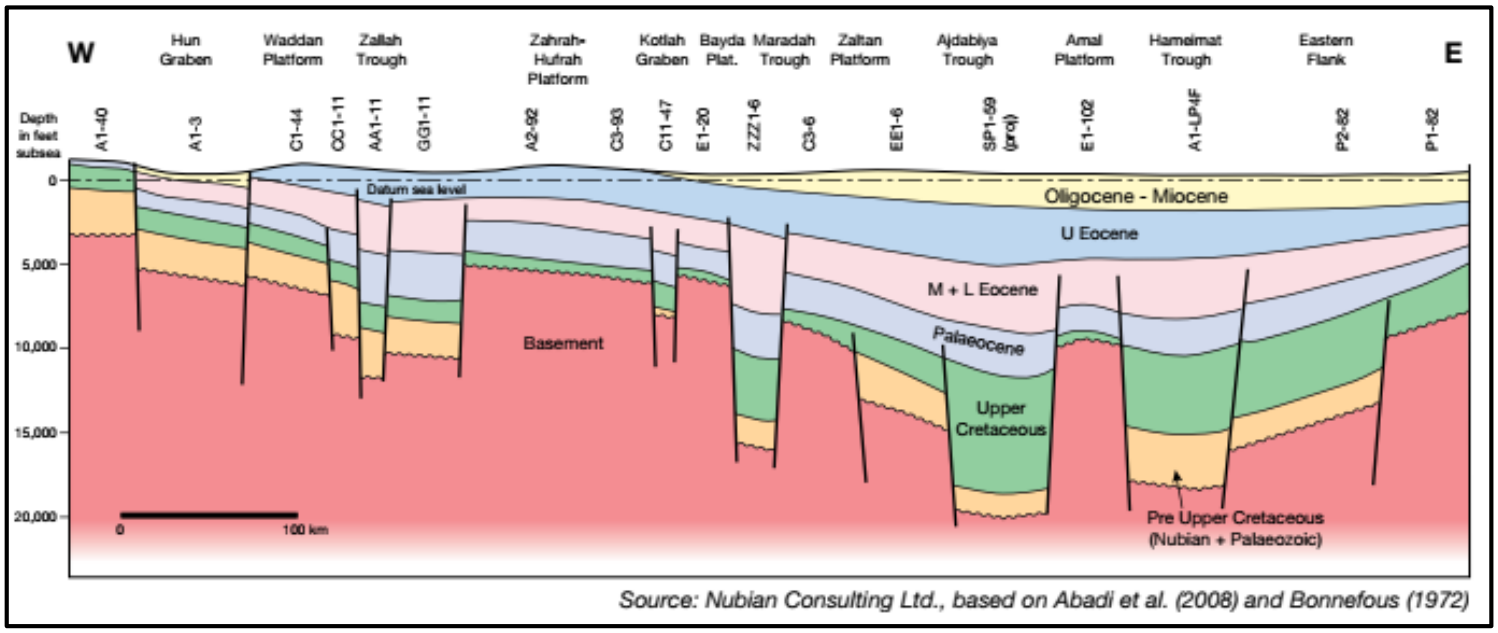

Figure 2. 5 : Sirt Basin W–E Regional Cross Section A- A` The Sirt Basin began its development in the mid-Cretaceous, following the collapse of the Sirt Arch and its fragmentation into a series of horsts and grabens.

2.3.1 Pre-Rift Sediments (Paleozoic to Triassic)

The Hofra Formation represented the pre-rift units of Cambro-Ordovician deposits, which consist of quartz sandstone with a small amount of shale, siltstone, and conglomerate (Barr &Weegar, 1972).

2.3.2 Syn Rift Basin Fill I (Late Jurassic - Early Cretaceous)

The Nubian sandstone represents the early syn-rift of Late Jurassic to late Cretaceous, with non-marine deposits, which consist of sandstone, siltstone, and shale and conglomerate (Barr &Weegar, 1972). The Nubian sandstone uncomfortably (Hercynian unconformity) overlies basement rocks or lower Palaeozoic formation.

2.3.3 Syn Rift Basin Fill II (Palaeogeon)

The Bahi Formation is characterized by Upper Cretaceous deposits in the North West Sirt basin, ranging from Cenomanian -Danian, which consists of interbedded sandstone, siltstone, conglomerate, and shale (Barr &Weegar, 1972).

The Maragh Formation was deposited at the same time in the eastern part of Sirt Basin that consists of sandstone, conglomerate, shale with minor carbonate, representing a transgressive cycle.

The Lidam Formation (Sirte Unconformity) represents the Upper Cretaceous shallow marine deposits and mainly consists of dolomite with mixing sand. It unconformably overlies the Bahi Formation, Nubian Formation, or Paleozoic and basement rocks. The Rakb Group consists of three formations, the Argub Carbonate, the Rachmat Formation, and the Sirt Shale in the North West (Barr &Weegar, 1972).

The Argub carbonate represents Turonian marine deposits, which consist mainly of dolomite with interbedded limestone and thin sandy strings. The Rachmat Formation

represents Coniacian to Santonian deposits consisting mainly of shale with minor limestone, sandstone, and inter-bedded dolomite (Barr &Weegar, 1972).

The Sirt Shale represents the Campanian deposits and consists of a shale sequence with thin limestone interbed (Barr &Weegar, 1972). The Kalash Limestone represents the Maastrichtian deposits and consists of argillaceous calcilutite with some interbeds of calcareous shale (Barr &Weegar, 1972).

2.3.4 Syn Rift Basin Fill III

2.3.4.1 Paleocene Sediments

The Hagfa Formation represents an open sea environment of the Danian deposits which is occurred throughout the central and western Sirt Basin.

It consists of shale with thin limestone interbeds. The upper member of the Satal Formation represents Danian deposits, consisting of fine-grained calcarenite in association with calcilutite (Barr &Weegar, 1972).

The Beda Formation is occurred in the southwestern part of the Sirt Basin and represents the Selandian deposit. It mainly consists of interbedded limestone lithofacies with subordinate dolomite and calcareous shale. This Formation becomes shalier in the basin's northwestern corner, indicating deposition in a shallow marine environment (Barr &Weegar, 1972).

The Khalifa Formation is located in the subsurface of the western and central basin and represents the Selandian-Thanetian deposits which consist mainly of argillaceous limestones which were deposited in shallow marine environments. In the upper part of the formation, the shale sequence was deposited in open marine environments in the southern part of the basin. The Jabal Zelten Group represents the Thanetian deposits

and it is composed of two formations, the Zelten Formation in the southern part and the Harash in the northern part of the basin. The Zelten Formation consists mainly of limestone with amounts of shale, and it is widespread in the western and central parts of the basin. The Harash Formation consists mainly of white to brown argillaceous calculatite and muddy calcarenite with thin interbeds of calcareous, fissile shale in the lower part of the formation, and it is located in the western and central section of the basin (Barr &Weegar, 1972).

The Khier Formation represents the Thanetian deposits which are characterized by open marine environments and consist mainly of shale with some clay, marl, and limestone.

In Eocene strata, the Gir Formation represents the lower Eocene deposits, and it is composed of three members. The Fasha Member consists of massive dolomite with a minor amount of anhydrite in the western part of the basin. The Hon Evaporate Member consists of a sequence of interbedded anhydrite and dolomite with minor shale in the western and central section of the basin, and the Mesdar Limestone member is characterized by open marine environments and consists mainly of massive limestone with thin beds of shale and dolomite in the central and eastern part of the basin (Barr &Weegar, 1972). The Gialo Formation represents the Middle Eocene deposits, which are characterized by shallow to open marine environments. It consists of a thick sequence of shallow marine limestone and is located in most of the basin except the northern part of the basin where the Gedari Formation was deposited (Barr &Weegar, 1972). The Augila Formation represents the Upper Eocene deposits, in the southeast and south-central part of the basin. The formation is composed of three members: the lower member which is characterized by open marine environments, and consists of soft shale with thin argillaceous limestone or dolomite interbedded, the middle member consists of soft, porous, glauconitic quartz sandstone, and the upper member which

characterizes shallow marine environments, and consists of hard, sandy, slightly glauconitic limestone. The upper part of the formation is unconformably overlain by the sandstone of the Arida Formation (Barr &Weegar, 1972).

2.3.4.2 Oligocene Strata

The Najah Group represents Oligocene deposits, located in the eastern and central of the basin: with the Arida Formation as a lower formation and Diba as an upper formation. The Arida Formation is located in the south-central part of the basin, subdivided into a lower unit which consists mainly of sandstone, and an upper unit consisting of shale. The formation represented a rapid change in the environment of deposition from continental sandstone in the southeast to carbonate to the north. The

Diba Formation consists of an alternating sequence of thick fine coarse sandstone units and thin soft shale and is located in the south-central part of the basin (Barr &Weegar, 1972).

2.3.5 Post Rift Basin Fill (Miocene)

The Maradah Formation represents the Miocene deposits, and consists of multiple lithofacies including interbedded shales, sandstone, sandy limestone, and calcarenites the formation contains several rapidly changing facies which represent an interfingering of various continental, littoral, and shallow marine environments (Barr &Weegar, 1972).

2.4 Tectonic history of Sirt Basin

The Sirt Basin covers an area of 600000 km^2 in central Libya. The basin is characterized by basin fill, which is Mesozoic and Cainozoic in age, and by the presence of platforms and deep Trough s. The main rift phase of the Sirt Basin began in the Cenomanian with the collapse of the Sirt-Tibestiarch. Five major grabens formed (Hun, Zallah, Maradah,

Ajdabiya, and Hameimat) which are separated by four major platforms (Waddan, Zahrah-Bayda, Zlatan, and Amal-Jalu) as shown in (Figure 2.6).

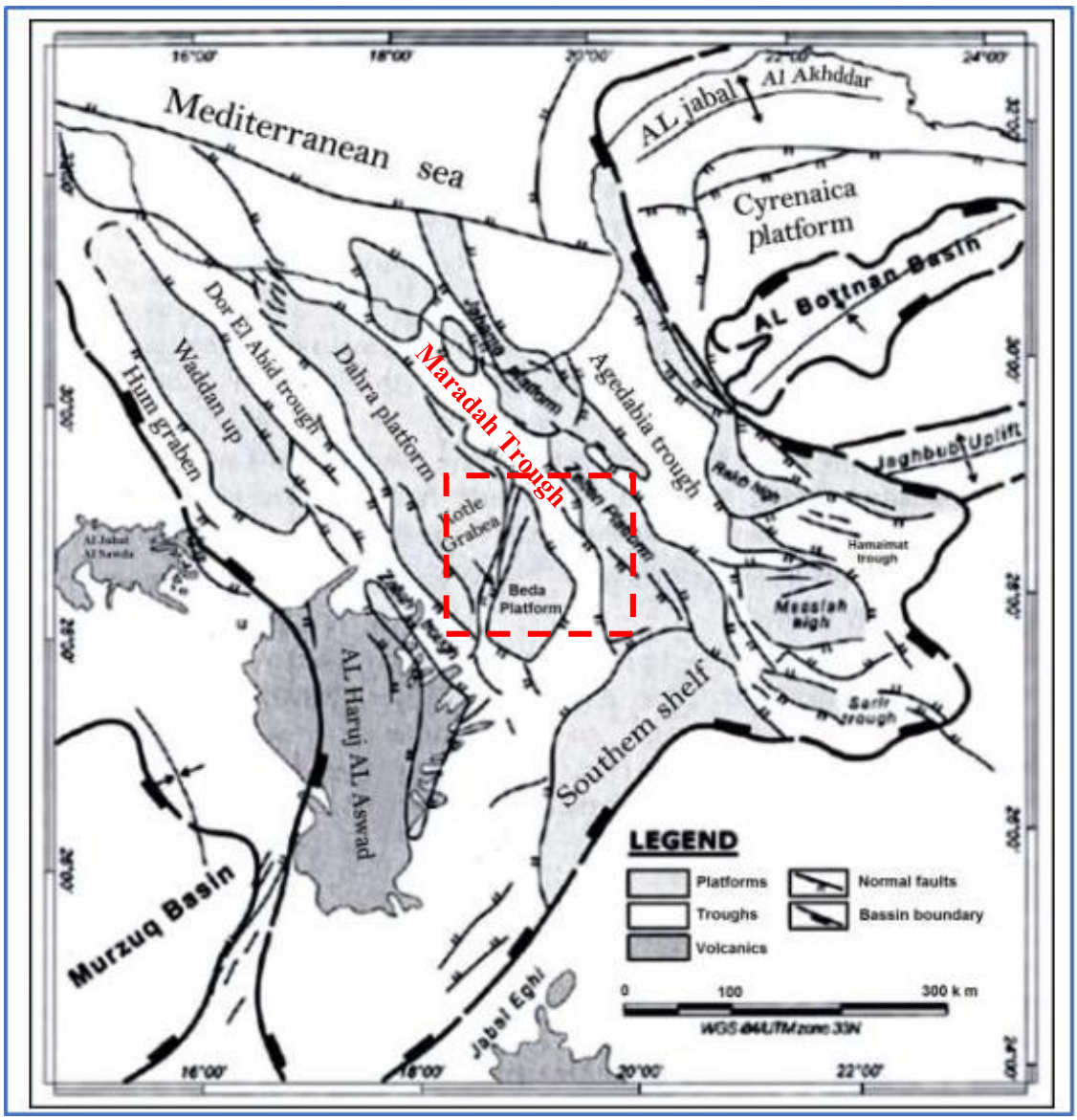

Figure 2. 6 : Tectonic map of Sirt Basin, Grey areas represent volcanism, thin lines major lineaments (Abadi, 2002) red rectangular represent the study area.

These structural features have great significance for the hydrocarbon migration from Trough s along the basement faults to platforms where most of the oil fields are known.

In the northwest of the basin main structural features orientation is generally northwest-southeast, in the eastern part of the basin it is east-west, and in the southwest part it is north-northeast south-southwest, this means that the basin may be related to a triple

junction, but the timing of tectonic activity in the eastern arm is not consistent with a triple junction (Barr &Weegar, 1972; Gumati&Kanes, 1985).

During the Late Cretaceous and Paleocene, a great thickness of shale and subordinate carbonates and evaporates accumulated in the Trough s, while a considerably reduced thickness of dominantly shallow marine carbonates was deposited on the platforms (Barr &Weegar, 1972; Gumati&Kanes, 1985).

The sedimentary succession of the Sirt Basin reflects its tectonic and structural evolution, which is related to the opening of the Atlantic Ocean and to the convergence of Tethys in Mesozoic and Tertiary times (Gras &Thusu, 1998).

The Sirt Basin developed following a sequence of tectonic events that led to the breakup of Pangaea. The breakup history of the Gondwana part of Pangaea commenced with the Late Carboniferous and Permian development of the Neo-Tethys and the development of rift systems in Gondwana (Ziegler, 2001).

Conant and (Goudarzi, 1970; Klitzsch, 1970) were the first who clearly explained the geological history and major structural elements of the Sirt Basin (Figures 2.6 & 2.7). Early in geological history, a long period of erosion prevailed throughout North Africa, and by the beginning of the Paleozoic Era, a great part of Libya had been peneplaned (Goudarzi, 1970).

Precambrian crystalline rocks are exposed in a limited and comparatively small area of south-central Libya, west of Jabal Eghi, in the Tibisti area, in the southeastern part near the border with Sudan and Egypt, at Jabal AlHasawinah north of Brak, and north of Waw Namus.

During the Cambro-Ordovician, up to 1000 m of quartzite sandstone were deposited throughout northern Libya (Anketell, 1996). Thinning of the Silurian succession across

the Sirt area, together with alkaline magmatism, presaged the uplift of the Tibisti-Sirt arch, during the Hercynian Orogeny (Klitzsch, 1996). Sedimentation continued in the adjacent basins to the east and west, while inversion of the region, together with increased igneous activity, continued during the Devonian to reach a maximum during the Perm-Carboniferous. During the Triassic-Jurassic, the eruption of basic lava accompanied post-Hercynian movements.

The Sirt Basin area remained a positive element nearly until the Latest Jurassic. The Sirt area gradually submerged, probably for the first time since the Early Palaeozoic, as a result of extension that led to the collapse of the pre-existing Sirt arch (Bonnefous, 1972; Burk & Dewey, 1974; Goudarzi, 1980; Klitzsch, 1970). (Figure 2.6) shows major structural elements of Libya, Caledonian-Hercynian and post-Hercynian volcanic, uplifts and basins.

The Sirt Basin area experienced stretching and down-faulting during Cretaceous time. Large-scale subsidence and block-faulting began in the latest Jurassic early Cretaceous. The basin underwent reactivation, both in the Late Cretaceous (Van Houten, 1983) and Paleocene time and continued into the Early Eocene (Gumati&Kanes, 1985). Volcanic activity resumed again in post-Eocene time, situated outside the Cretaceous rift at the western side of the Sirt Basin (Guiraud & Bellion,1995; Wilson, Guiraud, Moreau, & Bellion, 1998).

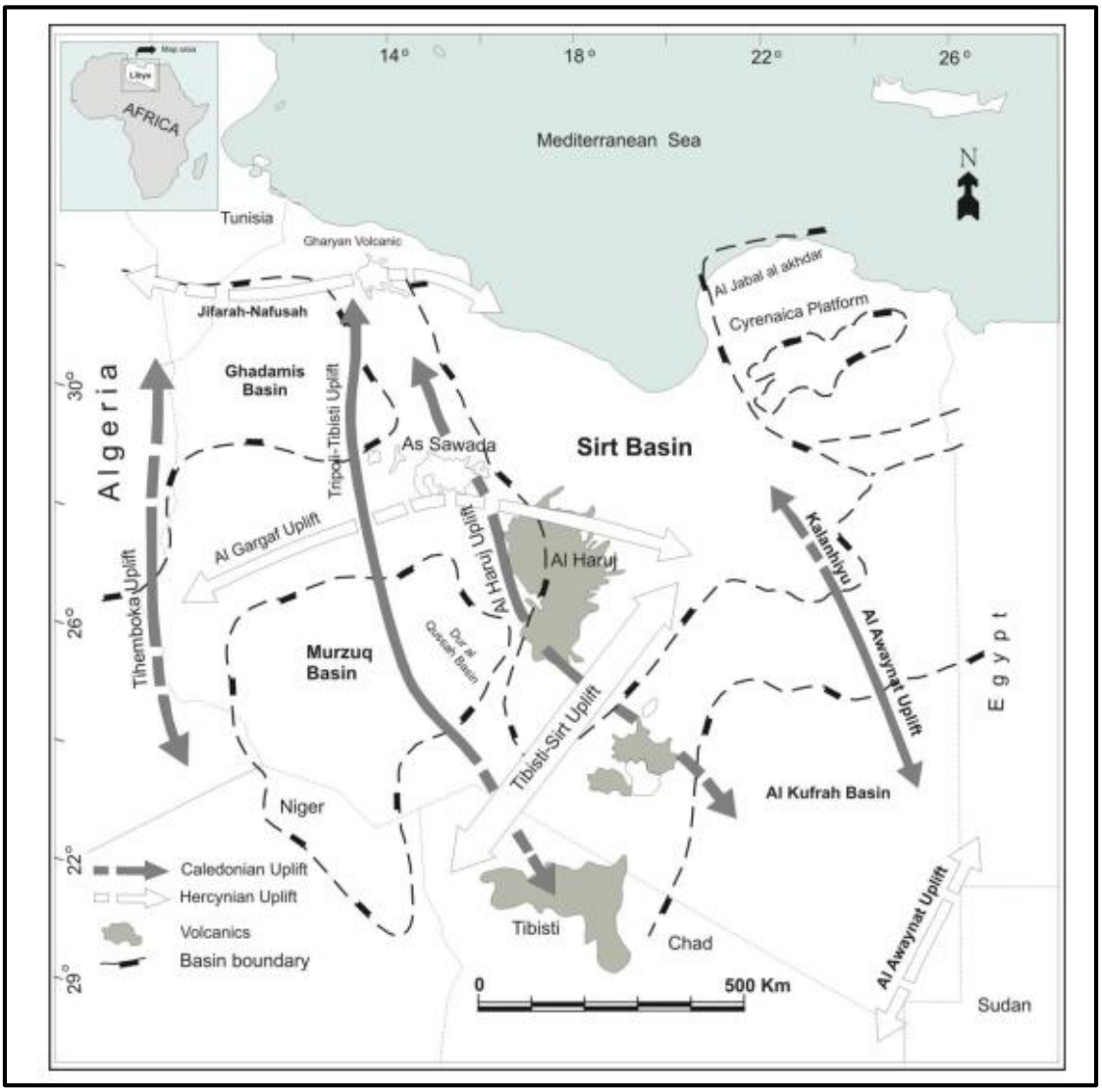

Figure 2. 7 : Major structural elements of Libya, Caledonian-Hercynian and post-Hercynian volcanic, uplifts and basins. (SWEI, 2010).

These generally volcanic episodes are believed to have been concurrent with movements along with deep-seated fractures (major basement fault zones), more likely re-activated during the Alpine Orogeny (Goudarzi,1980).

The rifting in the Sirt Basin took place along a weak zone between two African sub-plates during the Early Cretaceous (Burk & Dewey, 1974), as a result of extension that led to the collapse of the pre-existing Sirt arch as shown in (Figure 2.2). This event is attributed to the drift of the African Plate, which moved north-central Libya over a fixed mantle hotspot during the Early Cretaceous (Van Houten, 1983).

Subsidence of the Sirt Basin reached a climax during the Paleocene-Eocene according to (Gumati&Kanes, 1985) corresponding to a period of major crustal extension and reactivation of faults. (Anketell, 1996) mentioned that the Sirt Basin developed due to inter-and intra-plate movements as a result of the relative motion of the American, African and Eurasian plates during the opening on the Atlantic Ocean and the development of the Mediterranean on the foreland of the African Plate.

2.5 Structural elements of Sirt Basin

A vast amount of data is available for the Sirt Basin as a result of oil exploration activity over more than fifty years, these studies produced a thorough understanding of the basin, they all aimed to examine the fundamentals of the basin in terms of its origins and the traditions that the basin through. (Figure 2.8). Thousands of wells have been drilled, gravity, magnetic and seismic data have been acquired. As a result, the basin is far better known than any other area in Libya, although it can fairly be claimed that the deep Trough s are still imperfectly known. Within the Sirt Basin, several distinct major tectonic subdivisions can be distinguished. These will be summarized, based on available data from west to east.

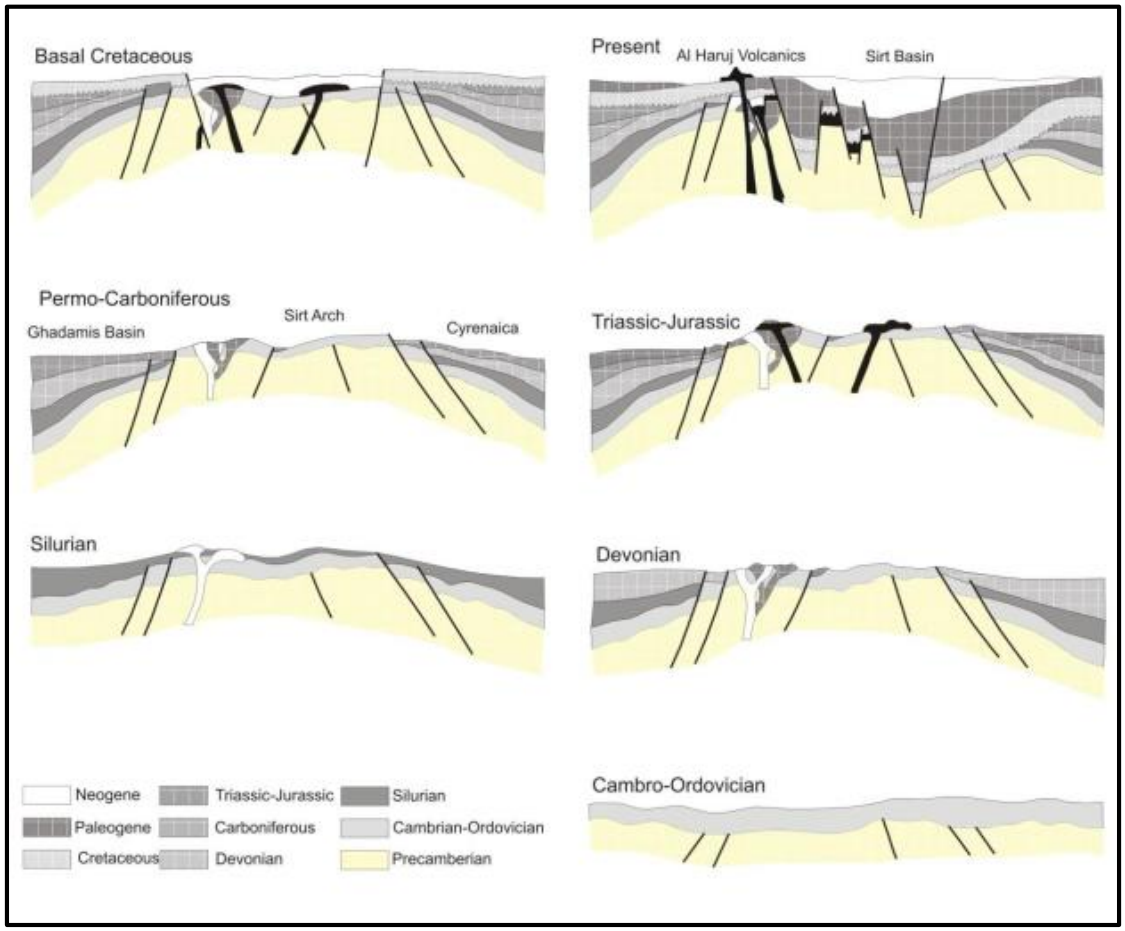

Figure 2. 8 : Structural development (E-W) of the Sirt Basin from the Lower Palaeozoic to the present time (Modified after (SWEI, 2010)).

- Hun Graben

The Hun Graben is an elongated structural feature measuring 300kmlong and averaging 40km wide, has a distinct surface expression, and forms a present-day fault-bounded depression indicating that it is one of the youngest tectonic elements in the region. The development of the Hun Graben, however, is controversial.

(Klitzsch, 1970) indicated that the Graben was downthrown 500-800mrelative to the Tripoli-Tibesti Uplift and also suggested that the graben was initiated before the Late Cretaceous and that the western margin was Paleocene in age.

(Cepek, 1979) estimated a vertical throw of 100-120m and an Oligocene age for the development of the Graben whilst (Abadi, 2002), suggested the major faulting occurring in post-Oligocene times (Figure 2.8).

- Waddan Uplift

The Waddan Uplift (Figure 2.2) is a gentle north-northeast tilted block, approximately 250 km long with a width of 105 km in the south, narrowing to 75 km in the north before it disappears below the coastal plain. The uplift terminates in the south against the northeastern extension of the Al Qargaf Arch (Figure 2.9) (Abdunaser, 2015).

The dominant fault trend is NNW-SSE with a subsidiary orthogonal set trending ENE-WSW. The northeastern margin of the Waddan Uplift is extensively faulted due to dextral shear along a WNW-ESE basement fault.

The southern end of the uplift has a convex morphology to the south and is characterized by a discrete fault-bounded margin with a down-throw to the southwest, south, and southeast. The western boundary is marked by the eastern boundary fault of the Hun Graben (Figure 2.9).

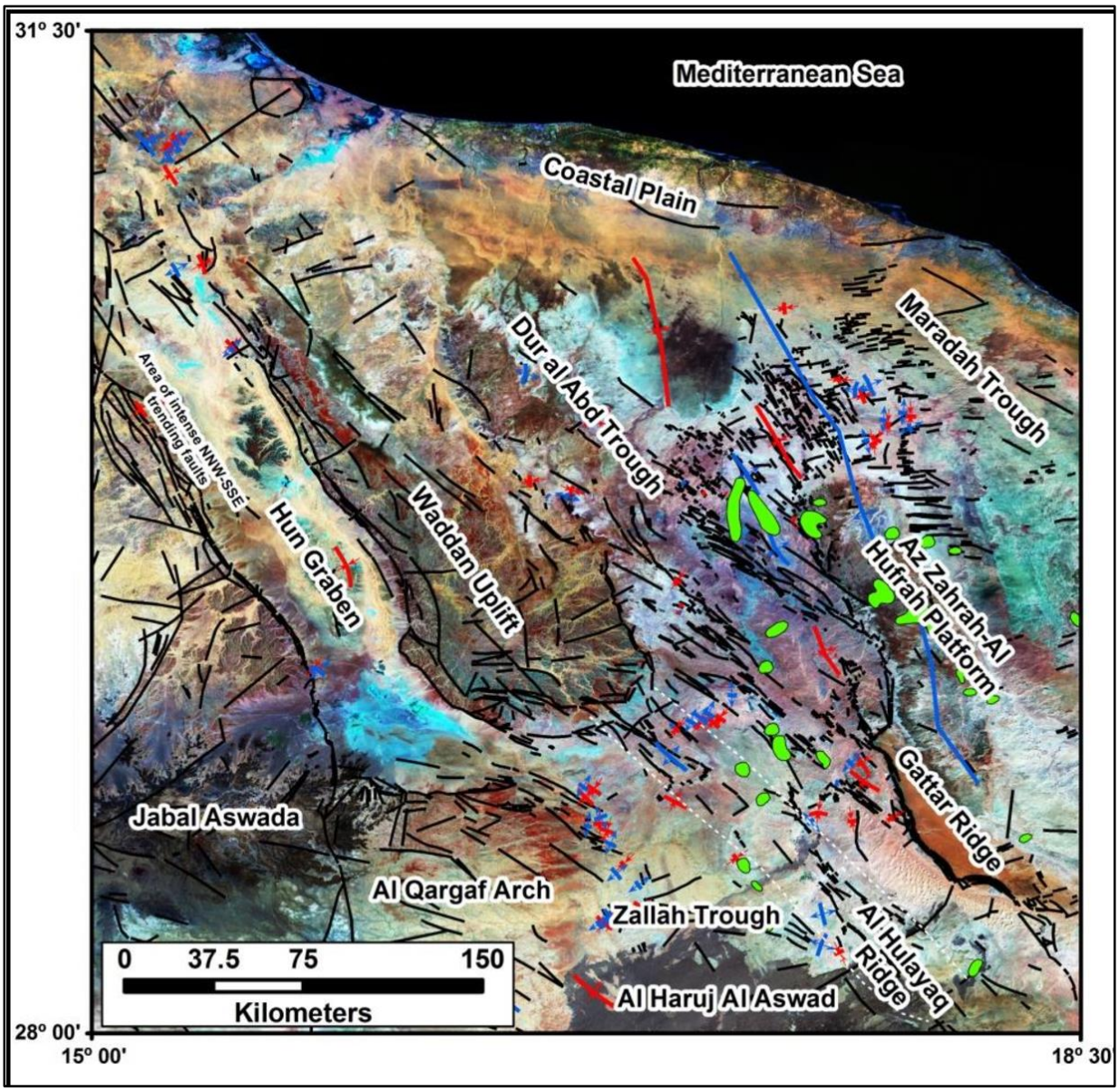

Figure 2. 9 : The Figures displays the interpreted segmented fault pattern composed of NW-SE and N-S to NNE-SSW striking fault systems that have formed at both the rift borders and within the basin. (K. Khalifa 2012)

As a general rule, the NW-SE faults (Figure 2.9) that are parallel to the major structural trend of the basin controlled the rate of rifting and subsidence whereas the NE-SW structure modifies the pattern formed by previous system to form the block structures. The topographically highest point of the Waddan Uplift is located towards the center. This area characterized is by radial drainage although the crest of the structure is marked by an NNW-SSE trending drainage divide, located some 20 km east of the western faulted margin of the Waddan Uplift (K. Khalifa 2012).

The internal structure of the Waddan Uplift is comparatively simple with an NNW-SSE trending trellised drainage pattern controlled by NNW-SSE trending, south-southwest down-throwing normal faults (antithetic to the northeast to north-northeast drainage direction).

The northern half of the platform is characterized by north and north nor the east-trending dendritic drainage pattern down the sub-horizontal dip slope of the structure. A more organized trellis drainage pattern is developed towards the northern end of the structure parallel to the NNW-SSE and ENE-WSW trending fracture system (K. Abdunaser & K. McCaffrey, 2015).

Elongate erosional escarpments of more resistant lithologies and/or fault scarps may also control linear NNW-SSE trending wadi channels. The southeastern part of the Waddan Uplift appears to be associated with a downthrown fault block which is defined by a broad low amplitude anticlinal structure developed in the Wadi Thamat Formation.

- Zallah Trough

The Zallah Trough (Figures 2.2 & 2.5) is situated in the southeast part of the study area and is an asymmetrical faulted graben that connects northwards with the Dural Abd Trough and southwards with the Abu Tumayam Trough where they appear more or less like a continuous low NW-SE trending embayment.

It is bounded by the Waddan Uplift to the northwest, the Al Qargaf Arch to the southwest, and the Az Zahrah-Al Hufrah Platform to the east, (K. M. Abdunaser & K. J. McCaffrey, 2015; Hallett & El Ghoul, 1996).

The depth to the top Cretaceous in the center of the Trough is about 7380' and to the base Mesozoic about 15748'. The upper Cretaceous is 6561' thick compared with only 984' on the adjacent platforms (K. M. Abdunaser & K. J. McCaffrey, 2015).

- Dur al Abd Trough

The Dural Abd Trough (Figures 2.2 & 2.5) represents a more or less continuous elongated low of three Trough s, including Dural Abd, Zallah, and Abu Tumayam Trough s from north to south respectively which runs from the Sirt embayment coast in the north to the southern (shelf) boundary of the Sirt Basin. Some authors believe that the Zallah Trough narrows northwards and becomes shallower to form the Dural Abd Trough (Abadi, 2002; K. M. Abdunaser& K. J. McCaffrey, 2015; Hallett, 2002).

The Dural Abd Trough separates the Dahrah -Al Hufrah Platform from the Waddan Uplift in the area of the Mabruk field and it is difficult to follow north of the Mabruk field where it loses its identity in the faulted northeast flank of the Waddan Uplift. The Dural Abd Trough is a 50km wide NW-SE trending, fault-bounded graben in the Mabruk area but broadens out further south and has the greatest fault displacement in the east. It extends approximately 175km northwards from the Facha field. The Dural Abd and Zallah Trough s seem to be in the first instance a continuous Trough that follows the NNW-SSE trending structural grain of the region, however, the data reveal a structure that acts as a bridge that separates them from each other possibly extending from northern Gattar Ridge to the southeastern part of the Waddan Uplift (ArRaqubah fault system (Abadi, 2002; Hallett, 2002).

The Dural Abd Trough is extensively faulted and characterized mainly by two fault trends, one that is parallel to the NNW-SSE dominant fault trend of the Sirt Basin and has an associated subsidiary later ENE-WSW transverse fault set and a second N-S trending fault set that are evident on the northeastern dipping flank of the Waddan Uplift and extend into the Dural Abd Trough . Displacement across the Graben bounding faults is approximately 250m. (Abadi, 2002; Hallett, 2002). Based on this surface

interpretation it is difficult to split the northern extension of Dural Abd Trough from the adjacent Az Zahrah-Al Hufrah Platform to the east.

The Mabruk field is the only field that lies within the Dural Abd Trough with the Facha field on its faulted western flank on the Az Zahrah-A Hufrah Platform.

- Abu Tumayma Trough

The Trough covers an area of about 850 km2. It had been assumed that the Abu Tumayam Trough t connects to the Maradah Trough over a structural saddle to the south of the Al Bayda Platform. The study by Hallett, 2002 provided evidence to show that most of this area is occupied by a broad horst and that any connection is likely to be very shallow.

- Dahrah-Al Hufrah Platform

The Dahrah-AlHufrah Platform is located between the Dural Abd Trough and Zallah Trough s to the west and the Maradah Trough to the east and is bounded on the south by the NNE-SSW trending Kotlath Graben which separates it from Al Bayda Platform (Figure 2.2).

The platform dips towards the northeast and its northeastern and northern boundary becomes indistinct in an area affected by wrench-faulting close to the present coastline (K. M. Abdunaser& K. J. McCaffrey, 2015). The platform occupies an area of about 40,000 km2. Depth to the top- Cretaceous ranges from about 2959' on the western margin near the Dahrah field to 5250' further north, and the thickness of the Upper Cretaceous is about 984'. The depth to the base of the Mesozoic strata ranges from about 4265' in the south to 6560' in the north (Abdunaser, 2015).

Depth to the top Cretaceous varies from 9842' in the center of the basin to 6561' in the north and south. Upper Cretaceous sediments are about 5905' thick in the Trough center compared with less than 492' on the adjacent Zaltan Platform. Depth to the Hercynian unconformity ranges from 15091' in the center to 11482' on the margin.

- Maradah Trough

The Mariah Trough (sometimes called the Al Hagfah Trough) is located in the northeastern portion of the study area. It is a deep fault-bounded graben extending for almost 400 km It is a narrow, NW-SE-trending basin bounding the Dahrah -Al Hufrah Platform to the west and swings to an NNE trend around the southern termination of the Al Bayda Platform and then shallows rapidly to the southeast onto the Southern Shelf (Hallett, 2002).

In the north, the Maradah Trough narrows and shallows rapidly between the Az Zahrah Al Hufrah Platform and the Shammar and An Nawfalfyah Highs. North of this it widens and deepens again towards the Sirt Gulf (Anketel 1996).

The dominant fault trend bounding the Trough is NNW-SSE with subsidiary NNE-SSW trending consistent with the Kotlath Graben and the basin southern shelf towards the south.

- Al Bayda Platform

Al Bayda Platform has NNE-SSW structural grain, More Similar to that of Al Kotlah Graben and Abu Tumamyan Trough than the Dahrah-Al Hufrah Platform Cambro-Ordovician rocks sub crop the Hercynian unconformity on the northern part of the Platform. And these rocks pinch out onto Precambrian Basement in the south. Depth to the top Cretaceous is 1300 m to 1800 m and the upper Cretaceous is about 300m thick.

Depth to the hercynianub conformity is bounded by the Zallah Trough north of Barrut Arch. and by the Abu Tumayam Trough to the south. To the east, the platform has faulted margin with the Maradah Trough . The platform covers an area of approximately 3200km2 (Hallett, 2002).

- Zaltan and Al Jahamah Platforms

The Zaltan and Al Jahamah Platforms, and their northward extension, the Shammar High and the Al Nuwfaliyah High, form a series of linked platforms extending from the Dayfah Field into the offshore north of An Nuwfaliyah (K. M. Abdunaser& K. J. McCaffrey, 2015). To the west, these elements are flanked by the Maradah Trough and to the east by the Ajdabiya Trough . Southwards the Zaltan Platform merges with the Southern Shelf. Depth to the top Cretaceous is 5413' at the Dayfah Field to 8694' Hutaybah. The thickness of the Upper Cretaceous is less than 656' on the Western margin thickening to 1968' on the eastern flank. Corresponding depths to the Hercynian unconformity are 6233' and 9186' respectively.

- Ajdabiya Trough

The Ajdabiya Trough covers an approximate area of 22,500 km2 (Hallett, 2002) and extends from the coast at Al Brayqah to the Kalanshiyu High in the south. The Ajdabiya Trough is the deepest in the Sirt Basin, containing 26246' of the post-Hercynian sediments (Hallett, 2002). The Ajdabiya Trough is the main depocenter for Oligocene and Miocene sediments in the Sirt Basin, with 4921' of Oligocene and 7874' of Miocene sediments in the center of the Trough . Active subsidence has continued to the present day. Upper Cretaceous rocks reach a thickness of 7874' in the southern Ajdabiya Trough compared with 1968' on the adjacent platforms, because of its great depth.

Chapter 3

3.1 Geophysical Data

In this study, the geophysical data including the gravity and magnetic data recorded, processed, and corrected, and then the conclusion of the subsurface phenomena will be obtained using the interpretation of this surface measured data.

3.2 Gravity Data

- Gravity Data Preparation

The gravity data was obtained from Libyan Petroleum Institute (LPI), Tripoli, Libya, from a total of 8871 Gravity stations at station spacing of 700–7000 m and over an area of approximately 10000 km^2.

For gridding the data, we converted the geodetic coordinates to x-y coordinates using projection Libya 2001 and Datum International 1924. The details will be provided later. Table (3.1).

A gravity survey was carried out in Sirt Basin Libya in 2006. About 8871 gravity data points were collected by the Libyan Petroleum Institute (LPI) Tripoli, Libya, covering an area of length of 100 km and width of 100km.

Figure 3.1 shows the distribution of gravity stations over the Maradah Trough. The survey lines laid out normally orthogonal to each other to cover all the area. The gravity data were gathered at an irregular spacing due to the topography of the area and due to the difficulty of accessing some points of the survey located on private property or in sensitive areas. The smallest grid spacing was 500 meters and the largest was approximately 1 km. The maximum gravity value is -2mGal, the minimum value is -33 mGal, and the generally negative values suggest that the applied density of 2670 kg/m3 is somewhat high, but as noted previously does not affect the pattern of anomalies.

The primary goal of studying detailed gravity data is to provide a better understanding of subsurface geology. The gravity method is relatively cheap and non-invasive.

It is also passive that is, no energy needs to be put into the ground to acquire data; thus, the method is well suited to a populated setting. The small portable instrument used also permits walking traverses.

Measurements of gravity provide information about the densities of rocks underground. There is a wide range in density among rock types, and therefore geologists can make inferences about the distribution of strata.

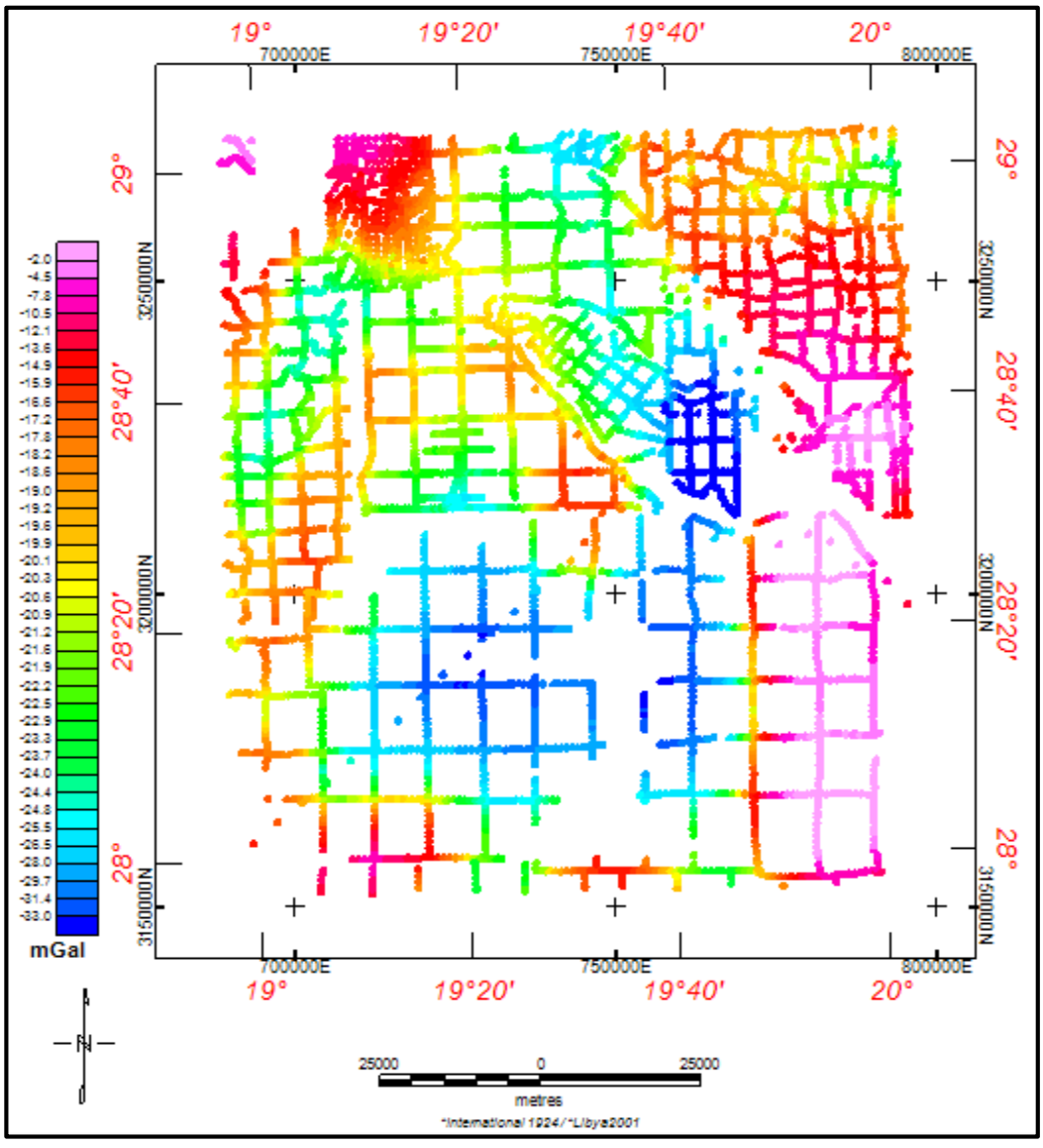

Figure 3. 1: The distribution of the gravity station location in the study area

The gravity method involves measuring the gravitational attraction exerted by the earth at a measurement station on the surface. The strength of gravitational field anomalies is directly proportional to the mass and therefore the density of crustal subsurface materials.

Anomalies in the earth's gravitational field result from lateral variations in the density of subsurface materials and the distance to these bodies from the measuring equipment, (Fig. 3.2).

For reliable interpretation of gravity anomaly, it is advisable to consult other geophysics data such as magnetic and seismic.

The general problem in geophysical surveying is the ambiguity in data interpretation of the subsurface geology. This arises because many different geologic configurations could reproduce similar observed measurements. This basic limitation is brought about by the unavoidable fact that geophysical surveying attempts to solve the difficult inverse problem.

The success of the gravity method depends on the different earth materials having different bulk densities (mass) that produce variations in the measured gravitational field.

These variations can then be interpreted by a variety of analytical and computational methods to determine the depth, geometry, and density that causes the gravity field variations.

For a better definition of the bodies causing the perturbations in the gravity field, the gravity data should be collected with small station spacing, such as 1km. For engineering investigations, this may be as low as 5 meters or less.

To further study the geological features within the Maradah, gravity data and its anomaly expressions were used and compared with the known geological features of the Maradah.

The source of used gravity data in this study is Libyan Petroleum Institute (LPI), it is a part of the Libyan Gravity Compilation Project (LGCP) that conducted by LPI 1992-2000. During which all the available gravity data from all different sources, such as National Oil Corporation (NOC), and the oil operation companies were collected and processed to produce the Bouguer Anomaly, merged into a single database and reprocessed with standard parameters.

Many gravity stations were measured and used to create a values matrix of Gravity anomaly with a (2000) m grid. Based on this grid described above the Bouguer gravity, anomaly map was built (Fig.3. 2).

3.2.1 Regional Gravity Compilation

(Essed, 1978) prepared the first compilation of the Bouguer gravity map of Libya, using data obtained from Shell Libya Oil Company, Libyan- American Oil Company, and Mobil Oil Company, He prepared the map from surveys conducted during the period from the late 1950s to the early 1960s.

These maps were tied to the gravity base section at Tripoli International Airport which has a Standard Gravity value of 979538.80 mGals. The compilation also tied Benina Airport near Benghazi which has a value of 979527.30 mGals, both of the base section values were adjusted 0 to The International Gravity Standardization Net 1971 (IGSN 71), which is 13.75 mGal less than the Potsdam datum. (Essed, 1978)

All the gravity data of Libya were compiled in 1988 nearly into a catalog by (Fairhead, 1988). The gravity map of Africa 1988 African Gravity Project (AGP) of the University

of Leeds Industrial Services was compiled from the data of academic, industry, and other sources. These data have been adjusted to the IGSN71.

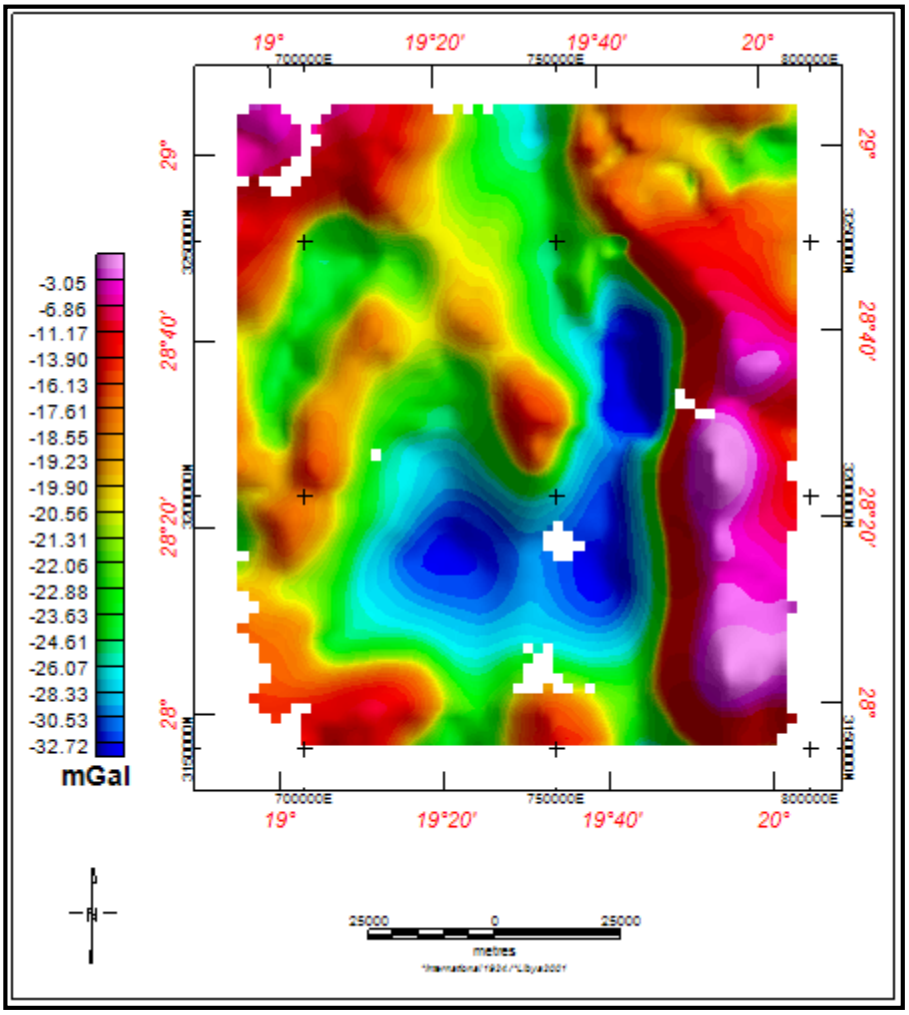

Figure 3. 2: Bouguer gravity anomaly map in the study area

In the 1988 catalog, the datum for each set of gravity data has been adjusted to IGSN71, and converted to the 1967 Geodetic Reference System (GRS67). Assuming a mean crustal density of 2.679kg/m3. The mean value of all gravity stations within each "5square" (equivalent to approximately 10X10 km) was substituted for the data before gridding.

During the period 1980, the Geodetic Survey Department of Libya (SDL) collected gravity data for all of Libya, these data have completed information (i.e., station

locations, elevations, observed gravity), which is based on the GRS67 formula (Geodetic reference system 1967).

3.2.2 Adjustment to a common datum and reduction densities

All gravity data from the (SDL) and LPI have been tied to the Geodetic Reference System 1980 (GRS 80), using the formula below (Moritz, 1980):

$g_{th}= 9.780327(1+0.0053024\sin^2\theta - 0.0000058 \sin^2 2\theta)\ ms^{-2}$

Where g_{th} is theoretical gravity in m s^{-2}(1 mGal= 10^{-5}m s^{-2}) and θ is latitude (in degrees) of the gravity station.

The Bouguer values were computed using a reduction density of 2670 kg/m3.

The data from AGP have been converted from the Gravity formula 1967 to the Gravity formula 1980, using the formula below (Moritz, 1980):

$g_{80} - g_{67}= (0.8316+0.0782 \sin^2\theta - 0.0007 \sin^4 \theta)$ mGal

Where θ is latitude (in degrees) of the gravity station and g_{80} Gravity formula 1980 and g_{67} gravity formula in 1967.

3.2.3 Projection, Gridding, and Contouring

Geosoft (Oasis Montaj) software was used for processing the Gravity data that was collected at irregular spacing. In this form, it is unsuitable for processing and contouring. For that reason, it is transformed to the grid by using the Oasis montage program based on minimum curvature surface methods (Table 3.1) (Briggs, 1974; Swain, 1976).

Projected Coordinate System (X, Y)	
X, Y channels	X, Y
Length units	Meter
Projection	Libya2001
Type	Lambert Conic Conformal (2SP)
Lat1, Lat2, Lat0, Lon0, FE, FN	17,33,0,17,500000,0
Datum	*International 1924
Ellipsoid	International 1924
MajAx, Eccen, PrimeMer	6378388,0.081991889999999998,0

Table 3. 1: Parameters of the coordinates system (projection Libya 2001) Oasis Montaj

The gridding interpolates the gravity anomaly values of the database to the square grid. The term grid refers to the files that contain the location (x,y) and data (z) gravity observation values, which are interpolated to create a regular and smoothly sampled representation of the location and data. This included Projection, Gridding, contouring, and plotting.

The data were available with latitude and longitude locations. For mapping purposes, the Lambert Conformal Conic Projection was chosen, because the longitude range straddled more than one UTM zone.

We used the minimum curvature facility within the Oasis montage software. It works well and is illustrative of the desire to honor individual data points as much as possible while realizing that gravity has an inherent smoothness due to the behavior of the Earth's gravity field. In this facility, the surface of minimum curvature is fitted to the

data points surrounding a particular grid node, and the value on this surface at the node is determined.

One can intuitively conclude that the proper grid interval is approximately the mean spacing between readings in an area The minimum curvature surface technique has been applied to data using different grid cell sizes (500, 1000, 1500, and 2000 m)

(Figs 3.3, 3.4, 3.5 and 3.6). The comparison suggests that 2000 m is the best grid cell size for this study (Fig. 3.7).

Gridding of the data had to be tight enough to capture the anomaly details here the data were recorded at close spacing, without needlessly creating enormous data files. For the gravity data, we used a range of cell sizes from 500 to 2000 to obtain an optimum value. One objective is to minimize the no-data gaps marked in Figures 3.3-3.7 as (Z1) (Z2) (Z3) (Z4) and (Z5).

When changing different grid cell sizes, we close some gaps in the area and the other gaps are closing (Fig. 3.7).

The trend continues, with extrapolation and interpolation gradually closing the no-data gaps as the cell size increases, with little loss of relevant detail. There is little difference between grid cell size 1500m and 2000m (Fig 3.7). So chosen the final “best grid cell size” at 2000m, because it represents the smallest final file size, with best interpolation and no significant loss of resolution (Fig. 3.8).

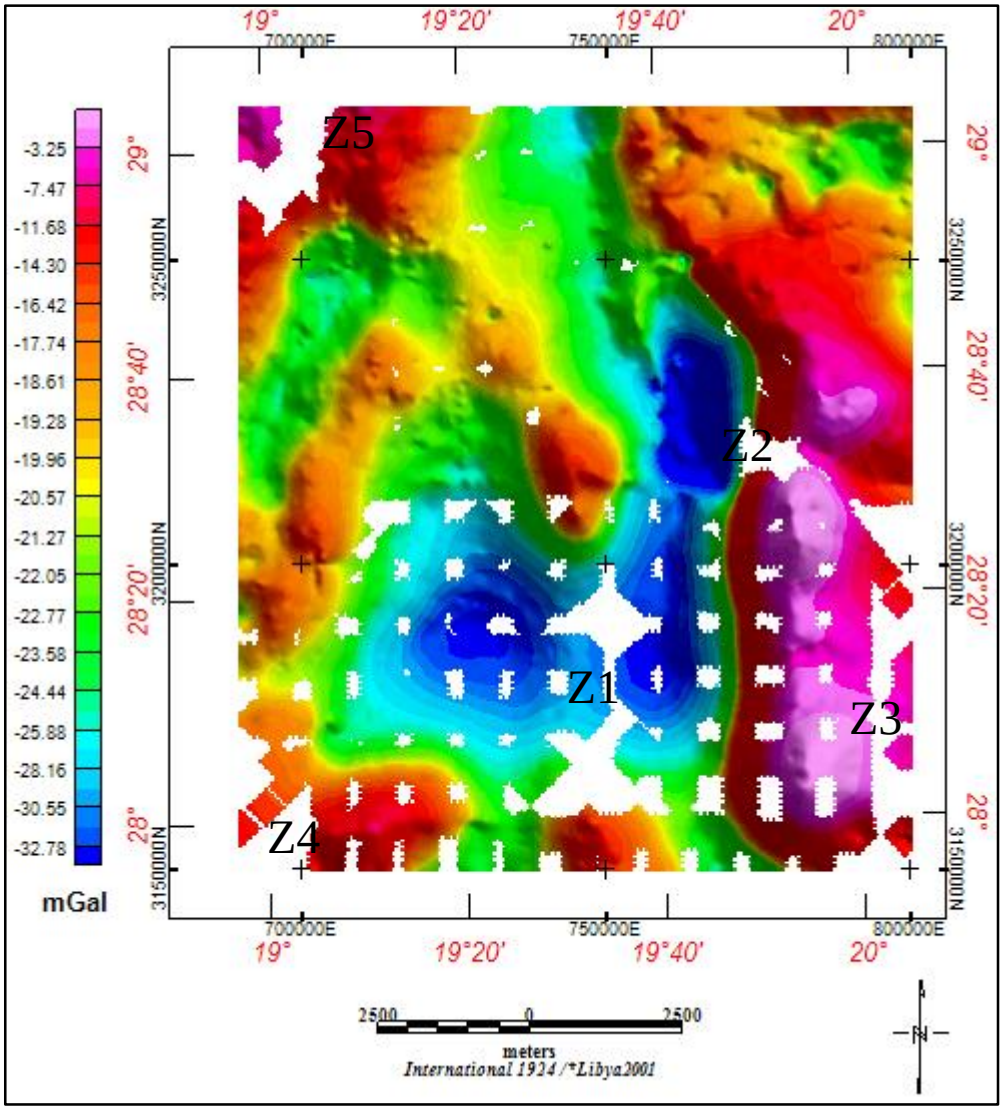

Figure 3. 3: Bouguer Gravity map in the study area with cell size 500 m we note the gap at area (Z1) (Z2) (Z3) (Z4) and (Z5)

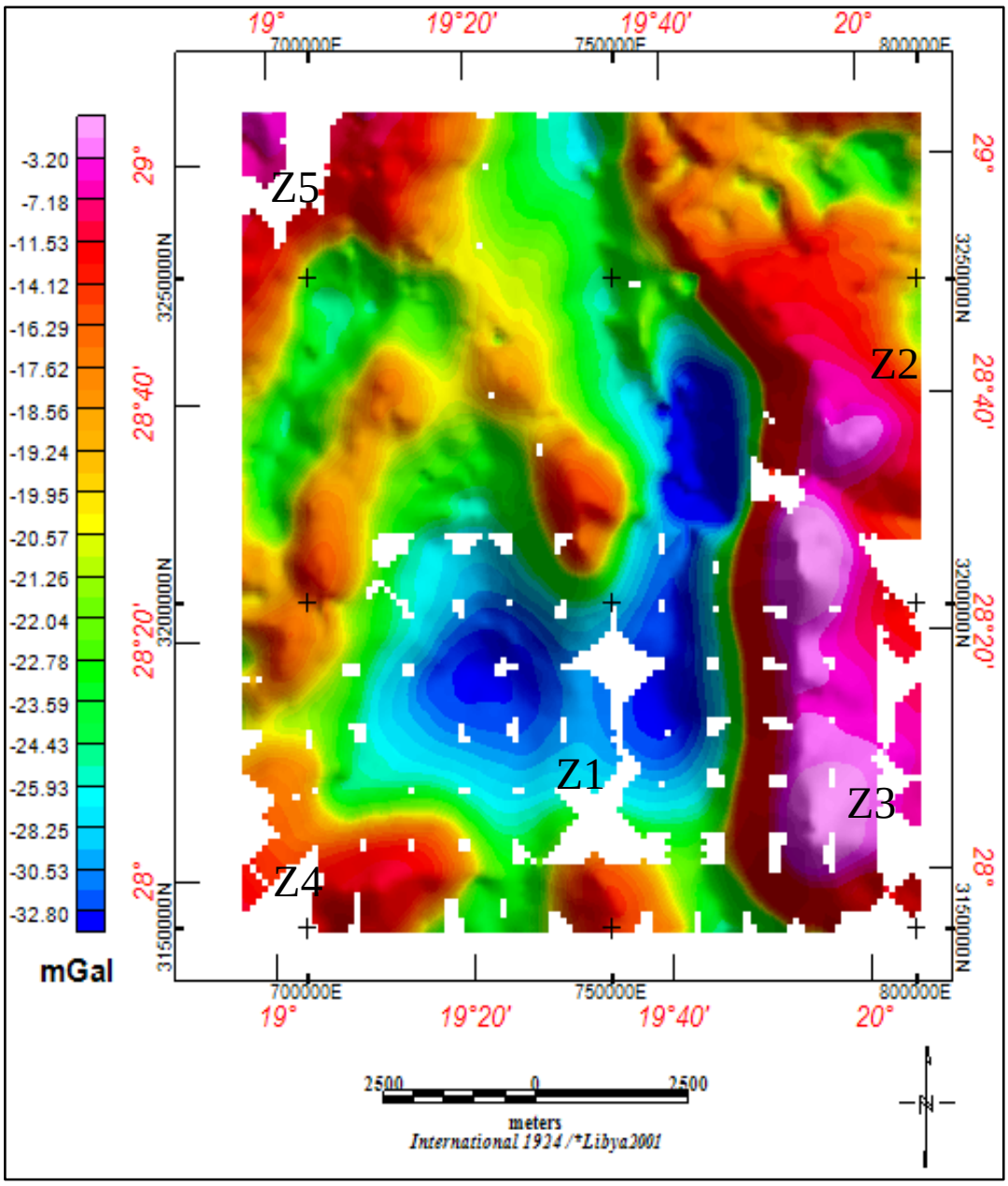

Figure 3. 4 :Bouguer Gravity map in study is with Grid cell size 1000 m

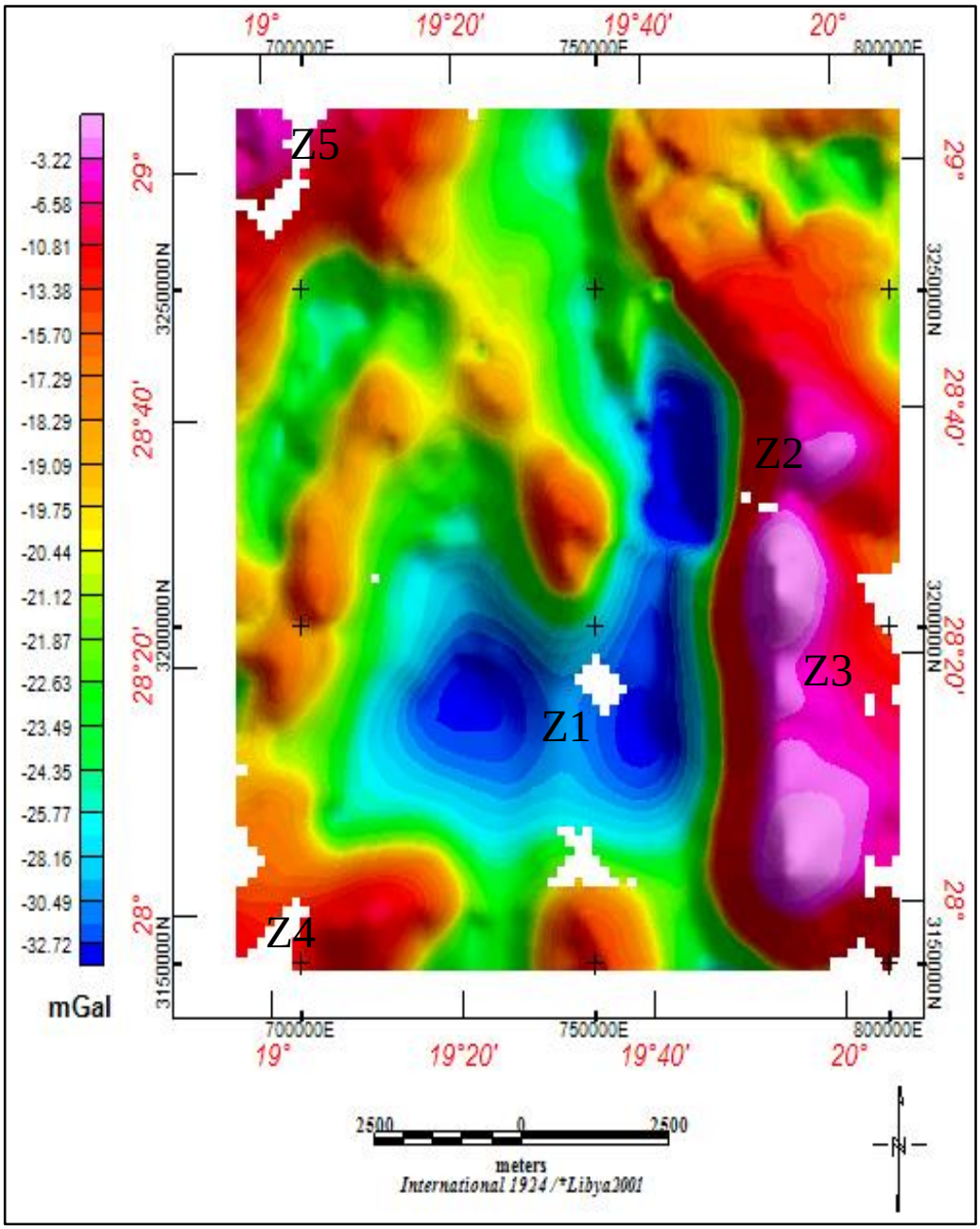

Figure 3. 5 : Bouguer Gravity map with cell size 1500 m

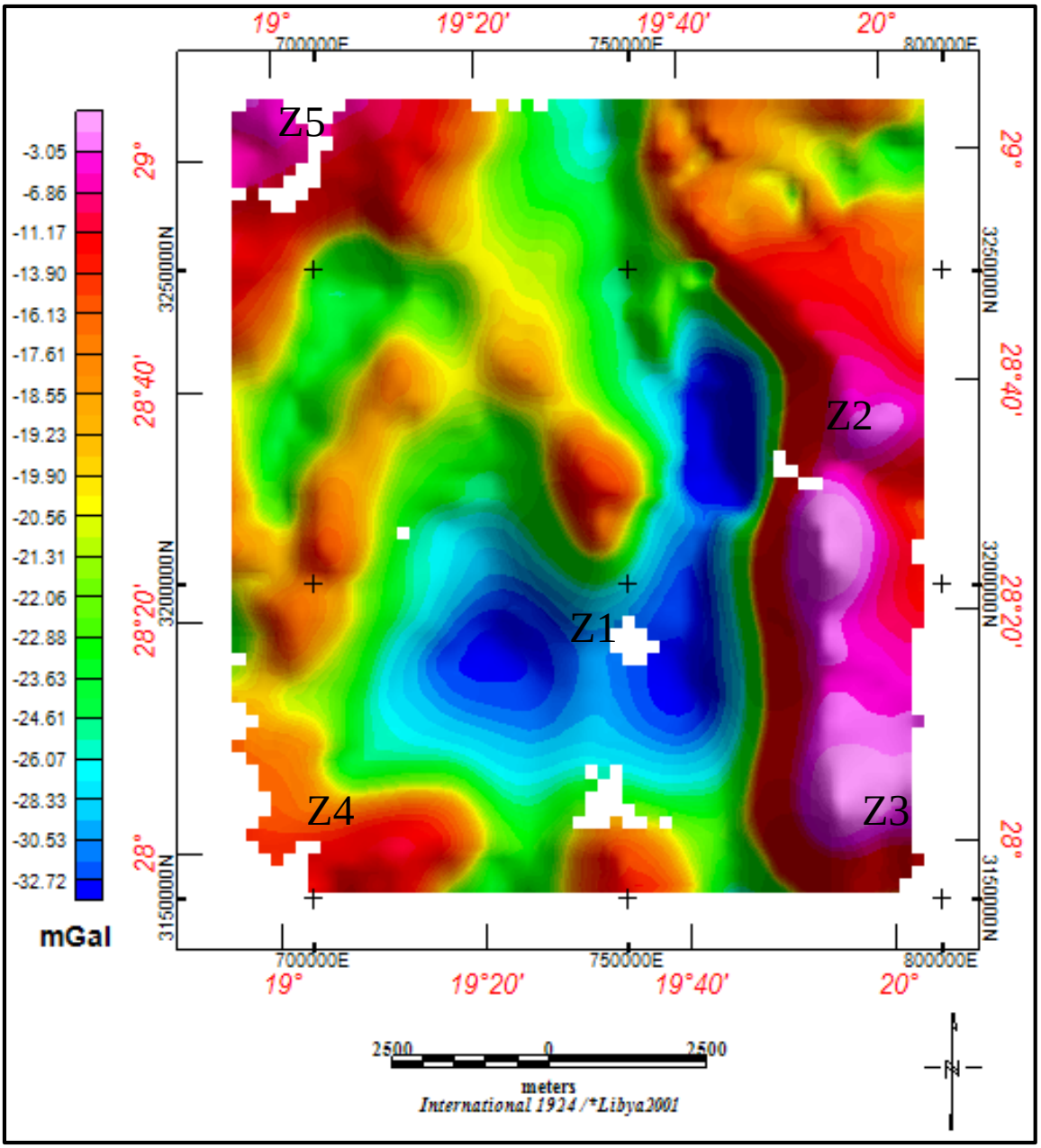

Figure 3. 6 : Bouguer Gravity map in study area with grid cell size 2000 m

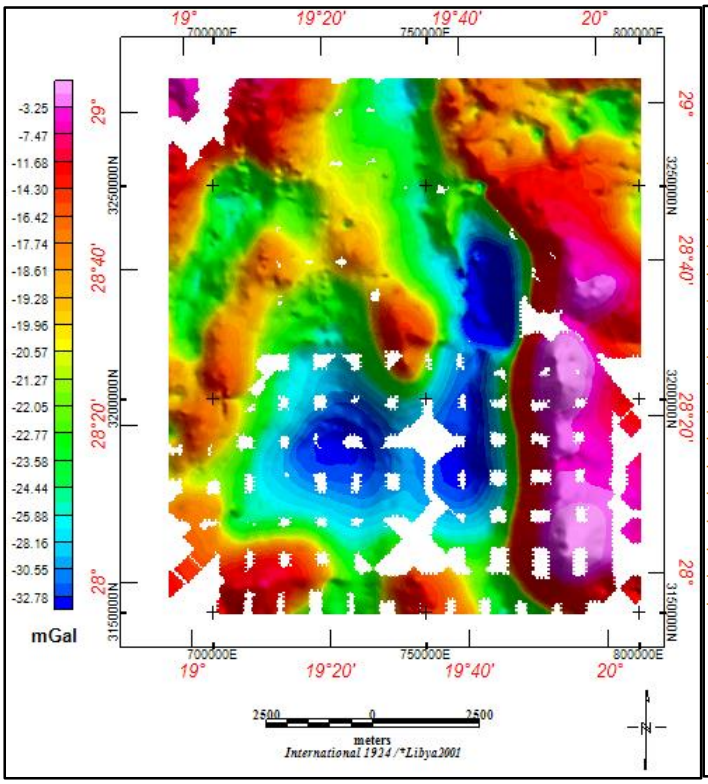

A= cell size 500m

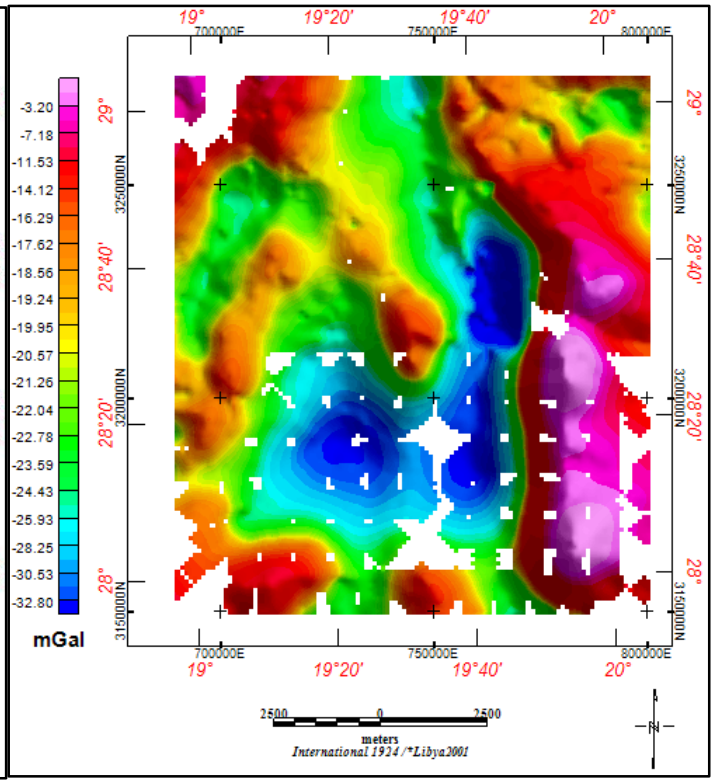

B=cell size 1000m

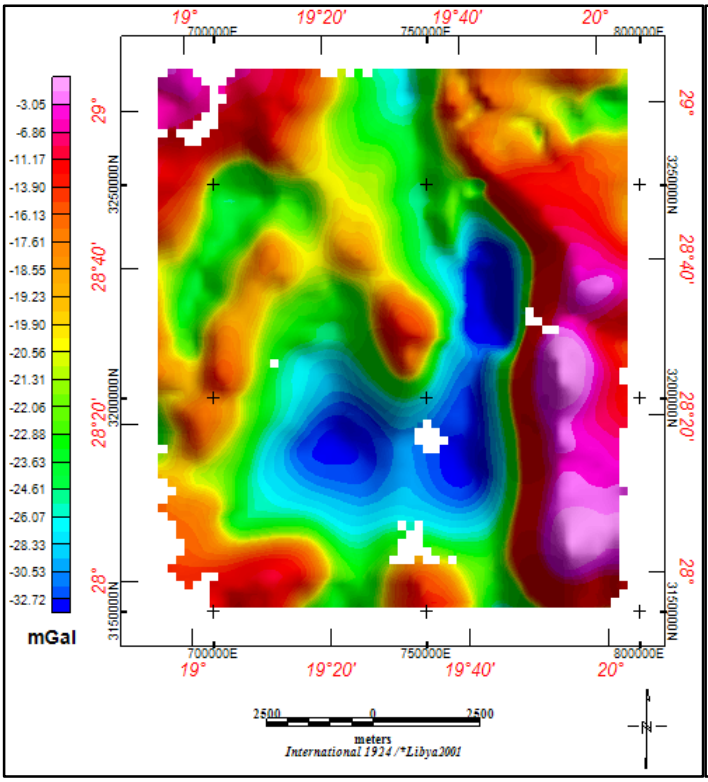

C= cell size 1500m

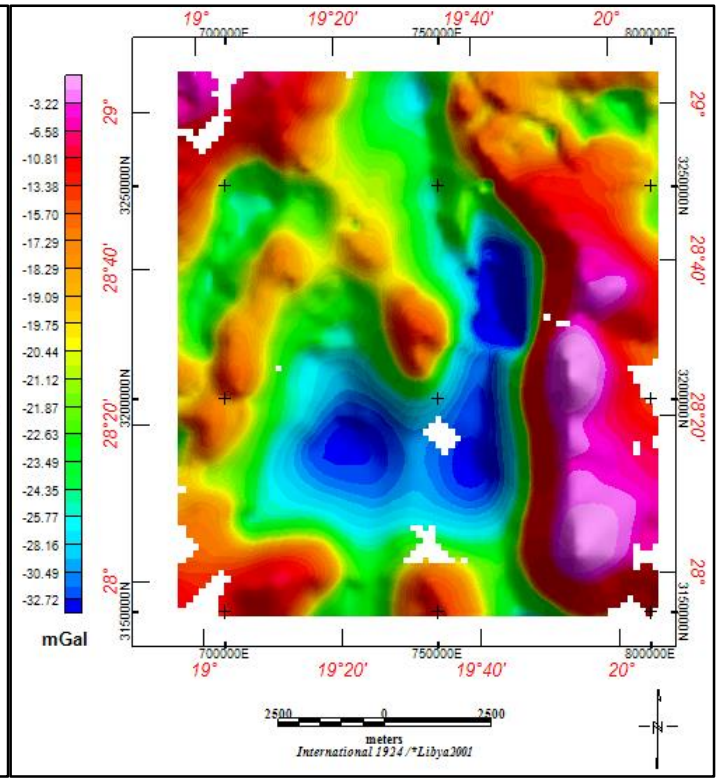

D=cell size 2000m

Figure 3. 7 : Bouguer gravity map of different grid cell size, A=500m, B=1000m,C=1500m,D=2000m

3.2.4 Bouguer Gravity Map

Gravity measurements are used to study the Earth's shape, composition, and structure. Variations in the density of bedrock and soil close to measuring points influence gravity's force in a discernible manner. This local variation of gravity can provide information about geological formations' position, shape, and structure. Measuring gravity has thus become an important method in geological mapping and exploration for mineral resources.

Total gravity is influenced primarily by the mass and figure of the Earth, local and regional topography, and centrifugal force due to the Earth's rotation.

Measured gravity values are reduced into gravity anomalies in such a way that the features under study stand out as clearly and correctly as possible.

As a result, there are several different ways to represent the measured gravity values such as Bouguer anomaly. Bouguer anomaly maps are the most common ones in geological applications, display the best subsurface density variations of basement rock.

The variations of the Bouguer anomaly can be enhanced by calculating 3rd vertical derivative, horizontal gradient or shaded relief maps. These help in perceiving, locating, delineating, and classifying geological formations and structures affecting gravity.

A sequence of gravity corrections is applied to the original gravity reading and resulting in various named gravity anomalies. The observed 69 gravity anomaly has been corrected for Earth rotation, latitude, tidal effects, local topography and gravity meter fluctuations.

The free air gravity anomaly has been corrected for the gravity effect caused by the elevation difference between the station and sea level (a correction for distance) and is a standard for oceanic gravity interpretation.

The Bouguer (*pronounced Boo-gay´*) gravity anomaly has been further corrected for the mass that may exist between sea level and the observer (a correction or mass) and is a standard used in geologic interpretation on land. A simple-Bouguer anomaly has undergone a simplified removal of topographic effects, which suffices in relatively flat areas.

A complete- Bouguer anomaly contains a terrain correction that uses a more complete representation of the local topography, which is necessary for accurate gravity values in mountainous areas.

The Isostatic (pronounced Isostatic) gravity anomaly is calculated by subtracting the gravitational effect of low-density mountain roots below areas of high topography. Gravity measurements are often processed to a complete-Bouguer or Isostatic gravity anomaly.

These data are then gridded, so that the randomly spaced data are converted to a representation of the gravity field at equally spaced locations.

Gravity anomaly maps can be shown as color figures with warm colors (reds and oranges) showing areas of higher gravity values and cool colors (blues and greens) showing lower values or as contour line maps, where each contour line follows a constant gravity value

The most of measurements were carried out by LPI. A total of many gravity stations was measured and used to create a values matrix of Gravity anomaly with a (2) Km

grid. On the basis of this grid described above the Bouguer gravity anomaly map was built (Fig. 3.8).

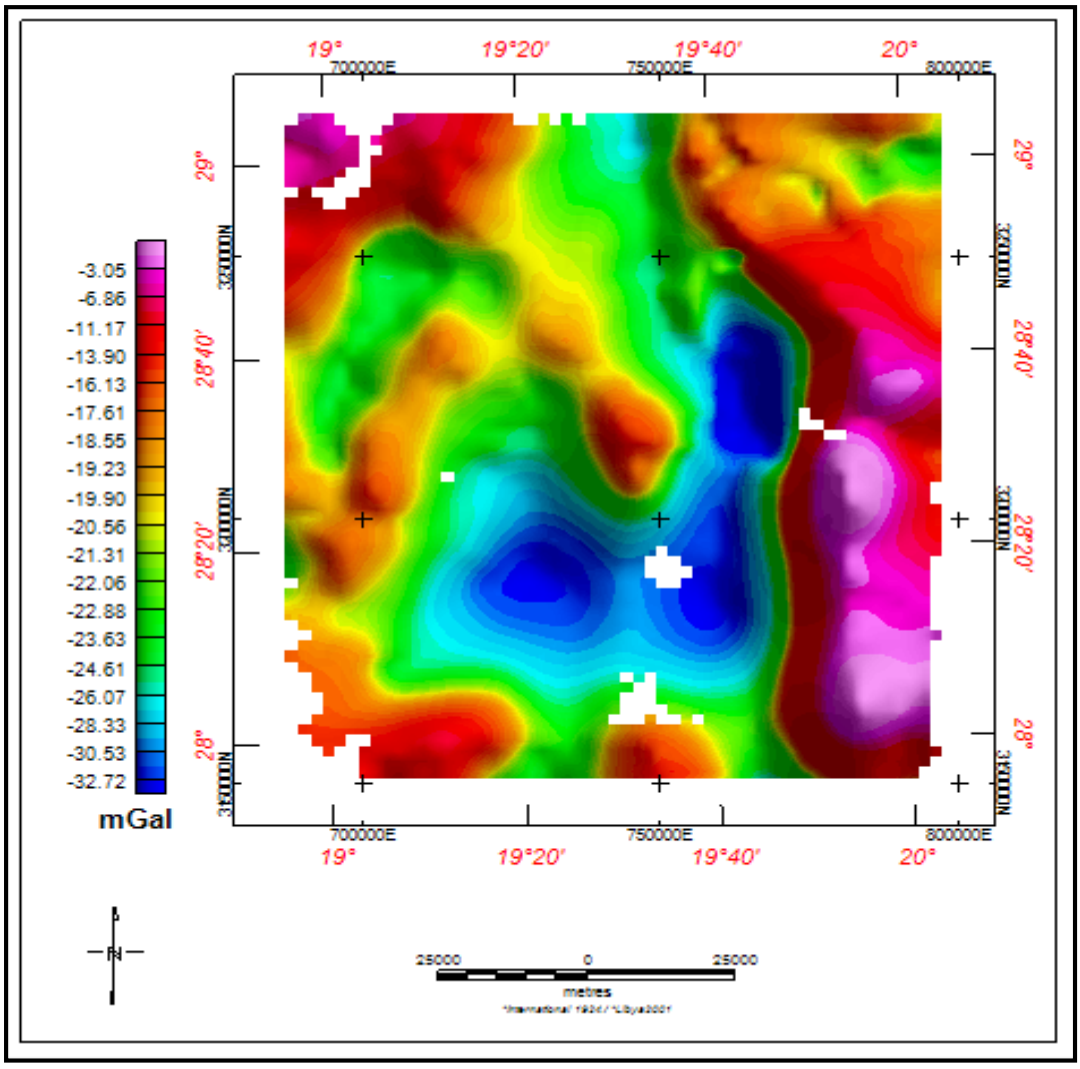

Figure 3. 8 : Bouguer gravity map of study area using Grid cell size 2000m

3.3 Gravity processing

After applying the next filtering and processing step, Bouguer anomaly maps are ready. in order to prepare the data for geophysical interpretation.

3.3.1 Filtering Techniques

The Gravity recorded at the Earth's surface is the collective effect of the sources of different levels from the surface downward to the Moho. The term filtering can be

applied to any of the various techniques that attempt to separate anomalies based on their wavelength and/or trend. In fact, fitting a low order polynomial surface (3rd order is used often) to a grid to approximate the regional as a common practice Then subtracting the values representing this surface from the original grid values creates a

Residual grid that represents the local anomalies.

- Total Horizontal Derivative

Total horizontal derivative method has been used extensively to locate the boundaries of density contrast from gravity and magnetic data (Phillips,2000) . The amplitude of the horizontal gradient (Cordell and Grauch,1987) is expressed as

$$G(x,y) = \left[\left(\frac{\partial g}{\partial x}\right)^2 + \left(\frac{\partial g}{\partial y}\right)^2\right]^{1/2} \qquad H(x,y) = \left[\left(\frac{\partial H}{\partial x}\right)^2 + \left(\frac{\partial H}{\partial y}\right)^2\right]^{1/2}$$

Where: (∂g/∂x) and (∂g/∂y) are the horizontal derivatives of the gravity field in the x and y directions. The total horizontal gradient of gravity data is calculated using fast Fourier Transform (FFT). (Cordell & Grauch, 1987) discussed the limitations of the horizontal gradient magnitude for gravity data. They concluded the horizontal gradient magnitude maxima can be offset from a position directly over the boundaries, if the boundaries are not near vertical and close to each other.

In the study area, the map of total horizontal gravity gradient anomalies was examined throughout the area. Some geologic faults are confirmed and others are delineated with more details Figure (3.32)

The horizontal derivative of potential field data is a technique used to enhance data. By taking the derivative along the x and y axis, this enhancement aims to define the anomalous body boundary and to separate with other anomalies through the relevance of analytical calculation.

- Regional and Residual of Gravity data

Measured gravity depends on Earth structures ranging from scales of 1m to 10,000 km, deeper density structures produce gravity anomalies with a long spatial wavelength. For a body such as a sphere, this would be expressed as a large value for the half-width (x½).

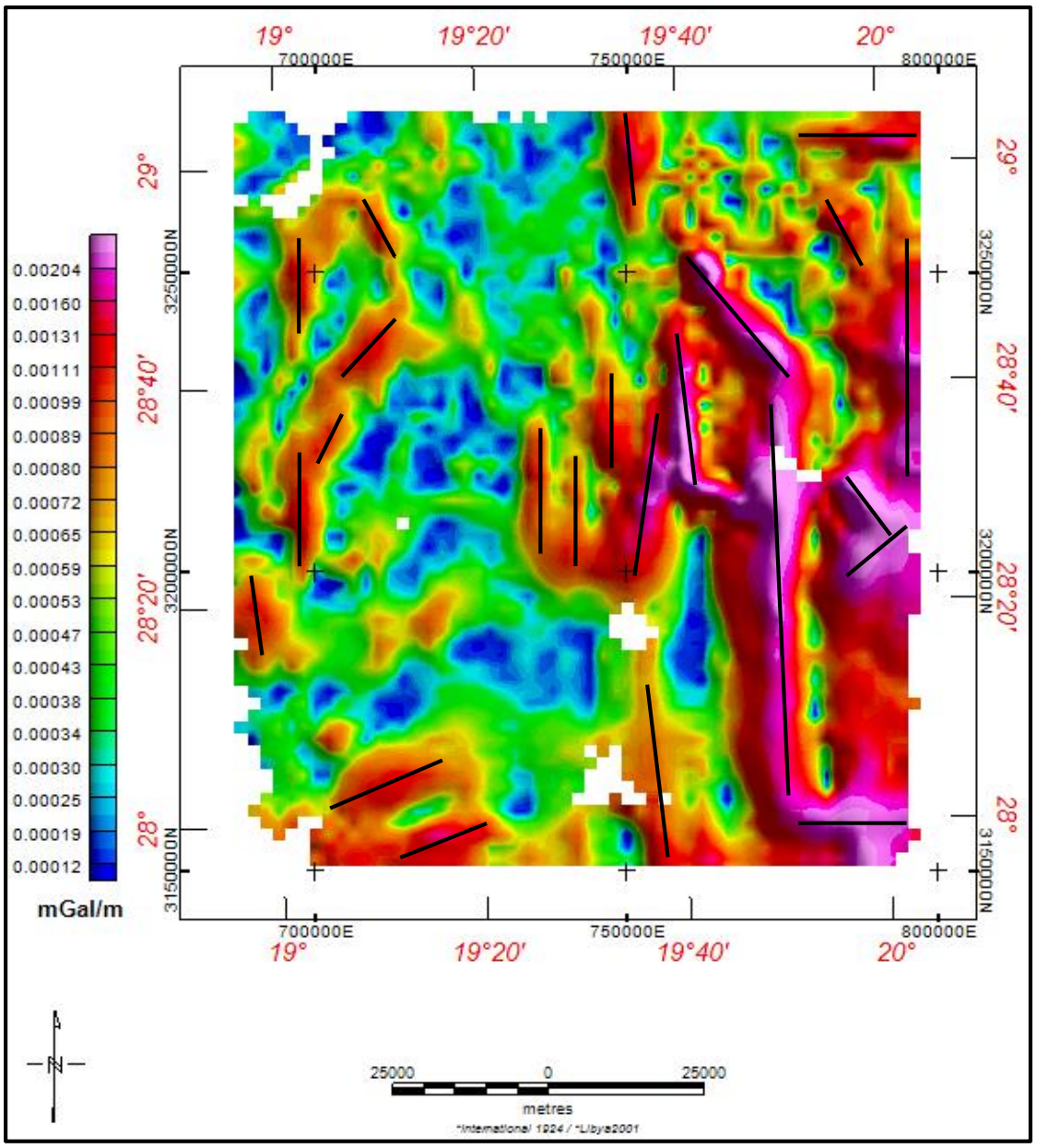

Figure 3. 9 : Total Horizontal Derivative Map of Bouguer Gravity data.

Similarly shallow density structures produce gravity anomalies with short spatial wavelengths or small half-widths.

Often the longer wavelength effects are called regional trends, while the shorter wavelength features are called residuals or anomalies. The distinction between the two is somewhat arbitrary.

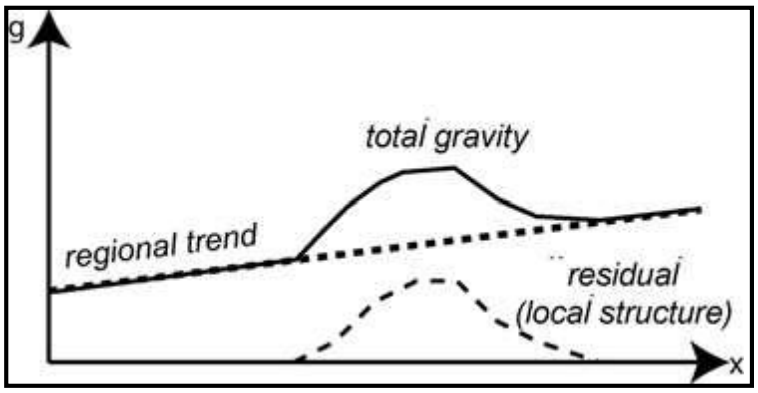

Figure 3. 10 : Regional and residuals separation

In shallow gravity exploration, we are generally interested in the short wavelength gravity anomalies. The long wavelength regional trends can make it difficult to analyses the short wavelength residuals. Thus, we need to find a way to remove the regional trends and emphasize the anomaly more clearly.

Regional trends may be computed by finding the straight line (or curve) that gives the best fit to the data. The regional trend is then subtracted from the Bouguer anomalies. However, care is needed not to eliminate useful data during this process.

Various techniques can be used to extract residuals and are effectively filtering techniques. More sophisticated analyses use formal filtering can be done after transforming to the Fourier domain.

The interesting anomalies on the gravity map frequently are masked by deep structures, which have low frequencies.

As a result, the separation between the two sources was carried out in three stages using the polynomial trend separation technique: Figure 3.11a and b_ Figure 3.13 a and b show the shape of total gravity field ؛Bouguer anomaly.

Comparing the corresponding maps, the first order regional map is adequate representations of the shallow residual gravity, whereas the similarity between the 2nd and 3rd order indicates that they are more reasonable. The 3rd order separation has been chosen and it will be accepted for further subsurface interpretation in the area (Figure 3.15) as it identified the target subsurface structures better than the Bouguer anomaly map, allowing a more quantitative interpretation.

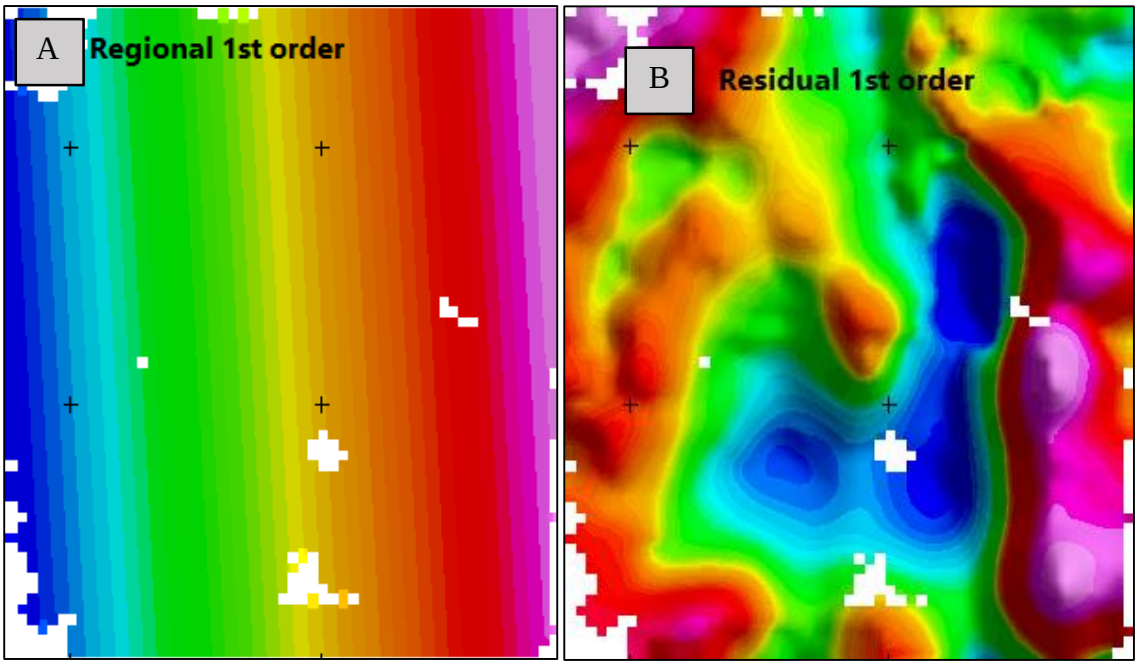

Figure 3. 11 : A and B: First-order Regional-Residual separation.

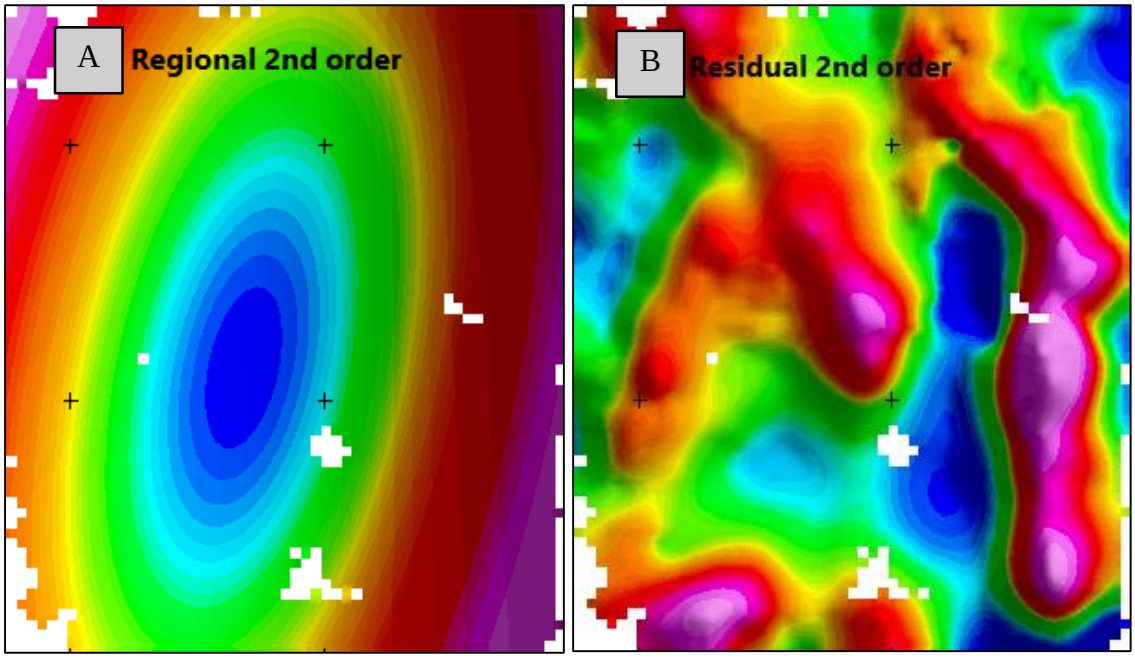

Figure 3. 12 : A and B: Second-order Regional-Residual separation

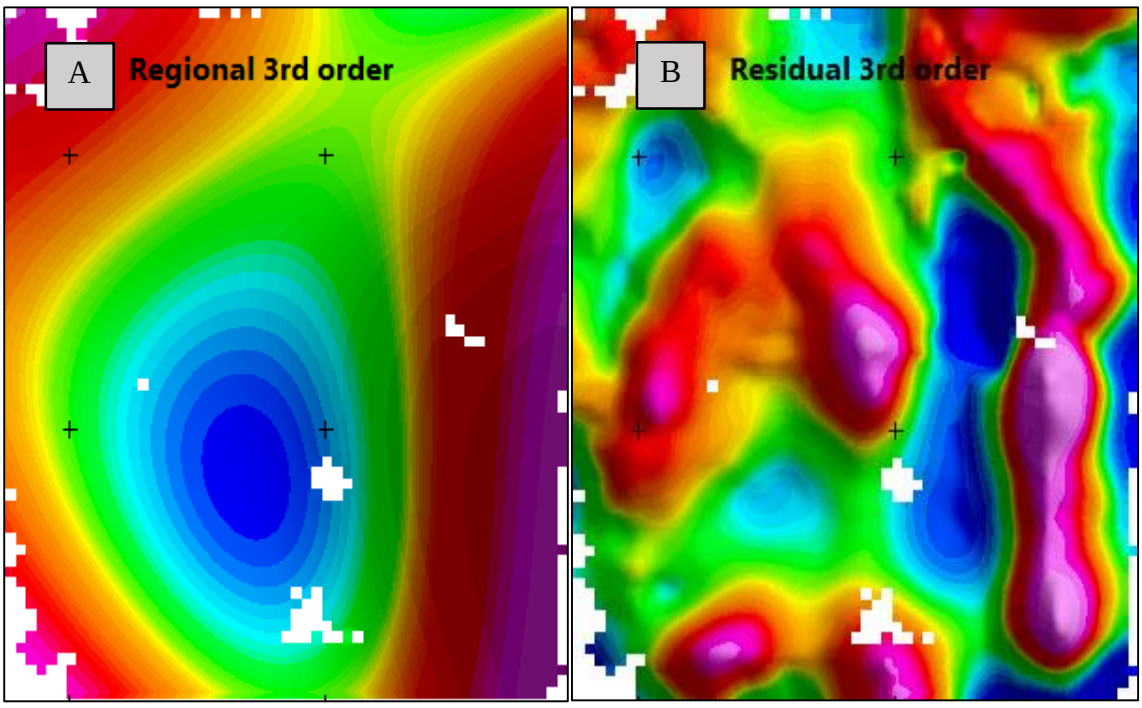

Figure 3. 13 : A and B : Third-order Regional-Residual separation.

- Residual Gravity Map

The residual gravity map corresponds to short wavelength fields of shallow bodies. The residual gravity map showed anomaly ranges from -15.39 to 18.44mGal. The distribution of anomalies is similar to the Bouguer anomaly map.

The residual map is dominated by a group of trends of high (positive) gravity, with intervening low (negative) gravity anomalies thought to represent sub-basins. The first trend running N-S in the right hand of the map can be divided into three main anomalies (H3, H6 and H7). H3 has the highest gravity value in the area (+18.44mGal), having a domal maximum, becoming elongated North-South, with a total area of 648 km2. Anomaly H6 peaks at +8mGal and is elongated North West-South East, with an area of about 249 km^2. The third anomaly in this trend is H7 appears to extend generally North East-South West and tends North East ward, has a peak value of +5.8mGal.

The other high anomalies H1, H2, H4, H5 have different value of gravity anomaly and different an area. H5 has a maximum gravity value of +7.7mGal, is elongated North-South and has an area of 108 km^2. H8 in the North West corner extends North East - South West with maximum gravity value of +3.7mGal and probably extends to the North East -South West of the area covered and has an area of 108 km^2. H1, H2 and H4 have maximum gravity value of +10.49, 6.79 and 8.52 mGal respectively .and an area of 186.55, 87.04 and 109.6 km^2 respectively.

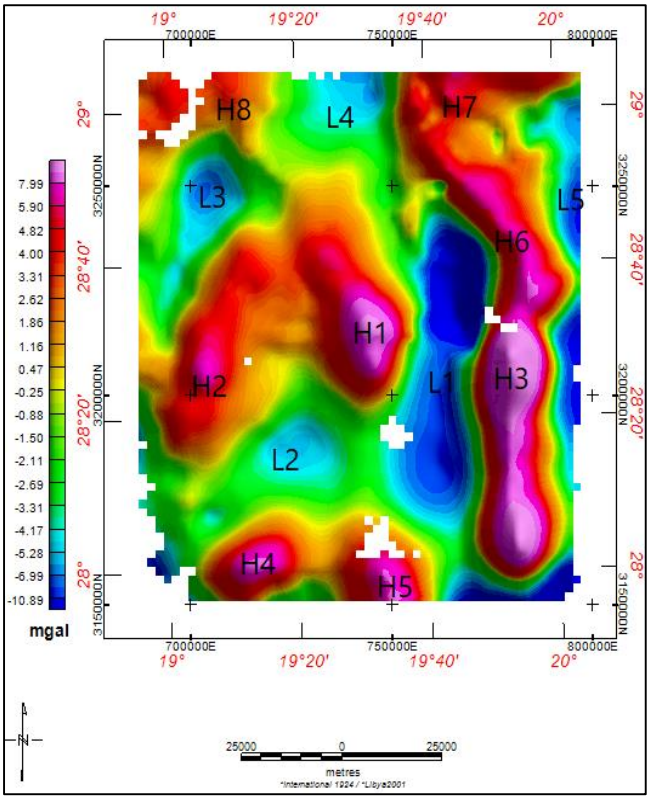

Figure 3. 14 : The 3rdorder of Residual of gravity anomaly

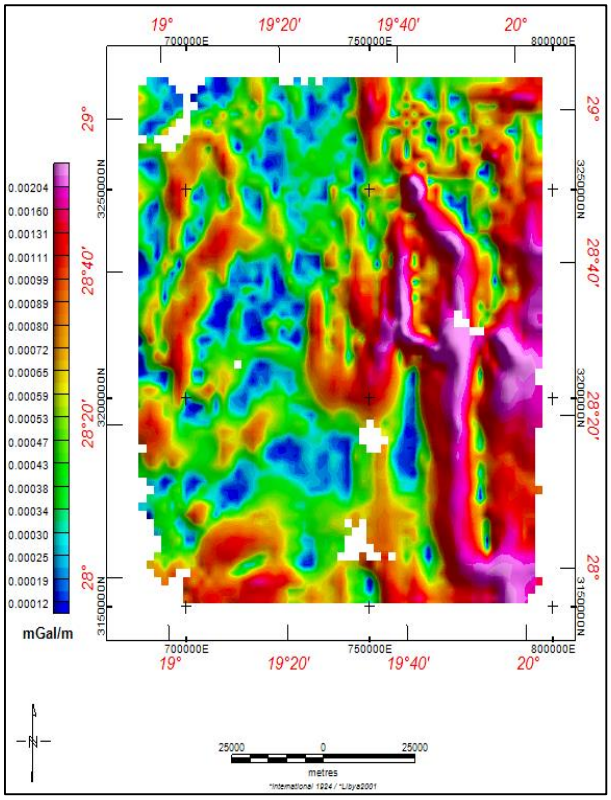

Figure 3. 15 : The total horizontal gradient of gravity anomaly

To extract further details and carry out a quantitative analysis of these anomalies some processing has been applied to the THG grid. First the upward continuation filters for a multi scales applied on the residual anomaly grid to obtain the residual grid at different levels (1, 2, 3, 5, 7, 9) km the result of these upward continuation will attenuate the high frequency (short sources) anomalies and emphasis the deeper (long sources) anomalies (Blakely, 1996), then for each upward level the vertical derivative gradient has been computed, finally we computed the THG for every grid that resulted from the previous step, and from this a set of maps have been created. Figure 3.16 a, b, c, d, e and f show these maps. By using these maps, further information can be determined about the anomalies which are defined on the residual map:

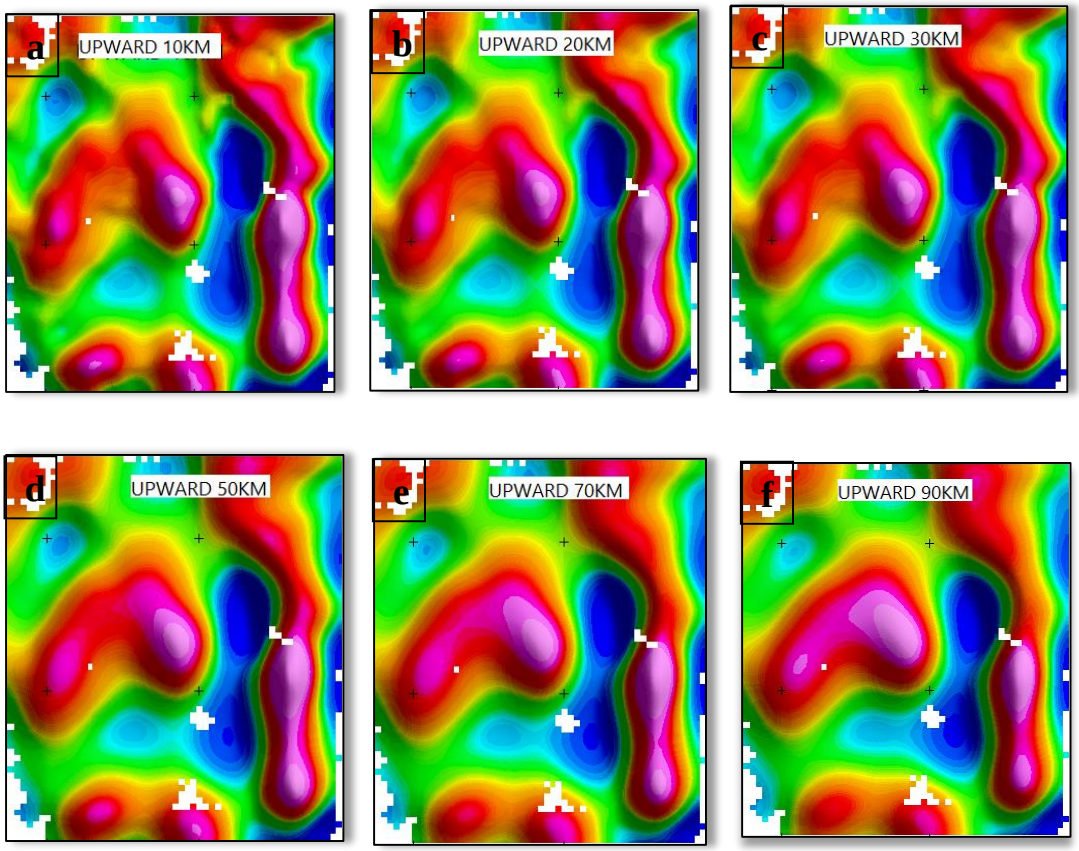

Figure 3. 16 : Various upward continuation anomaly maps of the Bouguer gravity, upward continued to residual gravity 1, 2, 3, 5, 7 and 9 km.

We applied this filter in the frequency domain (more properly the wave number domain) by using the Fast Fourier Transform (FFT) technique in Geosoft package software. All the upward continuation maps were examined and compared until there are no longer any noticeable changes among the subsequence upward continuation. maps.

3.4 Magnetic Data

The magnetic data for the Maradah Trough made available from the African Magnetic Mapping Project (AMMP) by Libyan Petroleum Institute (LPI). The Magnetic data was obtained from (LPI), from total of (3231) interpolated magnetic grid nodes.

This project was compilation off all available airborne, ground and marine magnetic data for the whole of the Africa. The data covers a variety of grid resolutions at constant 1km elevation terrain for this project. Previous and new data were merged into unified 1km grid. Also, the International Geomagnetic Reference Field (IGRF) was removed from the original data by using program which applied by Geosoft package software.

The inclination and declination in the center of the study area is 40.021˚,

-0. 268˚.respectively. (Fig. 3.17) shows the distribution of magnetic stations over the study area.

Magnetic surveys record spatial variation in the Earth's magnetic field. Variation in susceptibility is one of the phenomena that may be indirectly detected by magnetic surveys. This data will be used by the same approach as performed for the gravity data to investigate the anomalies in the earth's magnetic field resulting from the magnetic properties of the underlying rocks. The anomalies in the earth's magnetic field resulting from the magnetic properties of the underlying rocks.

The magnetic data for the Maradah Trough obtained and made available from (AMMP) by (LPI).

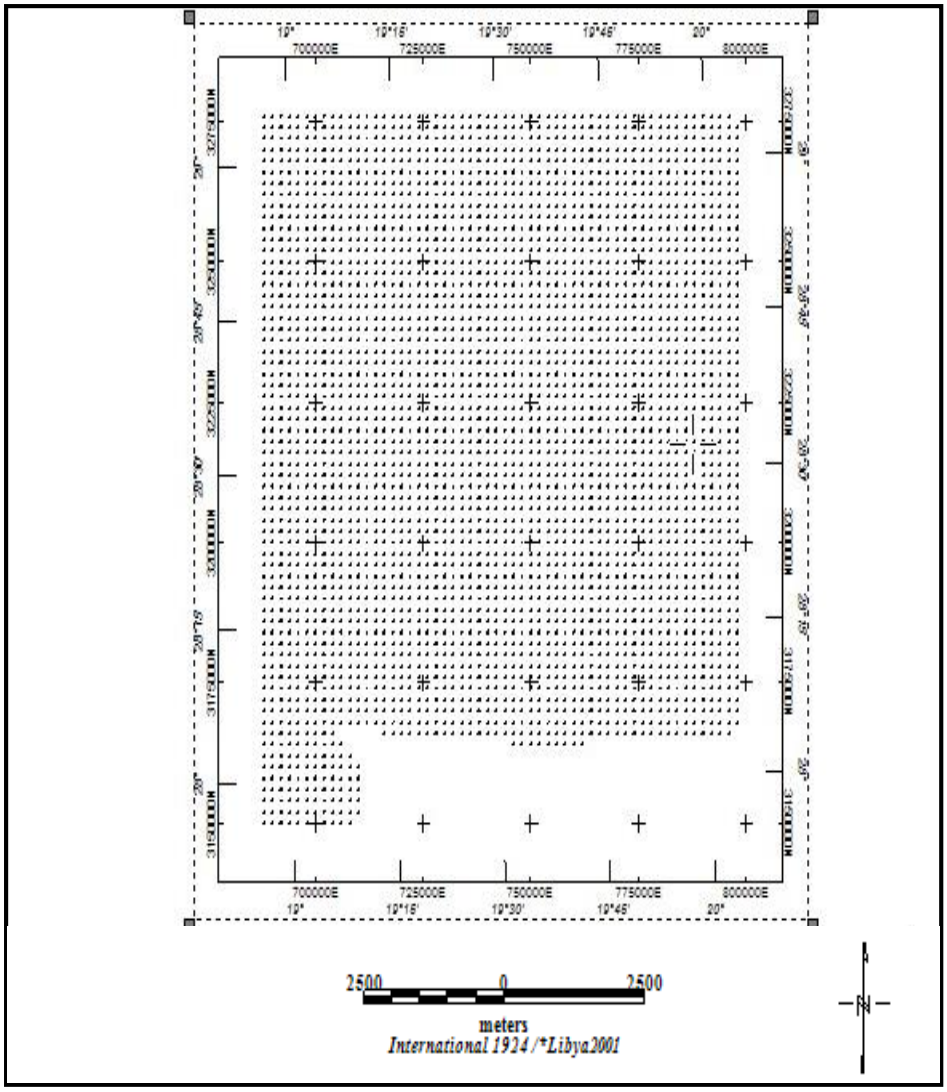

Figure 3. 17 : Magnetic station locations in study area

The minimum curvature techniques have been applied to magnetic data in order to get smooth gridding by using different grid cell size (250 ,500, 1000, 1500 m), (Fig. 3.18) show different grid spacing applied, it seems to be that 1000m is the best grid cell size

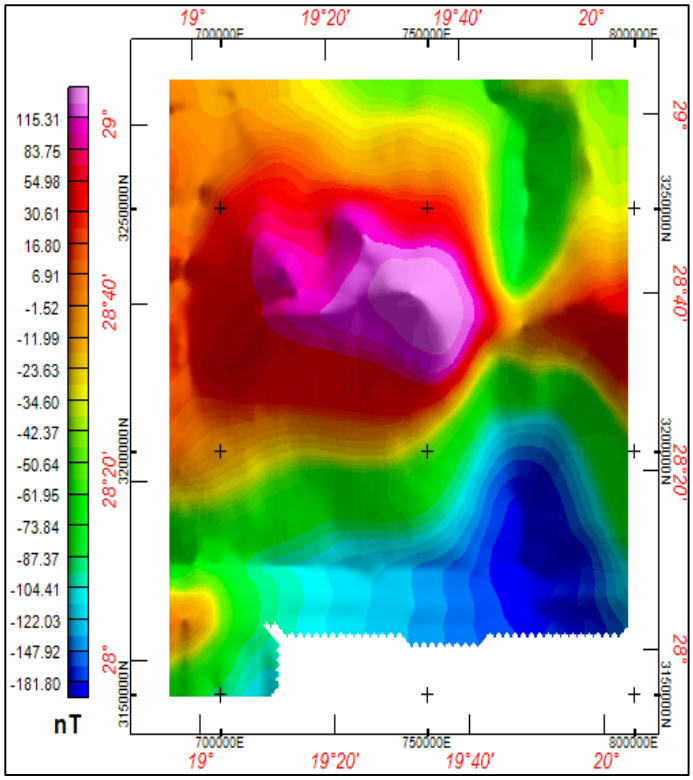

A = Cell size 250m

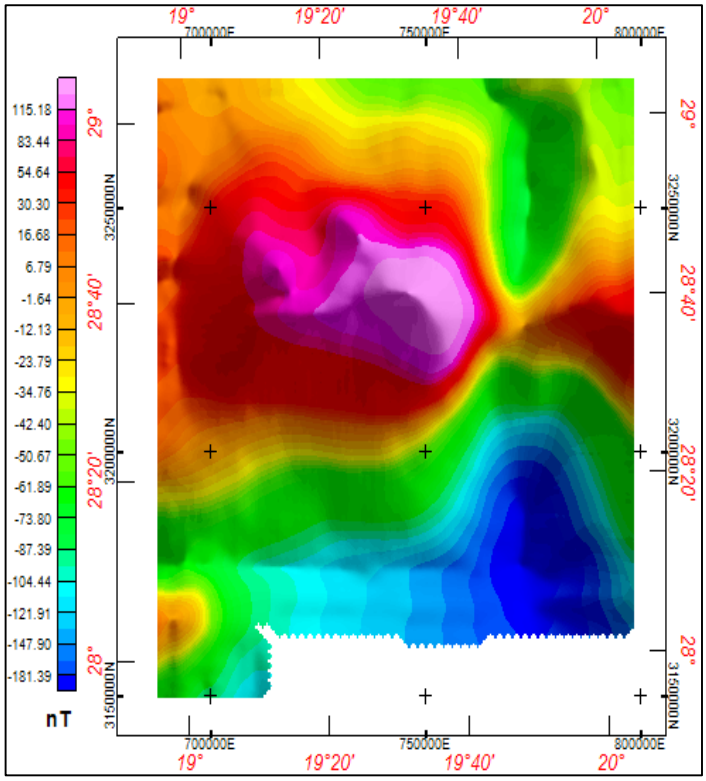

B = Cell size 500m

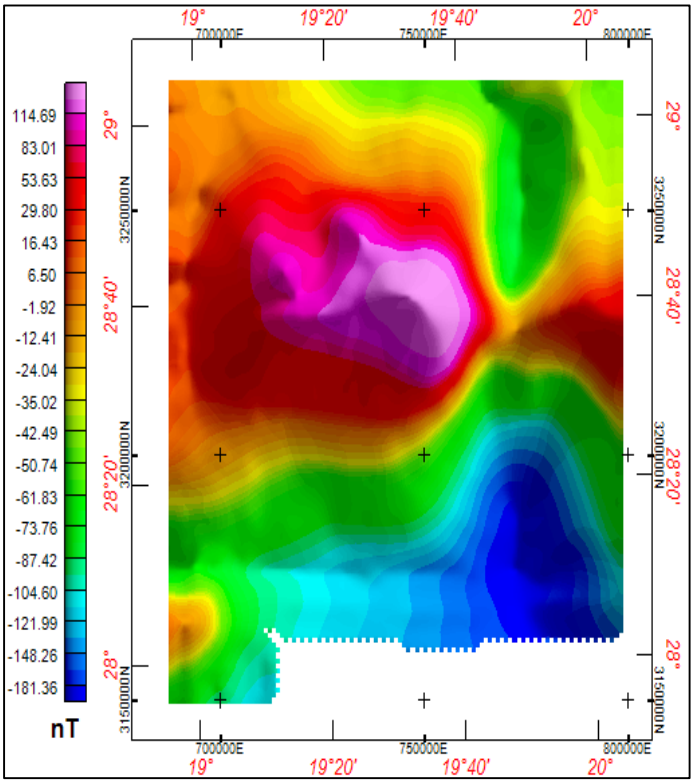

C = Cell size 1000m

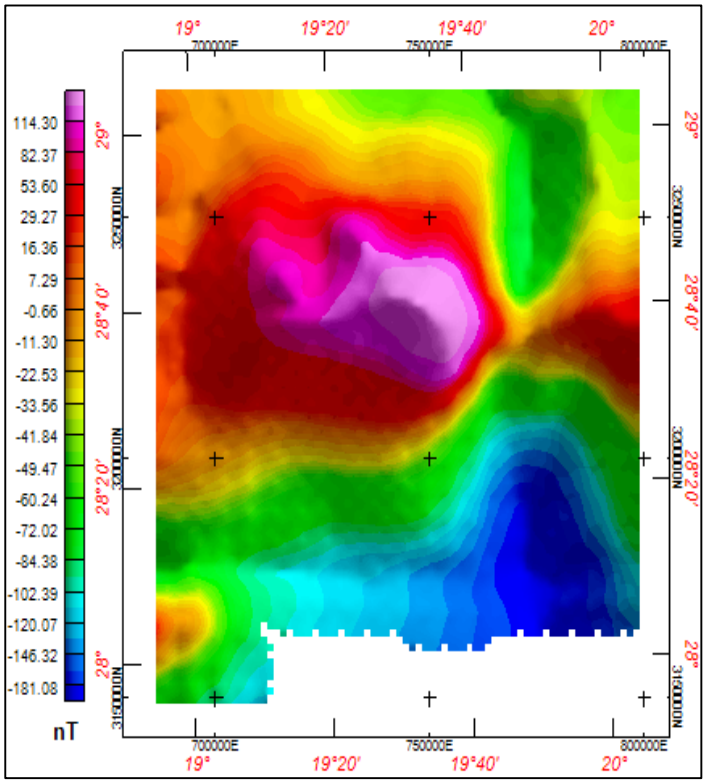

D = Cell size 1500m

Figure 3. 18 : Total Magnetic Intensity of different grid cell size A=250m, B=500m, C =1000m, D=1500m.

- Total Magnetic Intensity (TMI)

The total-magnetic-intensity (TMI) map of the Maradah through area was obtained to delineate the subsurface anomaly.

Figure 3.19 indicates TMI with ground magnetic data points. The ground magnetic anomalies range from -181.36 to 114.69nT and are characterized by both low and high frequencies of anomalies.

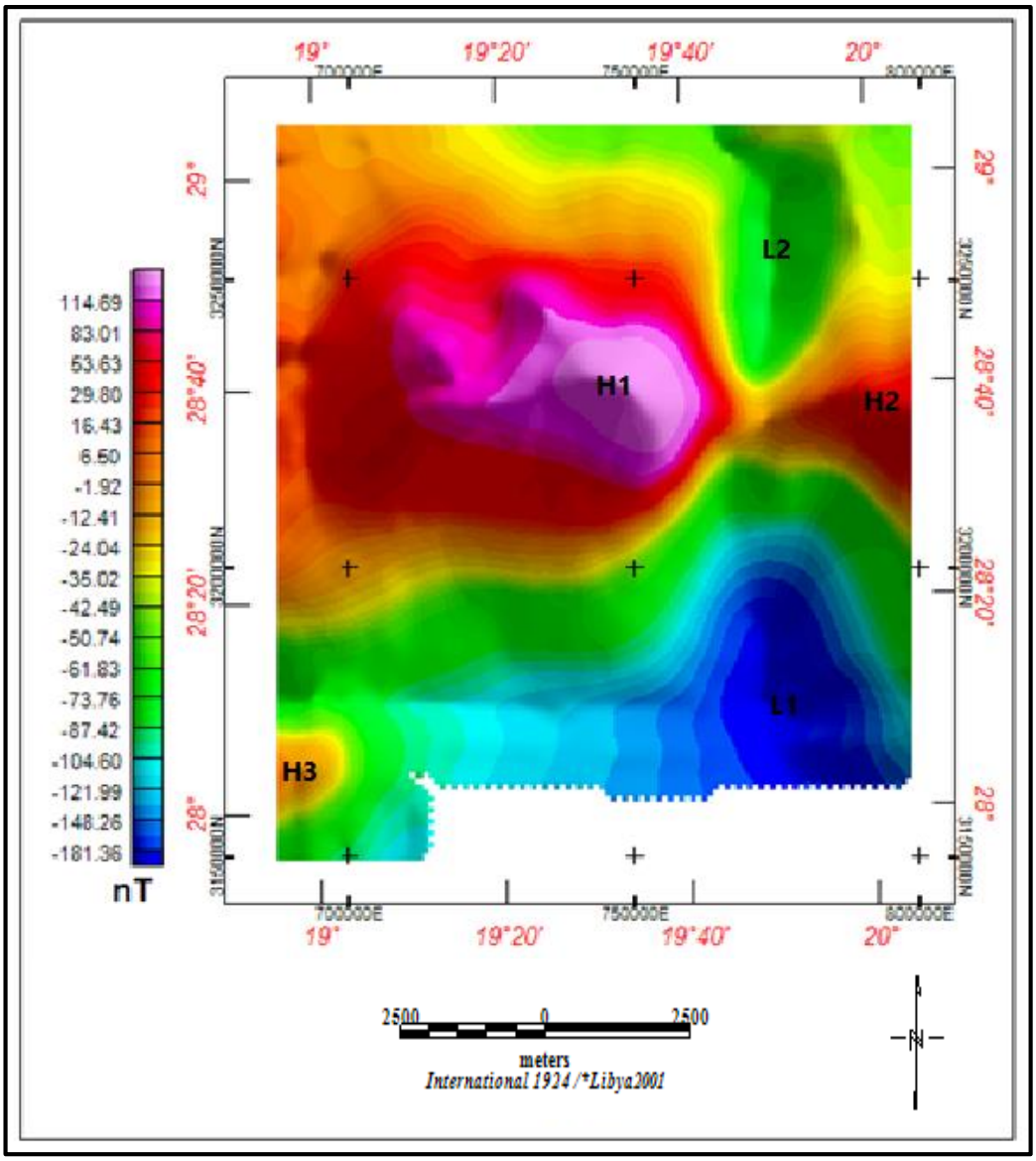

Figure 3. 19 : Map showing Total Magnetic Intensity of study area, grid cell size 1000m

The map reveals that dipolar (anomalies having positive and negative components) magnetic anomalies have a general (NE–SW) direction, which is in the center and south-East of the studied area .There is obvious dipolar magnetic anomaly (is in the center) In the Maradah prospecting area.

Negative magnetic anomalies observed on the total magnetic intensity map (TMI) are interpreted to define local sedimentary basins.

- Residual Magnetic Map

Usually, the magnetic map contains anomalies come from several sources. The regional anomalies are log wavelength anomalies due to deep density contrast. They are very important for understanding large scale structures of the Earth's crust, such as mountain, oceanic ridges and subduction zones. While, the short wavelength anomalies are due to shallow anomalies, which called residual, anomalies and they may be interest for commercial exploration. Geological knowledge is essential for interpreting the residual anomalies, short wavelength anomalies may be due to near-surface mineralized bodies. In sedimentary basin, short or intermediate wavelength anomalies may arise from structures related to reservoirs for petroleum or natural gas. The separation of anomalies of regional and residual is important step in the interpretation of magnetic map. There are several methods that used to separate the regional and residual such as graphical, polynomial fitting, upward continuation and wavelength filtering. For this study, upward continuation technique used to separate regional map from Residual map (Lowrie, 2007).

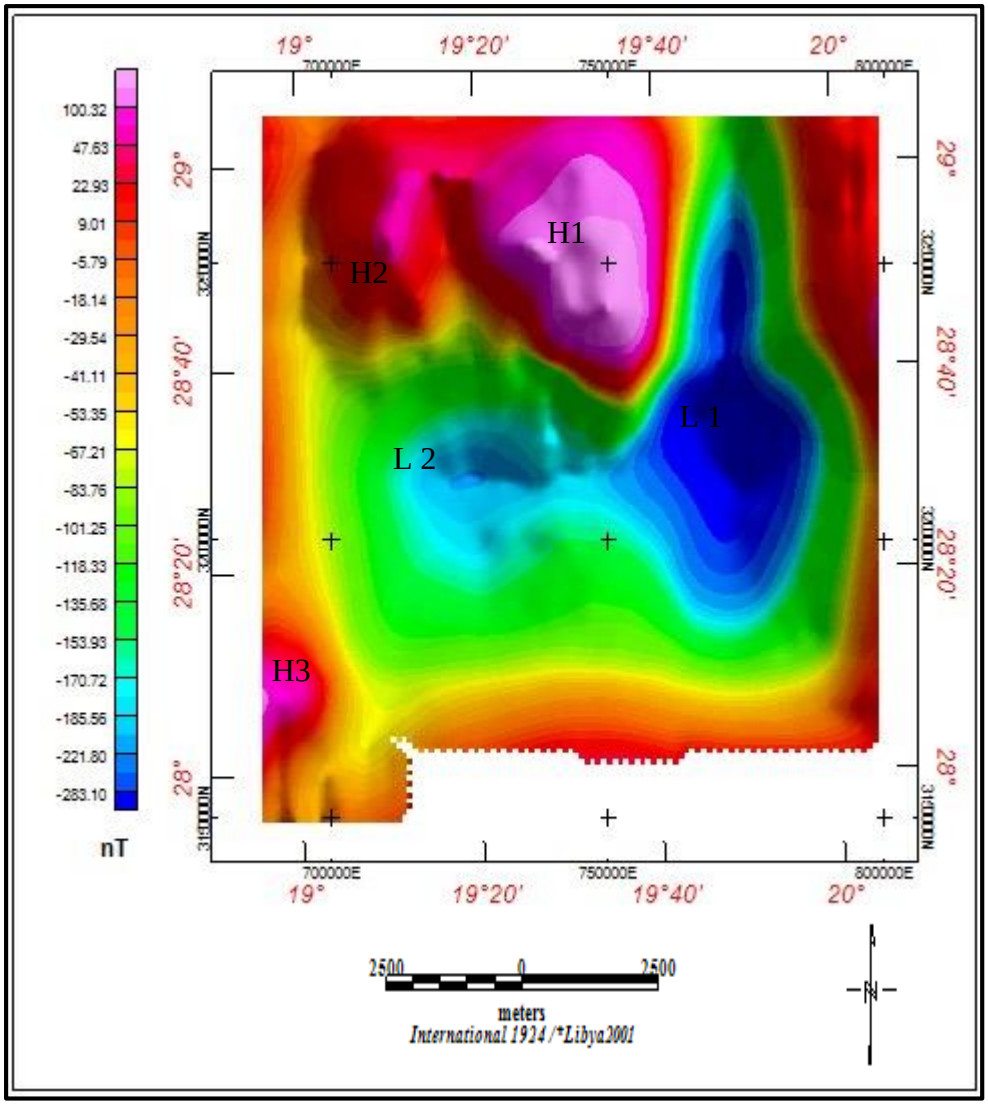

Figure 3. 20 : Map showing the 3rd order of residual magnetic map

The magnetic highs are located over the bodies which cause them. In particular the large amplitude magnetic anomalies HI, H2, and H3 (80-200) nT. The low negative magnetic anomalies are dominated the middle of the map which defined L1 and L2 (-120, -300) nT.

3.5 Magnetic processing

A reduction to the pole (RTP) filter for low geomagnetic latitudes was applied to the Residual Magnetic anomaly which is the Total Magnetic Intensity (TMI). Interpretation of magnetic data can further be helped by RTP in order to remove the influence of magnetic latitude on the anomalies, which is significant for anomalies caused by crust (Luo & al,2010). The inclination and declination were computed using the central coordinates of the study area, normally by extracting the values from the International Geomagnetic Reference Field (IGRF). It is possible to perform reduction to the pole or to any other magnetic latitude.

Reduction to the pole is the process of converting the magnetic field from magnetic latitude where the Earth's field is inclined, to the field at a magnetic pole, where the inducing field is vertical. When the Earth's field is inclined, magnetic anomalies due to induction have forms that are asymmetrically related to their sources, but when the inducing field is vertical, the induced anomalies are directly over their sources.

The same process can be used to convert magnetic fields between any two magnetic latitudes. Reduction to the pole greatly simplifies the interpretation of magnetic data, because at magnetic latitudes less than 50° the relationship of anomaly form to source geometry is often not obvious (Vacquier & Gary, 1951) as discussed by (MacLeod & al., 1993), problems can arise in the reduction to the pole process at magnetic latitudes less than 15°, as the Fourier domain process becomes unstable, owing to the need to divide the spectrum by a very small term. Some workers avoid this problem by limiting their transformations to greater than 15° and accepting the results. Others approximate the process by doing two transformations for smaller amounts, where the sum of the angles involved in the transformations equals the difference between the survey latitude and the pole.

Some workers avoid the issue altogether by performing a reduction to the equator. This does indeed produce anomalies that are symmetrically related to their sources;

However, such anomalies have elongations and subsidiary peaks that do not occur in polar anomalies and they are, consequently, more difficult to interpret

The Reduction-to-pole filter (Grant & Dodds, 1972) is

$$R_{TP}(\theta) = \frac{1}{[\sin(I) + i\cos(I)\ \cos(D - \theta)]^2}$$

Where: i, Θ, I, and D, are the imaginary unit, wave number direction ,magnetic inclination and magnetic declination of the magnetic anomaly respectively.

The inclination and declination in the study area which used for the RTP transformation were taken as 28˚ N and 20˚ respectively Inclination = 40.021 ˚, Declination = -0.268 ˚.

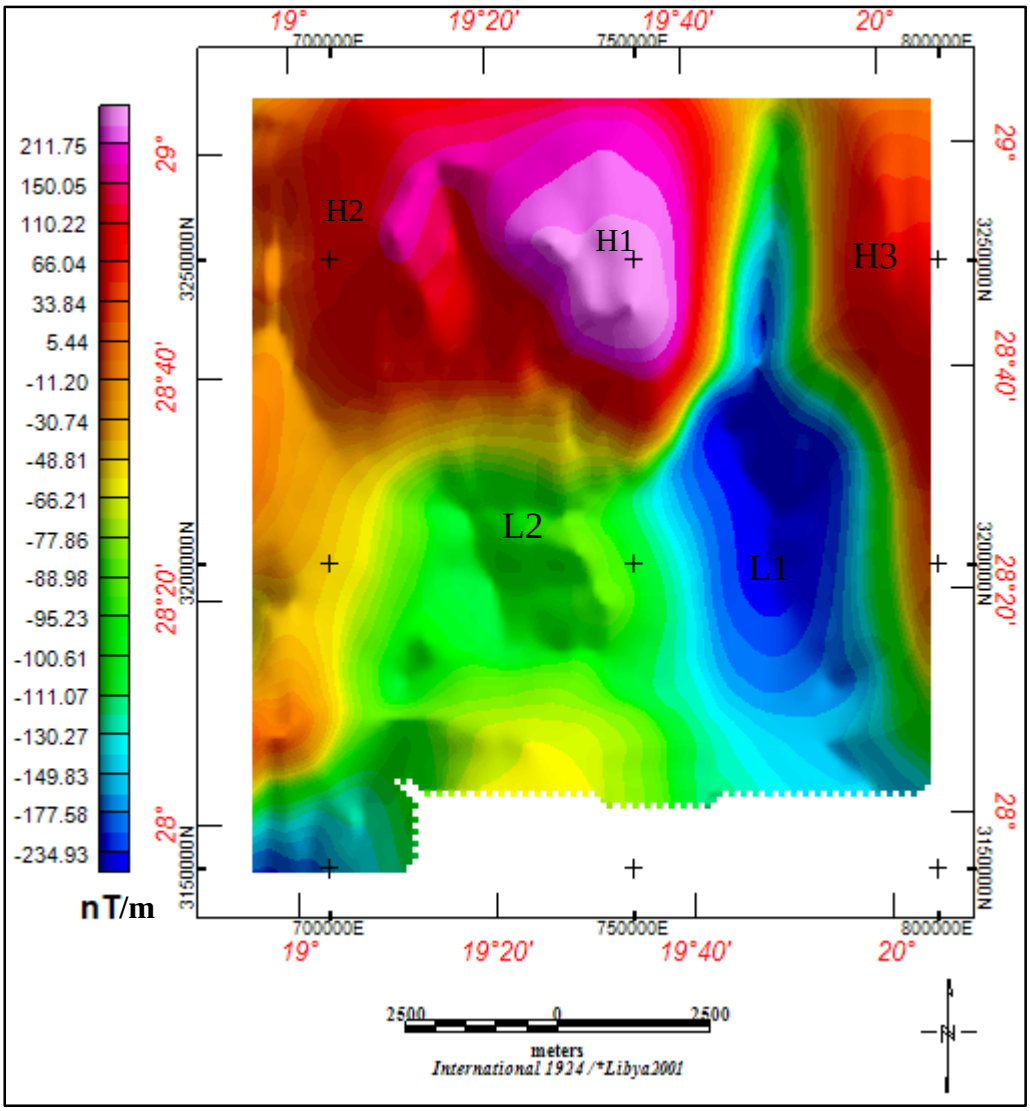

Figure 3. 21 : Map showing the reduction to the pole of the study area.

The reduction to the pole operation is a data processing technique that recalculates total magnetic intensity data as if the inducing magnetic field had a 90^0 inclination. Reduction to the pole makes the simplifying assumption that the rocks in the survey area are all magnetized parallel to the earth's magnetic field.

The total magnetic intensity was reduced to the magnetic pole in the Fourier domain by using the Geosoft package software, in order to remove magnetic anomaly distortion which caused by varying magnetization inclination and azimuth. RTP grids were easier to interpret than the TMI because replaced the anomalies directly above the source of the magnetic field.

After reduction to the pole (Figure 3.21), the anomalies, in general, become better defined. The maximum intensity of the main high positive anomalies increases, H1 and H3 are nearly completely merged into one large high.

H1, H2, and H3 increase to be 358nT, 70nT, and 164nT respectively. The area of H1/H3is2838 m^2 and the part of area H2 that shown in in the map is 555m^2. The contrast between the positive and negative anomalies is steeper, and the negative

anomalies increase as well, L1 and L2 have amplitude of -240 nT, -108nT respectively. With SE-NW-trending.

- Vertical Derivative (FVD)
- First vertical derivative

Vertical gradients of potential fields are also a mainstay of the interpretation process, principally because they sharpen the response of geophysical features. This filtering method is effective in enhancing anomaly due to shallow sources; it narrows the width of anomalies and also very effective in locating source bodies more accurately (Cooper and Cowan, 2004). Derivatives tend to sharpen the edges of anomalies and enhance shallow features. The vertical derivative map is much responsive to local influences than to broad or regional effects and therefore tends to give sharper picture than the map of the residual field intensity. Thus, the smaller anomalies are more readily apparent in area of strong regional disturbances. In fact, the FVD is used to delineate high frequency features more clearly where they are shadowed by large amplitude, low frequency anomalies.

- Second vertical derivative (SVD)

The second vertical derivative of magnetic fields is commonly used for resolution of anomalies in gravity and magnetic fields. It is also commonly used as an aid to geologic mapping i.e., for the delineation of geological discontinuities in the subsurface. Frequency domain methods for calculating second vertical derivatives often result in highly distorted outputs that cannot be reliably interpreted. The second vertical derivative of the magnetic field is the rate of change of the first vertical derivative in the vertical direction. Computation of the second vertical derivative significantly improves the resolution of closely spaced anomalies. The second vertical derivative can detect very small changes in the concentration of magnetic material within a given rock unit. Besides its utility for mapping contacts, patterns of second vertical derivative features indicate compositional and structural trends within a specific unit or domain.

- Total Horizontal Gradient of the 3rd order of residual magnetic anomaly

The total horizontal gradient of gravity data is calculated using fast Fourier Transform (FFT). (Grauch & Cordell, 1987) discussed the limitations of the horizontal gradient magnitude for gravity data. They concluded the horizontal gradient magnitude maxima can be offset from apposition directly over the boundaries, if the boundaries are not near vertical and close to each other. This method had the effect of highlighting high gradient areas which (for example) might occur at normal fault boundaries, making the technique useful for delineating structural trends. In the study area, the map of total horizontal gradient anomalies was examined throughout the area. Some geologic faults are confirmed and others are delineated. The Figure (3.22) showed strong horizontal gradients on the Central , Eastern and Southeastern parts of map.

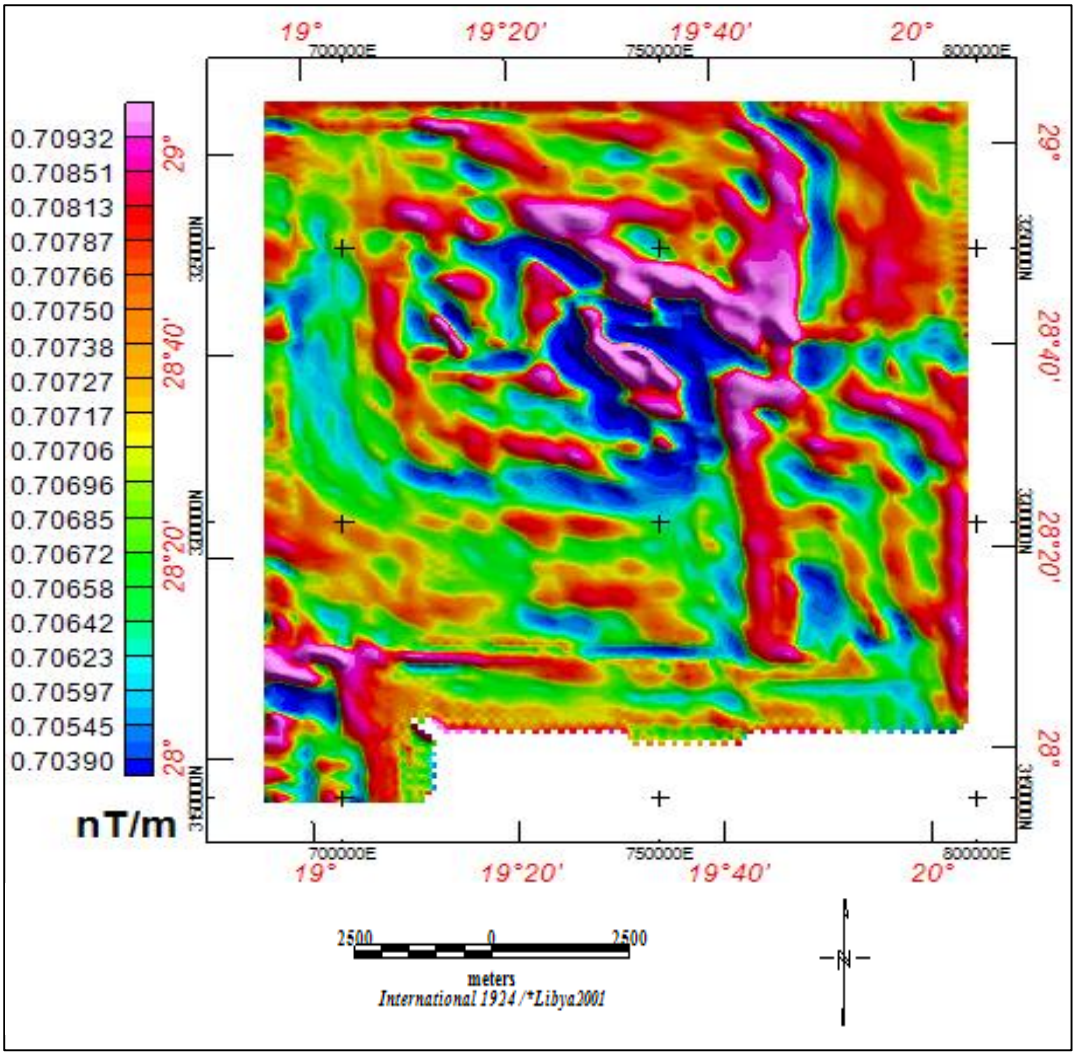

Figure 3. 22: Total Horizontal Gradient of RTP of magnetic anomaly

- Pseudo gravity Data

We Use the pseudo-gravity functional transform to enhance deep magnetic sources and enrich regional gravity data.

Magnetic anomalies are difficult to analyze and interpret because they are not always located in the vertical direction of the perturbing bodies. Depending on the parameters of the geomagnetic field, the shape of the anomalies cannot be uniquely related to a given source. The complexity of the magnetic field and of its anomaly-to-lithology relationship often complicates interpretation. The amplitude of the anomalies is

dominated by the magnetic bodies that are present in the shallowest geologic structures. This dominant influence of shallow geologic bodies makes the detection of the deeper geological sources, which contribute to the medium and long period components of the observed magnetic signal, difficult. Conventional filtering methods smear out the shallow sources which are not capable for separating the lower amplitude magnetic anomalies associated with the deeper magnetic source rocks Figure (3.23).

The magnetic anomaly is converted into the gravity anomaly with respect to Poisson's relation (Baranov, 1957), that would be observed if the magnetization distribution were to be replaced with an identical density distribution. (Baranov, 1957) called the resulting quantity a pseudo gravity anomaly

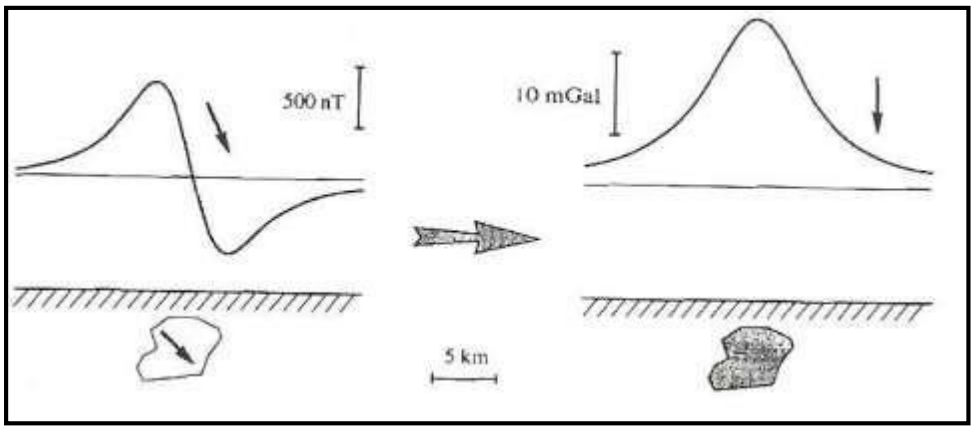

Figure 3. 22 : Magnetic anomaly and its pseudo gravity transform after (Blakely &Richard, 1996).

The transformation relates total magnetic intensity to vertical component of the gravity field g_z. The transform of the Poisson equation relating the gravity and magnetic field potentials expressed by:

$$U = \frac{J\ \partial g}{Gp\ \partial I}$$

Where U, g, I, J, ρ, G are, respectively, magnetic potential, gravitational potential, direction of magnetization, magnetization intensity, density and Gravitational constant.

Poisson's theory relates linearly the derivative of the gravity taken along the total magnetization vector direction and the magnetic potential due to a common, isolated source with constant density and magnetization distributions. From this theory, two very useful functional

Transformations for magnetic anomalies, the reduction-to- pole (RTP) and the pseudo-gravity (PSG) vertical integration were formulated by Baranov.

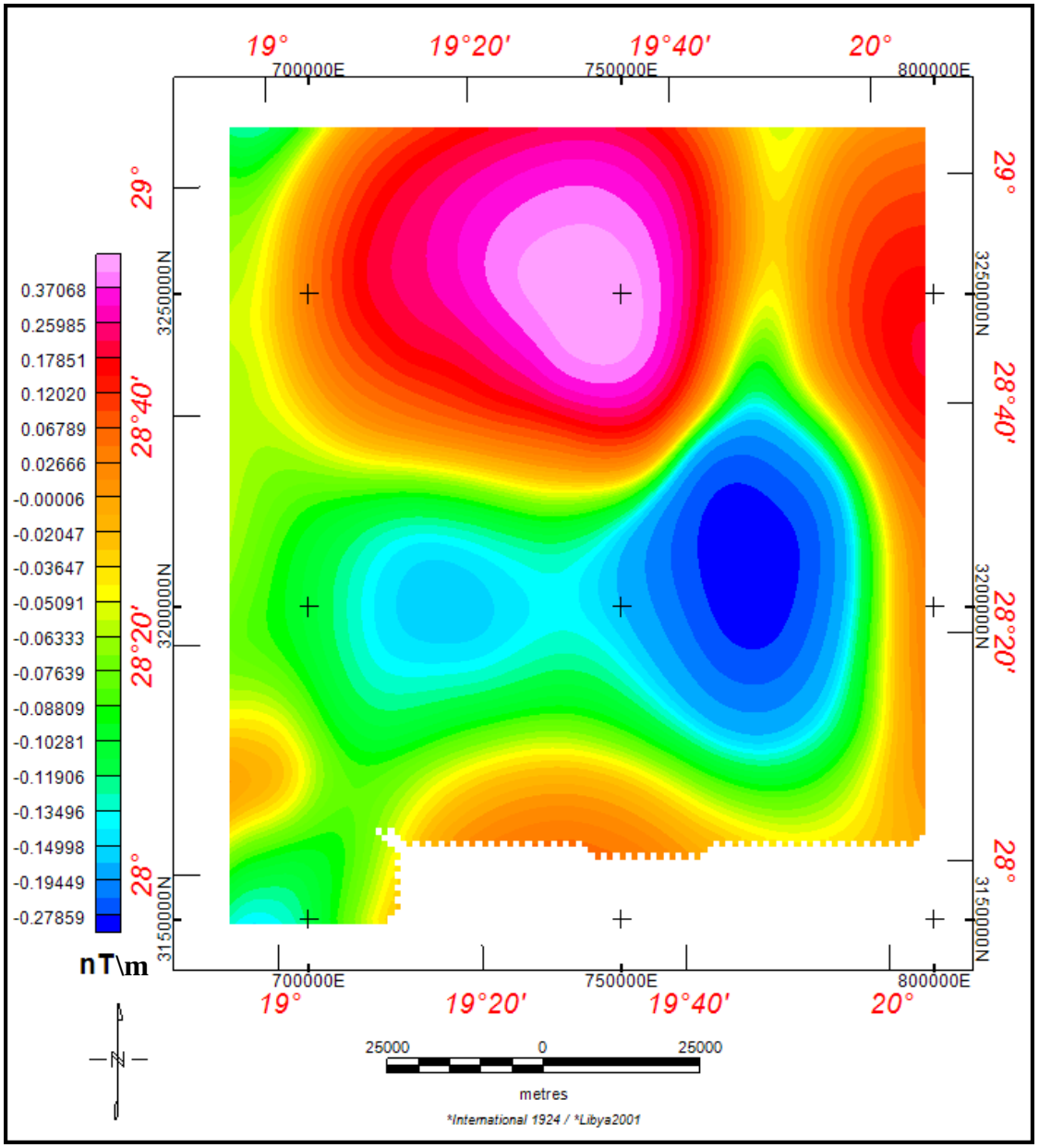

Figure 3. 23 : Map Showing Pseudo gravity anomaly map of the study area.

3.6 Depth estimation using power spectrum analysis and 3D Euler deconvolution

3.6.1 Depth estimation

Depth estimation techniques of the anomaly (Magnetic and Gravity) are depending on the common standard of the gradient of the anomalies, where the shallow sources are known by steep gradient and the broad gradient known as deeper sources.as in figure 3.25 (Grauch et al., 2003). However, in the interpretation it must be look at the influence of the properties of the source since broad shallow sources with a prospective change in properties can be interpreted in wrong interpretation as broad shallow sources، even though the influence of the broad shallow source with slow change could be interpreted as a deep anomaly. Furthermore, the adjacent and/or overlying sources could cause interference between anomalies and the depth estimation will be difficult (Grauch et al., 2006).

When the anomaly and noise are completely separated (where the perfect cases exist), the quantitative depth estimation using some techniques can be described as a final solution (Xiong, 2003). The power spectrum analysis is one of the methods used in this study. Spector and Grant (1970) described how the body or the depth of the magnetic layer can be revealed by occupation the slope of its power spectrum versus (Figure 3.26).by using the Oasis montaj-Geosoft software. The estimation of the source depth was produced using the plots of magnetic and gravity of the power spectrum.

3.6.2 The Spector and Grant method.

Spector & Grant (1970) approximated the susceptibility distribution in the space domain by a number of rectangular prisms. They derived a model power spectrum which includes a factor for the horizontal susceptibility variations and a depth factor

exponential of (*-2hr*), where *h* is the mean depth to the top of the prisms and *r* is the absolute value of the wave vector. Stating that:

$$e^{-2hr}$$

This term is invariably the dominating factor in the power spectrum', Spector & Grant introduced a method that estimates the depth to source directly from the slope of the log radially averaged power spectrum. This method enjoys continuing popularity, as can be seen from a number of recent publications (e.g. Ofoegbu & Hein 1991; Cowan & Cowan 1993; Hildenbrand, Rosenbaum & Kauahikaua 1993). An example of an interpretation by the Spector and Grant method is shown in (Figure 3.18) (after Hildenbrand et al. 1993).

A shortcoming of this method is that it only yields the depth to the equivalent layer and not the depth to the real sources, which may be situated anywhere above or below this layer. Spector and Grant's understanding of the power spectrum has another widespread application. If the slope of the log power spectrum indicates the depth to source, then a section with constant slope defines a spectral band of the potential field originating from sources of equal depth. Hence, it appears to be possible to separate the contribution of these particular sources from the rest of the field by band-pass filtering (Spector & Grant 1970; Jacobsen 1987; Cowan & Cowan 1993; Pawlowski 1994, 1995). Since the low-wavenumber (long wavelength) portion of the power spectrum is usually rather steep, this implies that long-wavelength anomalies necessarily originate from deep-seated sources.

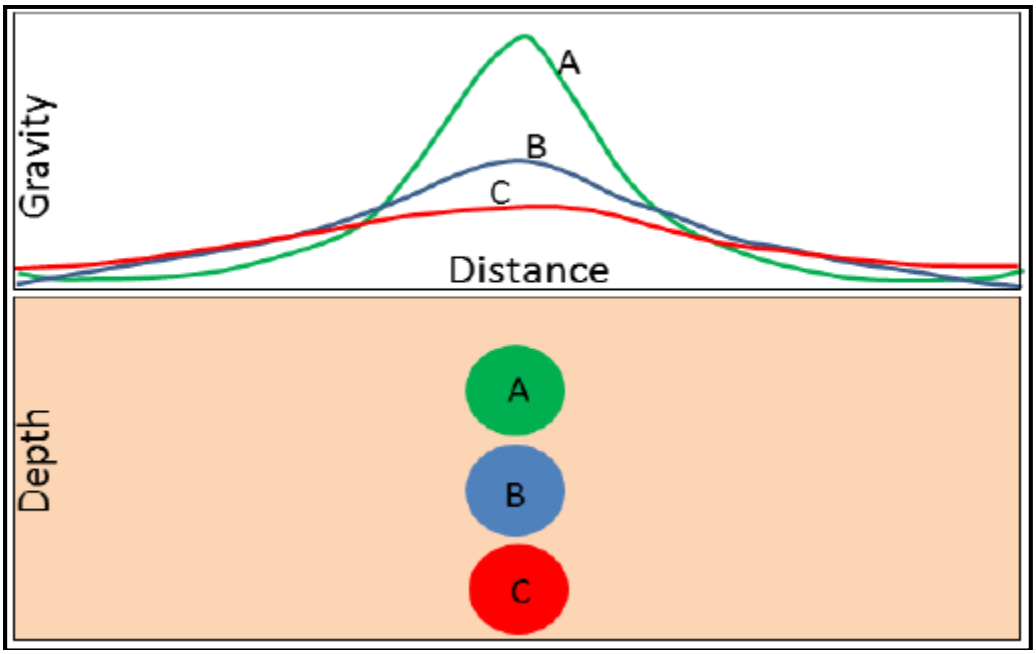

Figure 3. 24 : How the gravity anomalies are functioned in the depth of the source, Modified from (Chapin et al., 1999)

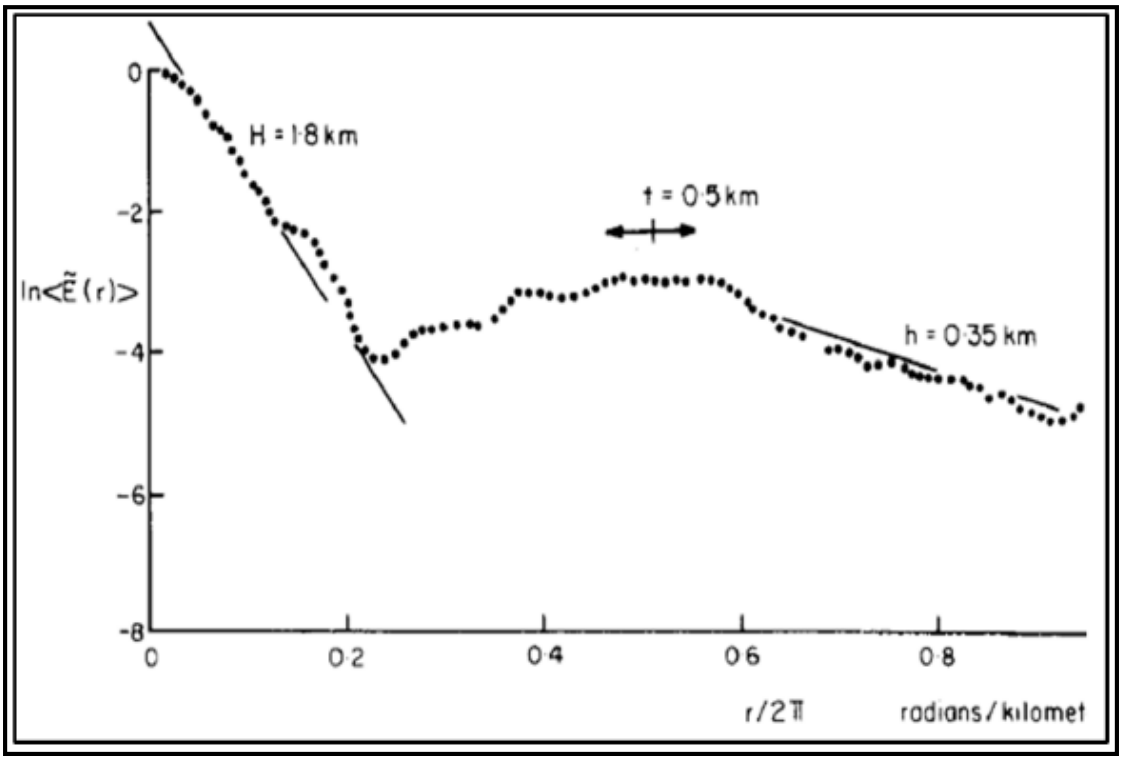

Figure 3. 25 : Power spectrum analysis and depth estimated of aeromagnetic data from Matonipi Lake area, Province of Quebec, Canada. Adapted from (Spector and Grant 1970).

The 3D Euler deconvolutions the second technique used, developed by Hood (1965) for the interpretation of the vertical gradient over a point and dipole in the aeromagnetic

data, and modified by others (et al Thompson, 1982) adapted the method for profile data interpretation. In 1990 the technique developed into girded 3D data by Reid and others. By this technique can be determined both the depth and the location of the gravity or magnetic bodies with an accuracy in this study area, the power spectrum of the gravity data (figure3.27a) shows that the curve split into a slice of different slop, the source depth can be derived using the expression $h=-S/4\pi$, where: h is the depth to the top of the source; S is the slope of the log (energy) spectrum.

On the graph, the maximum depth as shown is 14 km which is a relatively deep source (deeper than the basement), then there is the source depth which was certain to be the top of the deepest basement that has a depth of 6 km the depths 5.9km and 6.2 km also still within the range of the basement depth, the 2.8 km value related to a relatively shallow source. The same procedure was done to estimate the power spectrum of the magnetic data, which is shown in Figure 3.27b

the estimation of the depth (source) that derived by the power spectrum of the data (Magnetic) is almost the same values obtained from the gravity (more or less), and the causative sources of the high wavelet have approximately depth of 15.9 km. the magnetized rock of the basement has values (7.1,4.4 km), on the other hand, the sources of the short wavelet are about 3.7 km in depth.

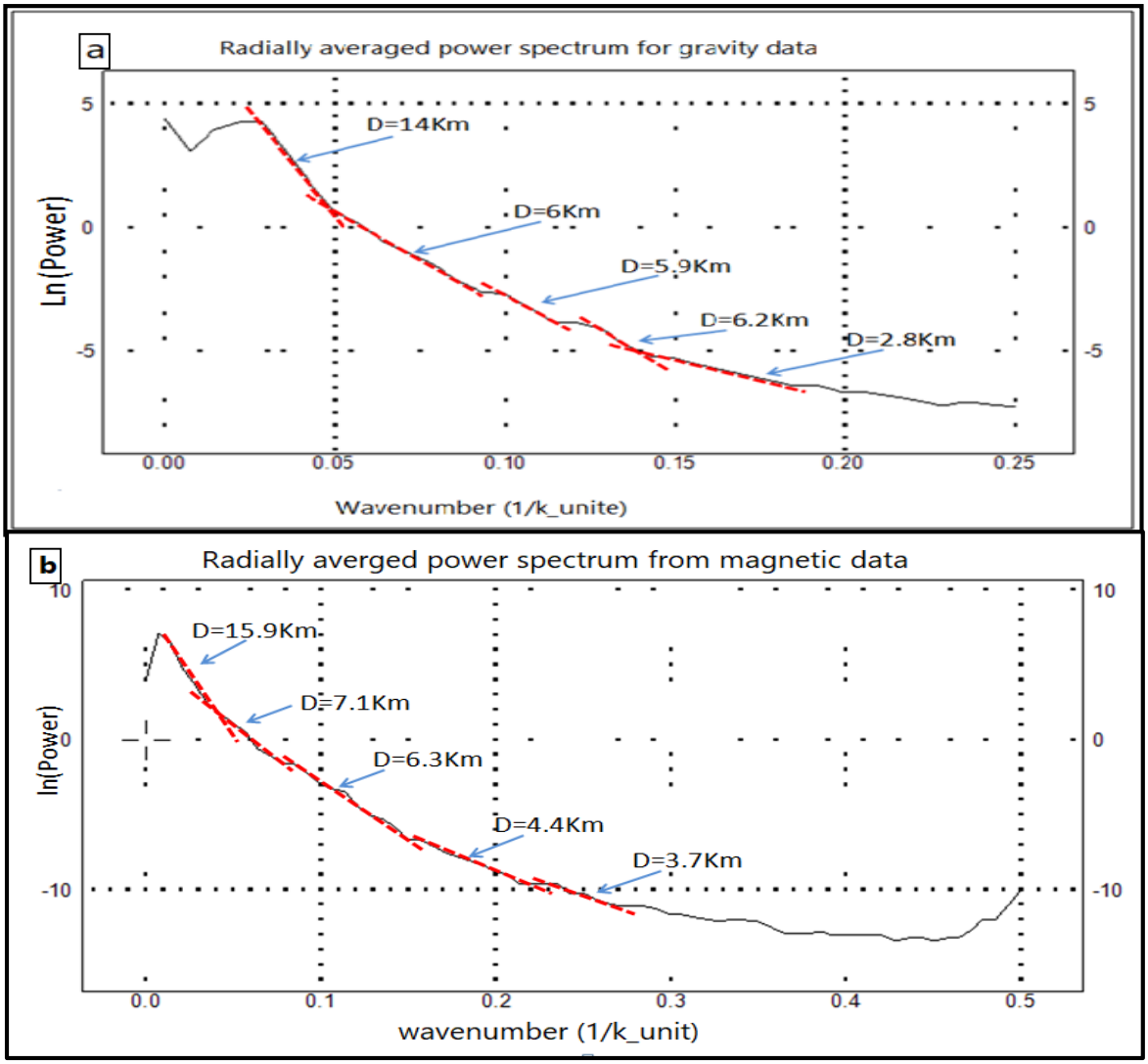

Figure 3. 26 : The depth estimation for the entire area by the slope of the radially averaged power spectrum. (a) From the gravity data. (b) From the magnetic data

3.6.3 3D Euler Deconvolution method.

Unfortunately, the power spectrum method does not readily resolve the location of the different sources on the map. To do this, 3D Euler Deconvolution was used. The depth determined by this method is based on the derivatives of the gridded gravity and magnetic data (Hsu, 2002). During the application of the technique, there are some parameters that should be specified to classify the results of the depth solution of the input grid. These parameters are:

I. Structural Index (SI): it is connected to the geometry of the geological source (guessed) that resulted from 3D Euler solving, Table 3.2 shows some deduced structures and corresponding

index value of these structures as it was obtained by the experimental modeling done by Reid et al. (1990).

II. Window Size: To give a solution, a window greater than 3x3 is needed, a 10x10 window size gives acceptable solutions (Reid et al., 1990), on the other hand, high-resolution data produce excellent outputs with a smaller window size for example (5x5), all results within this window have been assigned to the same source.

In general, the minimum depths returned in Euler deconvolution are of the order of the grid interval, while the maximum depths are about *twice the window size* (Reid et al., 1990; Geosoft, 2004).

III. Depth Tolerance: this factor is dominant for the number of the solutions (i.e. solutions will be refused if the uncertainty is higher than a specific percentage) (Reid et al., 1990). In purpose to determine all the possible sources, and to create the solution of the depth from all of the sources, the method was applied many times, each one of them has a different structural index value.

Structural Index		Structural Index Type	Inferred geological structure shape
Grav.	Mag.		
	0.0	contact	Two adjacent bodies
-0.5	0.5	Step	Fault
0	1	Line of poles	Dyke
1	2	Point poles	Vertical pipe (e.g., Kimberlite)
2	3	Point dipole	Point source (nominally spherical)
Key: Grav.= gravity, Mag.= Magnetic			

Table 3. 2 : Inferred geological structures and the corresponding structural index Obtained from structural index model that gave good results when applied on the real data from central England, Birmingham-Oxford ridge (Reid et al., 1990).

For the gravity:

The used structural index (SI) is (0.0) and the window size is (5.0) for the first trial. Figure 3.28 (a) illustrates the depth solution of the residual gravity map. These parameters gave the extreme depth solution number, it ranges from 1415m to 6989m, and as it noticed most of the results came from the edges of the anomalies. In the second test, the structural index was (0.5), the window size was (5.0), and 20% depth tolerance (default). Figure 3.28 (b) illustrates the solution of the depth of the second test parameters that related to the top of the source of the anomalies, the depth ranges from 3047m to 10830m. As obvious, these values confirm the results obtained by the power spectrum earlier

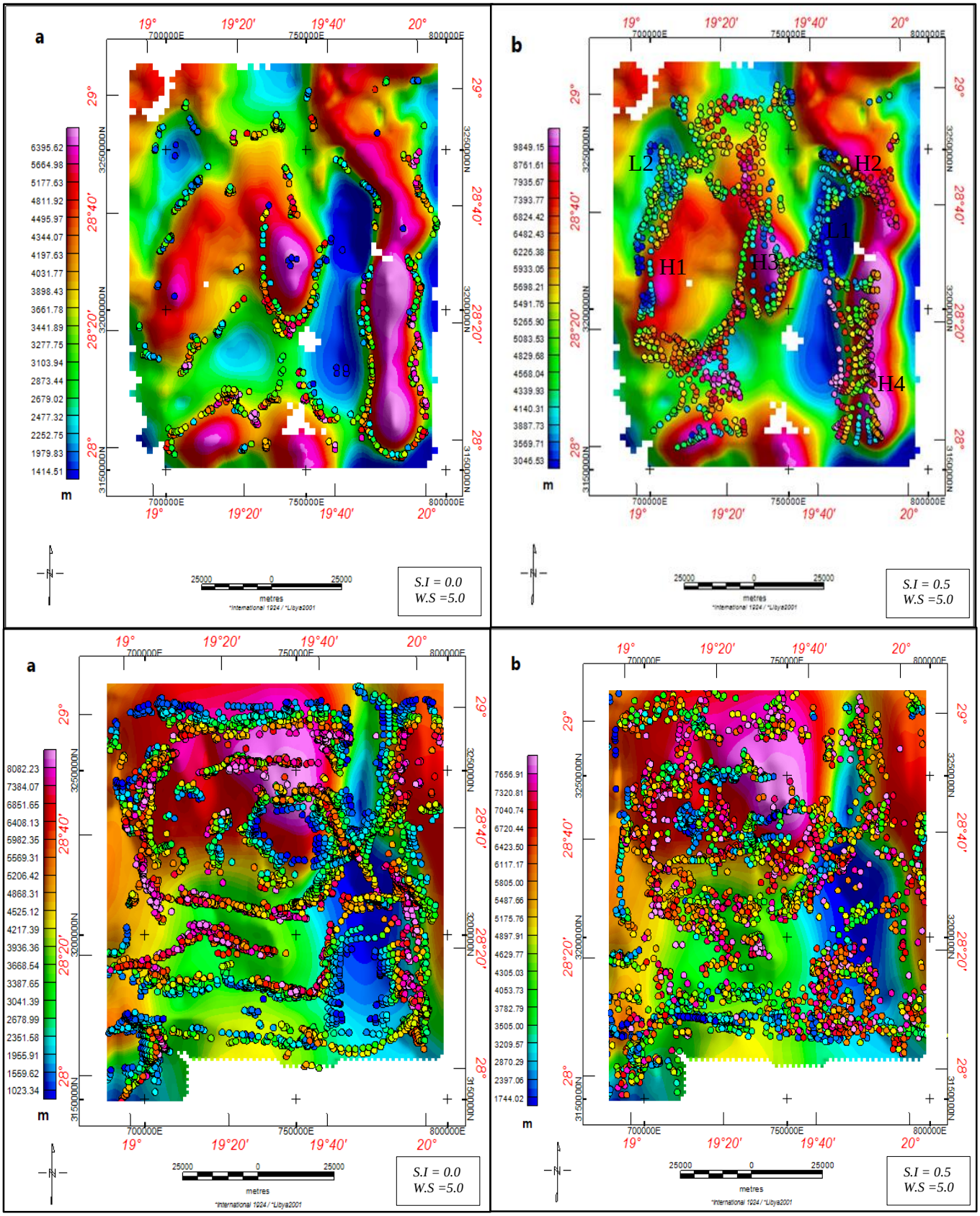

Figure 3. 27: (a) 3D Euler deconvolution depth-solution in the contacts area, (b) 3D Euler deconvolution depth-solution for the top of sources. Both maps are constructed and superposed on the *Residual map*.

For the Magnetic:

Figure 3.29 (a) shows the resulted depth solutions estimated by applying these parameters (SI = 0.0 and WS = 5.0), which gave solutions of the depth for the contacts, that range from 900 to 9000 m. the estimation of the depth to causative magnetic anomalies (SI = 0.5 and WS = 5.0), is shown in Figure 3.29 (b), depths range is from 1480 to 7000 m.

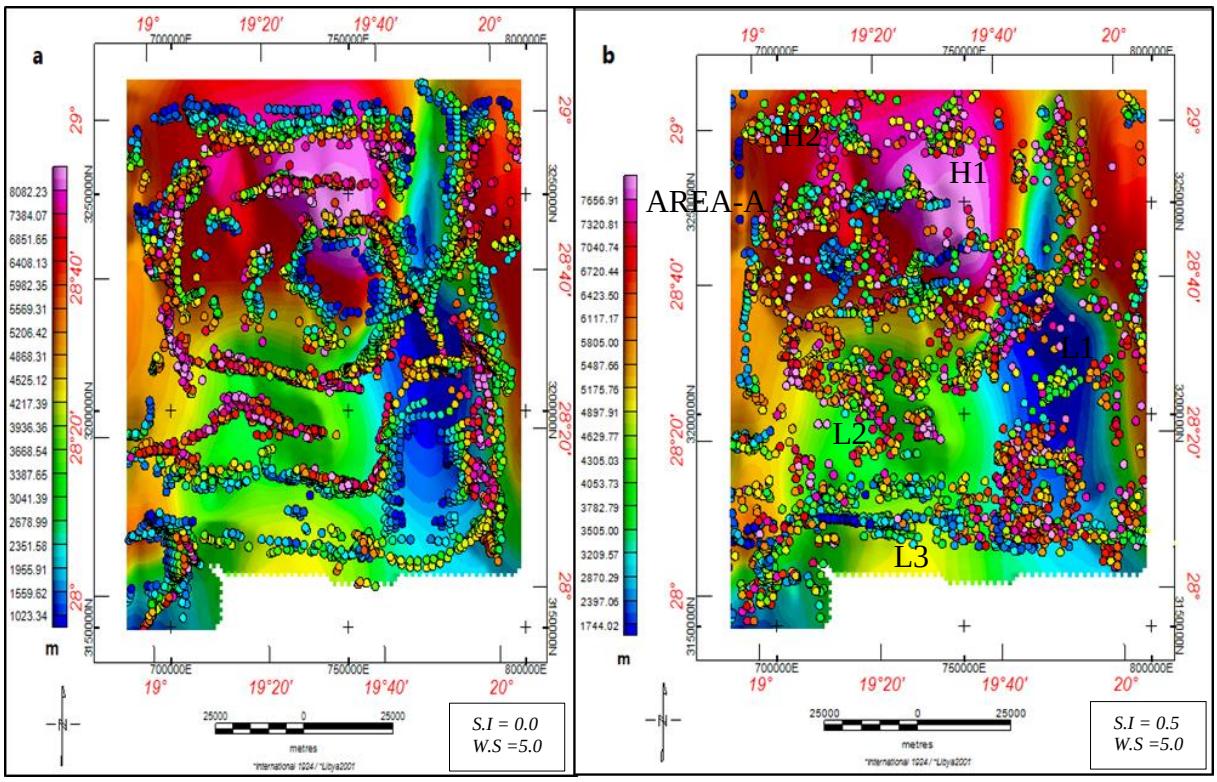

Figure 3. 28 : (a) 3D Euler deconvolution depth-solution in the contacts area, (b) 3D Euler deconvolution depth-solution for the top of sources. Both maps are constructed and superposed *on the RTP map.*

Some observations have been concluded from the Gravity map (Figure 3. 29: (b) the area of H1 has a range from 3400m-6000m (Ano. No 1) at East part, and Area of H2 has a range from 5800 m-9600 m (Ano. No 2), at the Northeast of the area. while the

depth of the center, area of H3 anomaly ranges from 3500m-6000m (Ano. No 3). H4 which located at south east has a range from 5500 m-9600 m (Ano. No 4). (Table 3.3): shows a summary of the depth of each gravity anomaly.

The area of L1 shows a depth range from 3000 m_5400 m (Ano. No 5). Where the depth solution values 3800 m_5500 m (Ano. No 6) appears within the area of L2 low.

Anomaly No	**Depth (m)**
1	3400-6000
2	5800-9600
3	3500-6000
4	5500-9600
5	3000-5400
6	3800-5500

Table 3. 3 : Summarize the Gravity anomalies and their depths as shown on the map

While the RTP map be divided into two areas; the upper part contains the deeper anomalies and lower part contains the shallower anomalies, for the area A the anomaly H1 which dominated the upper part of the map has an approximate range of 3200 m-8900m (Ano. No 1), the area of H2 which covers the northwest area of the map has a depth range from 4000 m-8000 m (Ano. No 2). While the area of H3 has a depth range from 2200 m-9200 m **(**Ano No 3). It appears that H1 and H2 come from the same source.

It is clear that some of the depth solutions mentioned previously is overestimating the depth to the top of the basement, which likely comes from dense structures within the basement.

the area **B** contains three anomalies. L1 shows a depth range from 3200 m_6700 m (Ano. No 4). L2 show depth solution values 2800 m_7000 m (Ano. No 5), the depth of the region of L3 ranges from 2000 m_4900 m (Ano. No 6). (Table 3.4): shows a summary of the depth of each magnetic anomaly as shown on RTP map.

Anomaly No	**Depth (m)**
1	3200-8900
2	4000-8000
3	2200-9200
4	3200-6700
5	2800-7000
6	2000-4900

Table 3. 4 : Summarize the Magnetic anomalies and their depths as shown on the map

3.7 Computer modeling.

Gravity modeling is usually the final step in gravity interpretation and involves trying to determine the density, depth and geometry of one or more subsurface bodies. The modeling procedure commonly involve s using a residual gravity anomaly. When modeling a residual gravity anomaly, the interpreter must use a density contrast between the body of interest and the surrounding material, while modeling Bouguer gravity anomalies; the density of the body is used. There are many different techniques available to perform the modeling procedure and they can be broken down into three main categories: 1) analytical solutions due to simple geometries, 2) forward modeling using 2-(two-dimensional), 2.5- (two and one-half dimensional) and 3-D (three-dimensional) irregularly shaped bodies, and 3) inverse modeling using 2-, 2.5- and 3-D irregularly shaped bodies. Most of these techniques involve iterative modeling (by the aid of a computer), where the gravitational field due to the model is calculated and compared to the observed or residual gravity anomalies. If the calculated values do not match the observed anomalies, the model is changed and the procedure is performed again until the match between the calculated values and the observed anomalies is deemed close enough.

This model has been chosen to cross the present structures. in its simplest form, the process of constructing an earth model is one of trial-and-error iteration in which one's knowledge of the local geology, data from drill holes, As the modelling proceeds, one must make choices concerning density and geometry of the bodies of rock that make up the model. with some constraints, one can usually feel that the process has yielded a very useful interpretation of the subsurface.

This profile length as, the density which used in this modeling were adopted mainly from two **wells** I48-13 and I10-13 (Figure 3.30).

3.7.1 Gravity model

Gravity modeling is usually the final step in gravity interpretation and involves trying to determine the density, depth, and geometry of one or more subsurface bodies. The modeling procedure commonly involve s using a residual gravity anomaly. When modeling a residual gravity anomaly, the interpreter must use a density contrast between the body of interest and the surrounding material, while modeling Bouguer gravity anomalies; the density of the body is used. There are many different techniques available to perform the modeling procedure and they can be broken down into three main categories: 1) analytical solutions due to simple geometries, 2) forward modeling using 2-(two-dimensional), 2.5- (two and one-half dimensional) and 3-D (three-dimensional) irregularly shaped bodies, and 3) inverse modeling using 2-, 2.5- and 3-D irregularly shaped bodies. Most of these techniques involve iterative modeling (by the aid of a computer), where the gravitational field due to the model is calculated and compared to the observed or residual gravity anomalies. If the calculated values do not match the observed anomalies, the model is changed, and the procedure is performed again until the match between the calculated values and the observed anomalies is deemed close enough.

This model has been chosen to cross some of the present structures in the area. In its simplest form, the process of constructing an earth model is one of trial-and-error iteration in which one's knowledge of the local geology, data from drill holes, as the modelling proceeds, one must make choices concerning density and geometry of the bodies of rock that make up the model. With some constraints, one can usually feel that the process has yielded a very useful interpretation of the subsurface.

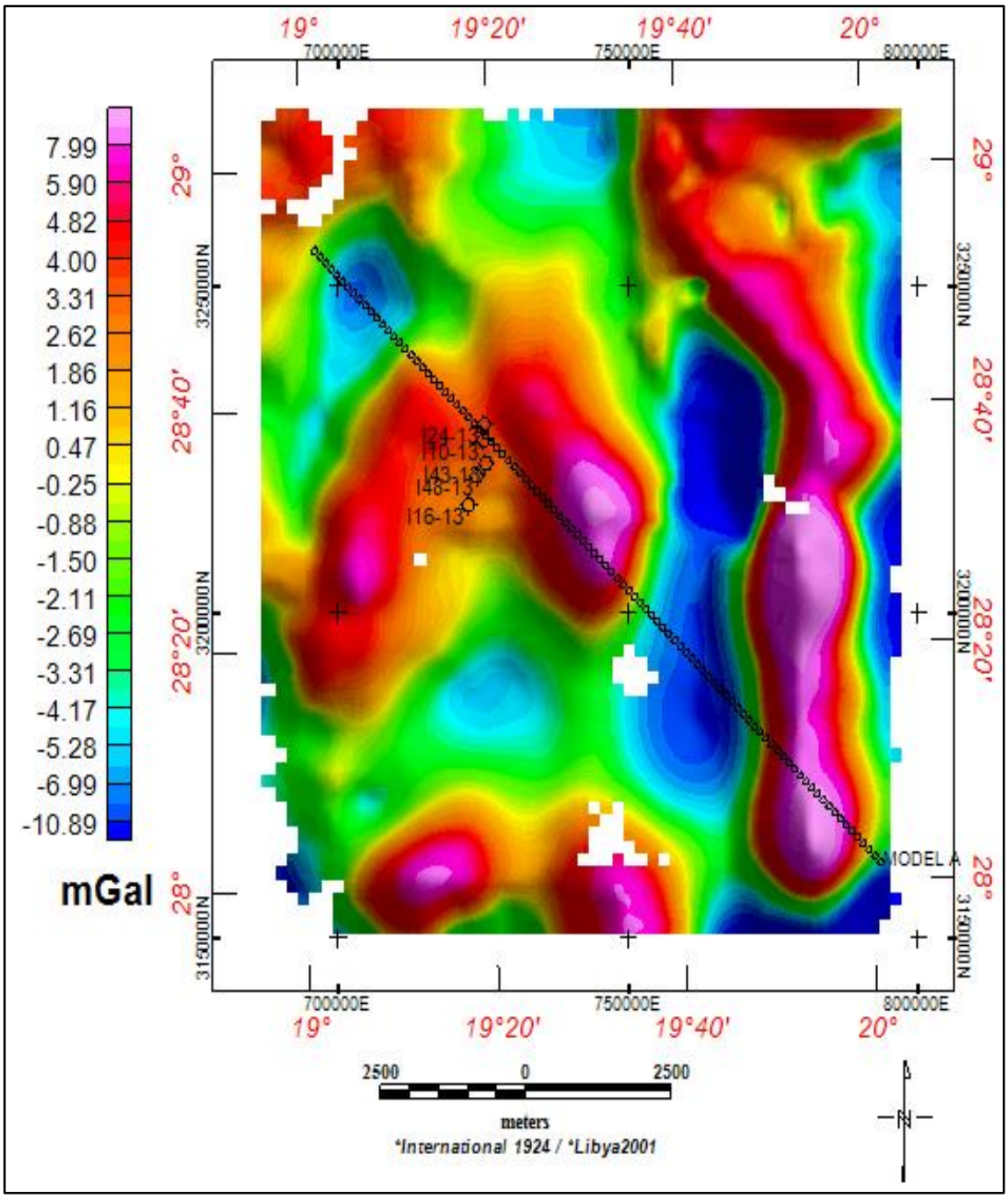

Figure 3. 30 : Location of the gravity profile A-B and the control points (boreholes). The map is constructed on the Residual anomaly map.

3.7.2 Model A-A1

Designed model A-A1 with a length of 135812 meters through the well I48-13 and l10-13 (Figure 3.30), the model (Figure 3.31) expressed a range of geological structures in the subsurface, and we have acquired a set of information (density, depth) of the strata from the wells mentioned above and from the previous studies, the densities are ranged between 1.8g/cc for the shallowest layer and 2.67g/cc for the basement. Table 3.5 show the final calculated density assigned to each package. these data were derived from the real well logs data.

Unit	Air surface	Pre- Eocene	Early- Eocene	landenian Eocene	Montian Palaocene
Density g/cc	0	1.8	2.3	2.35	2.38
Unit	Danian Palaocene	Maastrichtian Cretaceous	Cretaceous	coni/sant Cretaceous	Camp-Eord (Basement)
Density g/cc	2.39	2.40	2.42	2.51	2.67

Table 3. 5 : The average densities calculated for different Units from a group of wells. ***(Estimated from well logs data)***

The range of the gravity values along the profile is between 10.89 mGal and -7.99 mGal. Two factors have been taken into consideration when the strike of the profile is chosen, first is the good resolution of the gravity data, second to be traversing with a number of anomalies.

The model shows the average basement depth of ~3.2 km and the minimum of 2.1 km, while the maximum is ~4.2 km near the southeast part of the area. The model reveals that the area is affected by the tectonic events and subsidence that took place during the Cretaceous and Paleocene time which in turn occurred a number of natural faults on the layers and controlled their thickness and caused a lateral change in depth.

Figure 3. 31 : The gravity model A-A1, focuses on the upper part of the model and demonstrate the depositional strata with the main features dominated the area and basement morphology

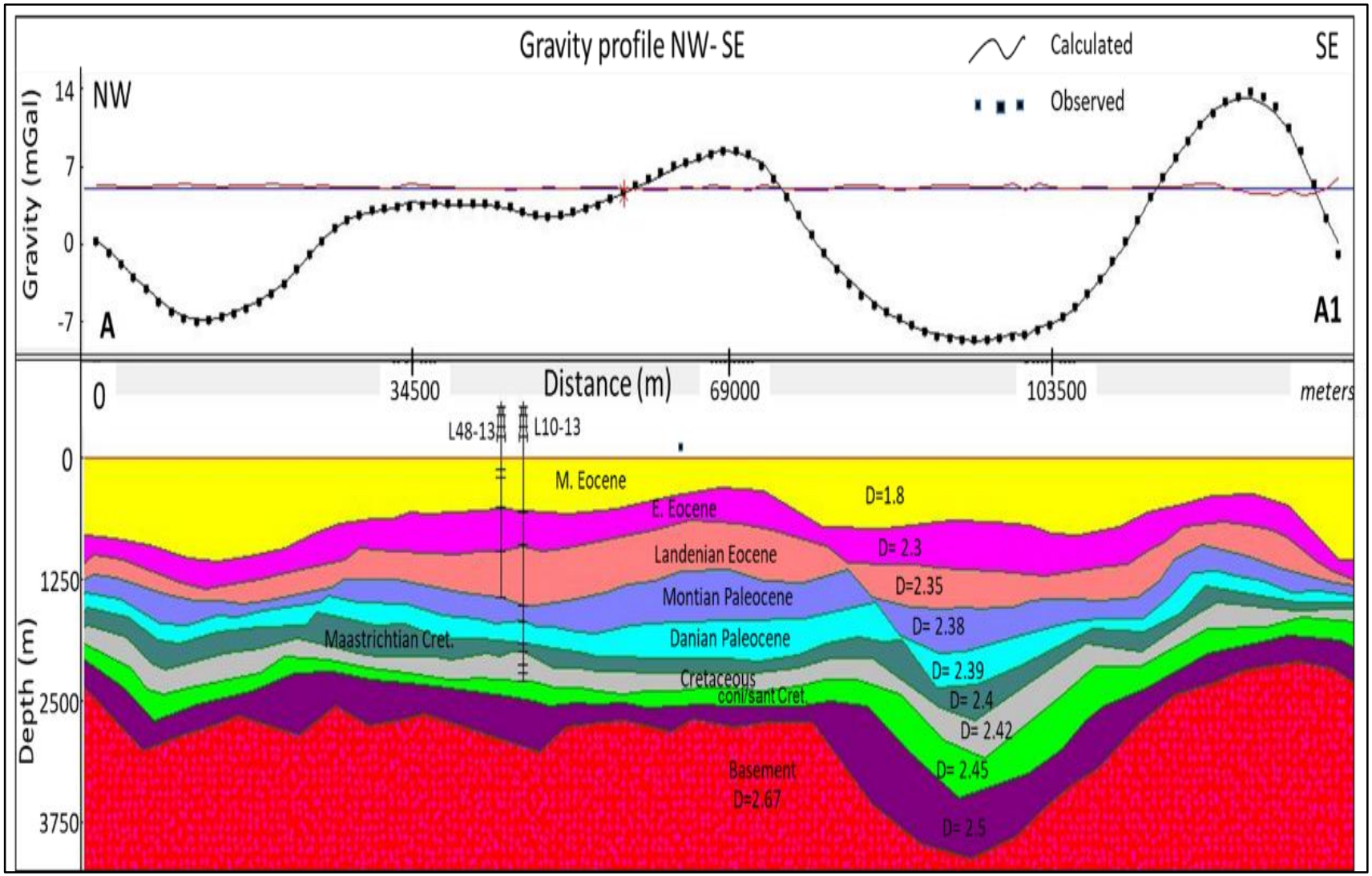

84

3.8 Tectonic map

The Area has undergone several phases of tectonic evolution, each of which is characterized by structural elements that differ in orientation (and thus in associated stress fields) and timing from the elements of other phases, which occurred during mid-Cretaceous and can be linked to the most recent evolution of the Sirt Basin.

Most authors believes that rifting began after the mid-Cretaceous, and during the Cenomanian and late Campanian it was the dominant force. Following this the rift infill episode started and persisted until the end of the Maastrichtian, after which much of the Sirt Basin experienced a sag subsidence. By the Oligocene the final tectonic stage was starting, in which northeast tilting dominated the area, In the Sirt Basin, the fracture zone formed in a series of NW-SE splays that controlled the Trough s location in the Sirt Basin, these Trough s can be considered as pull-apart grabens. According to the figure, the dominant fault trend bounding the Trough is NNW-SSE, with a subsidiary trending N-S.

The majority of faults within the study area are found within the center, as appeared in the (Figure 3.32). with trending NNW-SSE and N-S While there are some faults, the direction is NE-SW.as that appears in the bottom left side of the area.

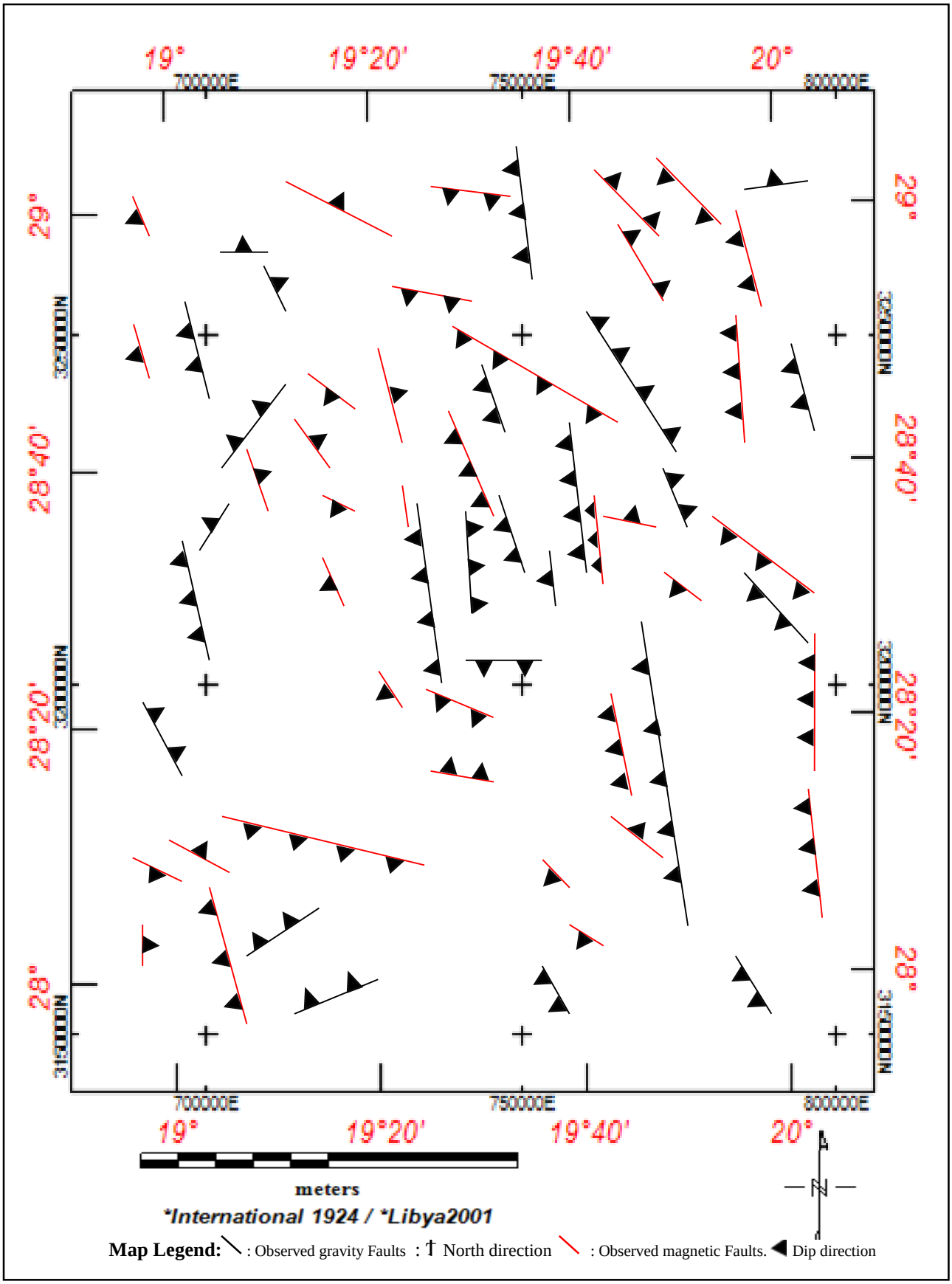

Figure 3.32 : General tectonic map of Sirt basin. Showing the minor and major faults. That dominated the area

Chapter 4

4.1 CONCLUSIONS

Gravity survey is a good tool and is widely used to investigate and interpret the subsurface geology, because it can cover large areas with cheaper cost than other geophysical tools like seismic. Different sorts of mapping were carried out to attempt to separate local and regional features. These maps demonstrate that the Marada Trough 's main structural features range in depth from shallow to deep.

The study area Maradah Trough in the far north and northeast and the trend of major structure is NNW-SSE.

Gravity anomaly commonly shows positive values in the north and northeast where there is high density resulting from Maradah Trough . The southern region is where the low anomalies are most prevalent.

The research indicates that there are a variety of local anomalies distributed throughout each study area, following regional gravity and bouguer anomalies are separated.

The residual gravity map revealed that there was a positive local anomaly in the north, south, north, and east as well as the southeast, on other hand a local negative anomaly in the lower center of the study area.

The Power spectrum analysis for the gravity data provided estimates a maximum depth of 14 km, indicating it a relatively deep source (deeper than the basement). The source depth, which is 6 km deep and was assumed to be the top of the deepest basement. The depths of 5.9 km and 6.2 km remain as well within the basement depths range. The anomalies that produced a range of 2.8 km were associated with a shallow source.

The depth (source) estimation produced from the data's power spectrum (magnetic) is nearly identical to the values determined from gravity (more or less).

The high wavelet's causal origins are located at a depth of 15.9 km, roughly. In contrast to the short wavelet sources, which are located at a depth of roughly 3.7 km, the magnetized rock of the basement has values between 7.1 and 4.4 km.

The purpose of the investigation was to extend the observed profile of the earth's gravitational effect across the present structural subsurface using a model of the earth

whose gravitational influence was predicted. According to the gravity models, the foundation beneath the gravity Trough s is rather shallow (about 2.1 km), but it is quite deep (about 4.2 km) beneath the positive anomalies. where the basement surface shows a maximum depth of 3.2 Km.

A new tectonic map has been created using the result of this research, indicating the location of the most significant anomaly, as well as the major and minor fault trending.

4.2 Future work

1 The results achieved in this study has to be verified using other methods such as well logging, seismic, etc.

2 More Gravity and magnetic modelling may be carried out later on to improve our present knowledge of the subsurface geology of Basin.

3 utilize the Backstepping technique of the wells data, will infer the evolution of the Sirt Basin and its subsidence history.

4.3 REFERENCES

Abadi, A.M. (2002) Tectonics of the Sirt Basin: Inferences from Tectonic Subsidence Analysis, Stress Inversion and Gravity Modeling. PhD thesis, Univ. Vrije, Holland, 187

A.M. Abadi, J.D. van Wees, P.M. van Dijk, S.A.P.L. Cloetingh, 2008,Tectonics and subsidence evolution of the Sirt basin, Libya, AAPG Bulletin 92(8):993-1027

Abdunaser, K.M, McCaffrey, K.J.W. (2014) Rift architecture and evolution: The Sirt Basin, Libya: The influence of basement fabrics and oblique tectonics. Elsevier, Journal of African Earth Sciences 100, p 203–226.

Abdunaser, K.M., McCaffrey, K.J.W. A (2015) new structural interpretation relating to the Sirt Basin, western Sirt Basin based on a new paleostress inversion.

Ahlbrandt, T.S. 2001. The Sirt Basin Province of Libya—Sirt-Zelten total petroleum system. US. Geol. Surv. Bull. vol. 2202-F. 29 pp.

Anketell, J.M. (1996) Structural history of the Sirt Basin and its relationship to the Sabratah Basin and Cyrenaica Platform, northern Libya. First Symposium on the Sedimentary Basins of Libya, Geology of the Sirt Basin, vol. 3. (eds.) M.J. Salem, M.T. Busrewil, A.A. Misallati, and M.A. Sola, Elsevier, Amsterdam, p. 57-89.

Baranov, V., and Naudy, H. (1957) Numerical calculation of the formula of reduction to the magnetic pole: Geophysics, 29: p. 67-79

Burk, K. and DEWEY, J. F. 1974. Two plates in Africa during the Cretaceous, Nature, 249, 313.

Barr, F.T. and Weegar, A.A. (1972) Stratigraphic nomenclature of the Sirt Basin, Libya.Petroleum Exploration Society of Libya, Tripoli, 179p.

Blakely, R. J. (1996) Potential theory in gravity and magnetic applications, second addition, published by the press syndicate of the University of Cambridge. First published 1995.

Bonnefous, J. 1972. Geology of the quartzitic" Gargaf Formation" in the Sirt Basin, Libya.

Briggs, I. C., 1974, Machine contouring using minimum curvature: Geophysics, 39, 39-48.

Chapin, D.L., Ander, M.E. (1999) chapter 15 ―Applying Gravity in Petroleum Exploration‖ in: Treatise of petroleum Geology/Handbook of petroleum Geology: Exploring for Oil and Gas Traps, **AAPG** special volumes. P. 15-1 to 15-28

Essed, A.S.: 1978, A reconnaissance Bouguer Gravity Anomaly Map of Libya. MSc. Thesis, Purdue University.

Fairhead, J, D. (1988) "A regional gravity study of the west African system and tectonic interpretation 141-159

Clark-Lowes, and M. W. Traut, 1998, Palaeozoic petroleum systems of North Africa, in D. S. MacGregor, R. J. T. Moody, and D. D. Clark-Lowes, eds.,Petroleum geology of North Africa: Geological Society of London, p. 7–68.

Cooper, G.R.J. and Cowan, D.R.: 2004, Enhancing potential field data using filters based on the local phase. Comput. Geosci., 32, 10, 1585–1591.

Conant, L.C. and Goudarzi, G.H. 1967. Stratigraphic and tectonic framework of Libya. Bull. Am. Assoc. Pet. Geol. vol. 51. p. 719–730.

Clifford, H.J., Grund, R. and Musrati, H. 1980. Geology of a stratigraphic giant: Messla oil field, Libya. In: Giant Oil and Gas Fields of the Decade 1968–1978. (ed. M.T. Halbouty). Mem. Amer. Assoc. Pet.Geol. No. 30, p. 507–524

Elakkari., 2005, Structural configuration of the sirt basin, geological resource management and environmental geology (GRMEG). p.1-5.

Gras, R. and Thusu, B. (1998) Trap architecture of the early Cretaceous Sarir Sandstone inthe eastern Sirt Basin, Libya. In: Petroleum Geology of North Africa. (ed.) D.S. Macgregor,

Goudarzi, G. H. 1980. Structure-Libya. The geology of Libya.Academic Press, Tripoli, III, 879-892

Guiraud, R. and Bellion, Y. 1995. Late Carboniferous to Recent, Geodynamic evolution of the west Gondwanian, cratonic, Tethyan margins. The Tethys Ocean. Springer.

Goudarzi, G.H. 1970. Geology and mineral resources of Libya: a reconnaissance. U.S. Geol. Surv. Prof. Paper No. 660, Washington 104p

Galushkin, Y., Eloghbi, S. and Sak, M. 2014. Burial and thermal history modelling of the Murzuq and Ghadames basins (Libya) using the GALO computer programmer. J. Pet. Geol. vol. 37. p. 71–93.

Grauch, V. J. S., Viki B. (2003) Aeromagnetic interpretation for understanding the Hydrologic framework of the southern Espanola basin, New Mexico. U. S. geological

Grauch, V. J. S., Hudson, M.R., Minor, S.A. (2006) Exploration geophysics, sources of a long-strike variation in magnetic anomalies related to intra-sedimentary faults: A case study from the Rio Grande Rift, USA V.J.S., 37: p. 372–378.

Gumati,Y. D., and W. H. Kanes, 1985, Early Tertiary subsidence and sedimentary facies—northern Sirt Basin, Libya: AAPG Bulletin, v. 69, p. 39–52.

Grant , Dodds 1972, Analytic Signal and Reduction-to-the-Pole in the Interpretation of Total Magnetic Field Data at Low Magnetic Latitudes. Elsavier

Hallett, D. (2002) Petroleum Geology of Libya, Amsterdam: Elsevier.

Hammuda, O.S. 1980a. Geologic factors controlling fluid trapping and anomalous freshwater occurrences in the Tadrart Sandstone, Al Hamadah al Hamra area, Ghadamis Basin. Second Symposium on the Geology of Libya, vol. 2. (eds. M.J. Salem and M.T. Busrewil), AcademicPress, London, p. 501–508.

Hassan, S.H., Chiarenzelli, J., Kendall, C.G. (2008) Cretaceous Source Rocks Potential of Northern Libya. AAPG, Annual Convention and Exhibition, Denver, Colorado.

Hassan, S.H., Chiarenzelli, J., Kendall, C.G. (2014), Hydrocarbon Provinces of Libya: A Petroleum System Study.

Hallett, D., and El Ghoul, A. (1996) Oil and gas potential of the deep Trough areas in the Sirt Basin, Libya, in Salem, M.J., El-Hawat, A.S., and Sbeta, A.M., (eds.) The geology of Sirt Basin: Amsterdam, Elsevier, v. 2: p. 455–484

Hallett, D, Petroleum Geology of Libya, “second edition”, 2014, “Geological map of Libya 1985”

Hsu Shu-Kun (2002) Imaging magnetic sources using Euler ‘s equation. Geophysical prospecting, 50, p. 15-25.

Hood, P. (1965) Gradient measurements in aeromagnetic surveying: Geophysics, vol. 30 (5),p. 891–902

Hildenbrand, Thomas G., Rosenbaum, Joseph G., Kauahikaua, James P. Aeromagnetic study of the Island of Hawaii, journal of geophysical research

Khalifa, m.,abdunaser (2012) structural style and tectonic evolution of the northwest sirt basin–cretaceous- tertiary rift, libya. doctoral thesis, durham university.

Klitzsch, E. 1970. Die Strukturgeschichte der Zentralsahara: Neue Erkenntnisse zum Bau und zur Paläographie eines Tafellandes.

Klitzsch, E. (1996) The structural development of parts of north Africa since Cambrian time. First Symposium on the Geology of Libya (ed.) C. Gray. Faculty of Science, University of Libya, Tripoli,

L. Cordell et al. (1987). Mapping basement magnetization zones from aeromagnetic data in the San Juan basin, New Mexico

Lowrie, W. (2007) Fundamentals of Geophysics. Cambridge University Press, Cambridge, UK.

Massa, D. and Delort, T. 1984. Evolution du bassin de syrte (Libye)
du cambrien Butt, A.A. 1986. Upper Cretaceous biostratigraphy of the Sirt Basin, northern Libya. Rev. Paleobiol. vol. 5. p. 175–191.

Moritz, H. (1988) GEODETIC REFERENCE SYSTEM 1980, Geodesists handbook from Bulletin Geodesique, Vol. 62 (3)

MacLeod , 1993-D Analytic Signal in the Interpretation of Total Magnetic Field Data at Low Magnetic Latitudes, springer.

Ofoeghu, C.O. and Hein, K. (1991) Analysis of Magnetic Data over Part of the Younger Granite Province of Nigeria. Pure and Applied Geophysics, 136, 173-189.

Pomeyrol, R. 1969. A catharsis on the term Nubian Sandstone. In: Geology, archaeology and prehistory of the southwestern Fezzan, Libya (ed. Kanes, W.H.). Petroleum Exploration Society of Libya, Eleventh Annual Field Conference, p. 131–138

Phillips, J.D. (2000): A Comparison of the Horizontal Gradient, Analytic Signal, and Local Wavenumber Methods. 402-405

R.T.J. Moody, D.D. Clark-Lowes, Geol. Soc. Special Publication No. 132, p. 317-334.

Richard, C.S, Stephen A.S (1998) elements of petroleum geology, second edition, USA, Elsevier.

Reid, A.B., Allsop, J.M., Granser, H., Millet, A.J., Somerton, I.W. 1990. "Magnetic interpretation in three dimensions using Euler Deconvolution", Geophysics, 55(1), 80-91.

Rusk, 1999, Exploration geology and geophysics of Libya: Tulsa, Oklahoma, Masera Corporation, 205p.

Rusk, D. C., 2002. Libya: Petroleum potential of the underexplored basin centers—A twenty-first-century challenge, in M.W. Downey, J. C. Threet, and W. A. Morgan, eds., Petroleum provinces of the twenty-first century: AAPG Memoir 74, p. 429–452.

Spector, A., Grant, F.S. 1970. "Statistical models for interpreting aeromagnetic data", Geophysics, 35(2), 293-302.

SWEI, G. 2010. Sedimentology, Diagenesis and Reservoir Characteristics of Eocene Carbonates Sirt Basin, Libya. Durham University.

Thompson, D.T. 1982. "Euldph-A new technique for making computer assisted depth estimates from magnetic data", Geophysics, 47(1), 31-37.

Tawadros, E.E., Rasul, S.M. and Elzaroug, R. 2001. Petrography and palynology of quartzites from the Sirt basin, central Libya. J. Afr. Earth Sci., vol. 32. p. 373–390.

Van houten, F.B. 1980. Latest Jurassic-early cretaceous regressive facies, northeast Africa craton. Bull. Amer. Assoc. Pet. Geol. vol. 64. p. 857–867.

V.J.S. Grauch et al (1987). Limitations of determining density or magnetic boundaries from the horizontal derivative of gravity or pseudo gravity data Geophysics.

VAN HOUTEN, F. B. 1983. Sirt Basin, north-central Libya: Cretaceous rifting above a fixed mantle hotspot? Geology, 11, 115-118

Vacquier & Gary, 1951, Method and apparatus for measuring intensity of magnetic fields, nature.

Wilson, M., and Guiraud R. (1998) Late Permian to Recent magmatic activity on the AfricanArabian margin of Tethys, in D. S. Macgregor, R. T. J. Moody, and D. D. Clark-Lowes, (eds.) Petroleum geology of north Africa: Geological Society (London) Special Publication 132, p. 231–263.

Williams, J.J. 1968. The sedimentary and igneous reservoirs of the Augila oil field, Libya. (eds. F.T. Barr,) Geology and Archaeology of Northern Cyrenaica, Libya. Petroleum Exploration Society of Libya, Tenth Annual Field Conference. p. 197–206.

Xiong, L. (2003) On the use of different methods for estimating magnetic depth: Society of Exploration Geophysicists the Leading Edge, vol. 22 (11) p.1090–1099.

Ziegler, P.A., Stampfli, G.M., 2001. Late Paleozoic Early Mesozoic plate boundary reorganisation: collapse of the Variscan orogen and opening of Neotethys. In: Cassinis, R. (Ed.), The continental Permian of the Southern Alps and Sardinia (Italy) regional reports and general correlations: Annali Museo Civico Science Naturali, Brescia, 25, pp. 17–34

Citation

https://www.geomatrix.co.uk/tools/magnetic-field-calculator/

(www.Geosoft.com